TU/e technische universiteit eindhoven

DAF A PACCAR COMPANY

# The Dynamic Behaviour and Stability Control of a Truck/full-trailer combination

**MSc Thesis**

Remco E. Mansvelders

DCT 2006.137

December 2006

*Thesis directed by:*
Prof. dr. Henk Nijmeijer (TU/e)
dr. ir. Ron Hensen (DAF-Trucks)
dr. ir. Igo Besselink (TU/e)

*Master thesis committee:*
Prof. dr. Henk Nijmeijer (TU/e)
dr. ir. Ron Hensen (DAF-Trucks)
dr. ir. Igo Besselink (TU/e)
dr.ir. Frans Veldpaus (TU/e)

**University of Technology, Eindhoven**
Department of Mechanical Engineering
Dynamics and Control Group

**DAF-Trucks, Eindhoven**
Technical Analysis Group

# Abstract

Vehicle safety remains an important topic in the automotive industry due to the large number of vehicle accidents each year. One of the causes of vehicle accidents is due to vehicle instability phenomena. Vehicle instability phenomena can occur by unexpected road changes, during full-braking, obstacle avoidance or severe manoeuvring. Three main instability phenomena can be distinguished: the yaw-rate instability, the rollover and the jack-knife phenomenon. Vehicle stability control systems have been developed to detect and counteract vehicle instability phenomena and to prevent vehicle accidents eventually. Unfortunately a stability control system does not yet exist for a truck/full-trailer combination.

In this report a methodology is presented for analyzing the yaw-rate instability, the rollover phenomenon and the stability margins of a truck/full-trailer combination around various trajectories. Therefore a one-track 3-dimensional dynamic vehicle model is derived and the corresponding non-linear equations of motion are determined.

The yaw-rate instability is studied using a vehicle handling diagram and shows that the vehicle combination is understeered for various circle trajectories. The rollover phenomenon is studied by deriving the maximum allowable lateral acceleration by which the vehicle combination will not rollover. To analyse the stability margins of the truck/full-trailer autonomous dynamics an analytic approach is used by which the non-linear equations of motion are linearized around various straight-line and circle trajectories.

Final part, the observability and controllability are analyzed of the truck/full-trailer combination around specified trajectories. Various sensors and actuators are placed on the vehicle combination to verify which combination can be used for a future stability controller design. This study shows that a minimal forward velocity is required to ensure that the computed observability and controllability are correct. An extra sensor and actuator is necessary to estimate and control the states around a straight-line trajectory.

# Samenvatting

Voertuigveiligheid is een belangrijk onderwerp in de automobielindustrie door het grote aantal ongelukken elk jaar. Een oorzaak van voertuig ongelukken is toe te schrijven aan het instabiel worden van een voertuig. Voertuig instabiliteit kan worden veroorzaakt door veranderingen in het wegdek, remmen en uitwijkmanoeuvres. Voertuig instabiliteit kan worden onderverdeeld in drie categorieën: gier snelheid ('yaw-rate') instabiliteit, rollen ('rollover') en het scharen van een voertuig combinatie ('jack-knife'). Voertuigstabiliteit regelaars zijn ontwikkeld om voertuig instabiliteit situaties te herkennen en in te grijpen om ongelukken te voorkomen. Echter bestaat er geen stabiliteit regelaar voor een vrachtwagen combinatie met een volledige bakwagen ('truck/full-trailer combination').

In dit verslag wordt een methodiek gepresenteerd om de yaw-rate instabiliteit, rollover en stabiliteitsmarges van de truck/full-trailer combinatie te kunnen analyseren. Hiervoor is een 3-dimensionaal voertuig model opgezet en de behorende niet-lineaire bewegingsvergelijkingen afgeleidt.

De yaw-rate instabiliteit is bestudeerd met het gebruik van een 'vehicle handling diagram' en toont aan dat de vrachtwagen onderstuurd is voor verschillende cirkel trajecten. Het rollover fenomeen is bestudeerd door het afleiden van een maximaal toelaatbare laterale versnelling waarbij de voertuig combinatie niet omrolt. Voor de analyse van de stabiliteit marges van de autonome truck/full-trailer dynamica is een analytische benadering toegepast waarbij de niet-lineaire bewegingsvergelijkingen rond diverse rechtuit en cirkel trajecten gelineariseerd zijn.

Tenslotte is de observeerbaarheid en controleerbaarheid van de truck/full-trailer combinatie bestudeerd rond verschillende trajecten. Sensoren en actuatoren zijn geplaatst om na te gaan welke gebruikt kunnen worden voor een toekomstig stabiliteit regelaar. Een minimale voorwaartse snelheid is vereist om te garanderen dat de berekende waarneembaarheid en controleerbaarheid correct zijn. Een extra sensor en actuator zijn noodzakelijk om de toestanden van de truck/full-trailer combinatie te bepalen en te regelen rond een rechtuit traject.

# Acknowledgements

Thanks to: dr. ir. Ron Hensen for providing me the opportunity for this interesting final thesis research. Also for his guidance, brainstorm sessions, enthusiasm, support and improving my knowledge to success this research. dr. ir. Igo Besselink for his excellent vehicle dynamics knowledge, providing me literature, suggestions, support and feedback during the research. Also thanks to Prof. dr. Henk Nijmeijer being the chairman during this final thesis and our monthly meetings. Thanks for providing me excellent feedback on the research results and interim reports and monitoring the quality of the research.
Also thanks to the people of the Technical Analysis department of DAF Trucks, who provide me the opportunity to work for nine months in a great environment during my thesis. Thanks for the technical assistance, support, personal advices and great coffee talks.
Lastly, I'd like to thank my family and friends who supported and encourage me in all things, this work included.

I would like to thank everybody spending time, support and effort to my final thesis.

# Contents

# Nomenclature

### Acronyms

| Acronym | Description |
|---|---|
| ABS | Anti-lock Braking System |
| c.o.g. | centre of gravity |
| $_{Circle}$ | Nominal circle trajectory |
| CM | Controllability Matrix |
| DAE | Differential Algebraic Equation |
| ECU | Electronic Control Unit |
| ESC | Electronic Stability Control |
| ESP | Electronic Stability Program |
| GM | Gain Margin |
| IC | initial condition |
| LHP | left half-plane (of a complex plane) |
| MF | Magic formula (tyre modelling) |
| MIMO | Multiple Input Multiple Output |
| NHTSA | National Highway Traffic Safety Administration |
| ODE | Ordinary Differential Equation |
| OM | Observability Matrix |
| PM | Phase Margin |
| SISO | Single Input Single Output |
| $_{SL}$ | Nominal straight-line trajectory |
| SMC | Sliding Mode Control |
| SUV | Sport Utility Vehicle |
| SVD | Singular Value Decomposition |
| TWR | Track Width Ratio |
| VSC | Vehicle Stability Control |

## Symbols

| Symbol | Description | Value | Unit |
|---|---|---|---|
| $\mu$ | friction | | $[-]$ |
| $\pi$ | pi | 3.1415... | $[-]$ |
| $\psi$ | yaw angle | | $[rad]$ |
| $\varphi$ | roll angle | | $[rad]$ |
| $g$ or gravity | gravitational acceleration | 9.81 | $[m/s^2]$ |
| $M$ | mass | | $[kg]$ |
| $a_y$ | lateral acceleration | | $[m/s^2]$ |
| $T_{kin}$ | kinetic energy | | $[J]$ |
| $U_{pot}$ | potential energy | | $[J]$ |
| $D_{diss}$ | dissipation energy | | $[J]$ |
| $Q_{ex}$ | generalized external applied forces | | $[N]$ |
| $F$ | force | | $[N]$ |
| $T$ | torque | | $[N]$ |
| $I$ | mass inertia | | $[kgm^2]$ |
| $C$ | lateral tyre cornering stiffness | | $[N/m]$ |
| $F_y$ | lateral tyre force | | $[N]$ |
| $\delta$ | steering angle | | $[rad]$ |
| $\alpha$ | side slip angle | | $[rad]$ |
| $U$ | forward velocity | | $[m/s]$ |
| $V$ | lateral velocity | | $[m/s]$ |
| $\mathbf{A}$ | state space system matrix | | $[-]$ |
| $\mathbf{B}$ | state space input matrix | | $[-]$ |
| $\mathbf{C}$ | state space output matrix | | $[-]$ |
| $\mathbf{D}$ | state space feedthrough matrix | | $[-]$ |
| $e$ | state tracking error | | $[-]$ |
| $q_i$ | generalized coordinate | | $[-]$ |
| $\mathbf{L}$ | proportional gain | | $[-]$ |
| $\mathbf{K}$ | state feedback gain | | $[-]$ |
| $x$ | state vector | | $[-]$ |
| $u$ | input vector | | $[-]$ |
| $y$ | output vector | | $[-]$ |
| $\theta$ | parameter vector | | $[-]$ |

# Chapter 1

# Introduction

## 1.1 Vehicle safety

Vehicle safety remains an important topic in the automotive industry due to the large amount of vehicle accidents each year. The National Highway Traffic Safety Administration (NHTSA) [fSN04b] shows that in the year 2004, 42,636 people lost their lives in the estimated 6,181,000 vehicle accidents in the United States. In these accidents 2,788,000 people were injured and 4,281,000 crashes involved property damage. The economic cost of the number of vehicle accidents in the US in the year 2002 was estimated at 230,6 billion dollar.

One of the causes of vehicle accidents are vehicle instability phenomena. A vehicle has become unstable when the driver is unable to control the vehicle by steering or by a throttle/braking input. Typical examples of vehicle instability phenomena are skidding (also called yaw-rate instability) and the rollover of the vehicle. Vehicle stability control systems, such as the Anti-lock Braking System (ABS) and the Electronic Stability Program (ESP), have been developed to detect and counteract vehicle instability phenomena and to prevent vehicle accidents eventually.

Large trucks (total mass greater than 4,500 [kg]) accounted for 8 percent of all vehicles involved in fatal crashes and accounted for 4 percent of all vehicles involved in injury and property damage crashes [fSN04b]. One of the causes of commercial vehicle accidents are vehicle instability phenomena which are difficult to recognize by the driver. The driver obtains a reduced feeling of instability phenomena by the suspended cabin and the low stiffness of the chassis. Also with the large height of the center of gravity (c.o.g.) and the varying cargo, the load condition, of a commercial vehicle the driver can over-estimate the permissible speed while taking a curve which can result in vehicle instability, for example rollover of the vehicle. With the aid of vehicle stability control systems the number of commercial vehicle accidents, which are related to vehicle instability phenomena, can be reduced. Another benefit is a securer transport of expensive cargo. Nevertheless nowadays only, a minority of the commercial vehicles are equipped with these vehicle stability control systems.

Bosch GmbH and WABCO are manufacturers of vehicle stability control systems for commercial vehicles. WABCO has developed the Electronic Stability Control (ESC) system for tractor/semi-trailer combinations. An example of a tractor/semi-trailer combination is shown in figure 1.1. The ESC system measures the steering angle, lateral acceleration and yaw-rate

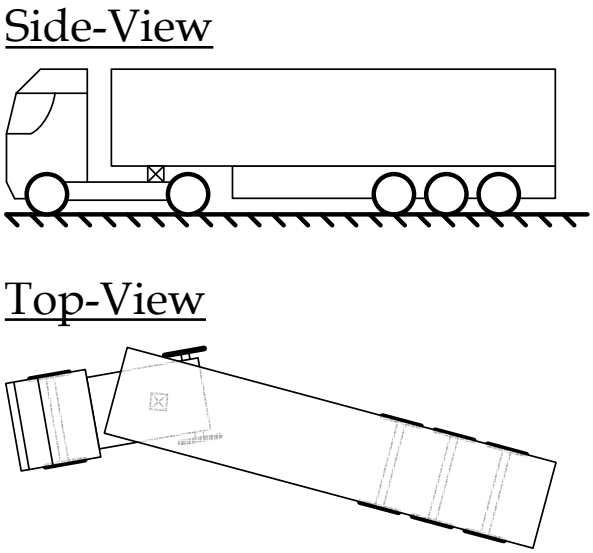


Figure 1.1: Tractor/Semi-trailer combination

of the tractor. This stability system can prevent vehicle instability phenomena by actuating on the engine torque, selective braking of the individual wheels of the tractor and/or simultaneous braking of the rear wheels of the semi-trailer.

## 1.2 Problem statement

Apart from a tractor/semi-trailer combination, the truck/full-trailer is another common commercial vehicle configuration. This vehicle combination exists of a full-trailer which has front and rear axles and is connected by a drawbar to the truck, as shown in figure 1.2. The drawbar is fixed to the front axle of the trailer and can rotate around its vertical axis. In comparison with the tractor/semi-trailer combination this commercial vehicle has an additional rotation point. A stability control system does not yet exist for this commercial vehicle combination and it is currently being developed by WABCO.

The main purpose of the stability control system is to prevent the truck/full-trailer instability phenomena. The instability of the truck/full-trailer combination appears when a combination of degrees of freedom exceeds a certain margin. The new stability control system has to influence all degrees of freedom to obtain a desired dynamic behaviour of the truck/full-trailer combination.

To avoid sensor communication between the trailer and the Electronic Control Unit (ECU) of the truck, the controller design is restricted by the fact that sensors can only be placed on the truck. On the other hand, control intervention can be applied by braking on both the truck as well on the full-trailer. Control intervention can consist of selective braking of the individual wheels of the truck and/or simultaneous braking of all wheels of the full-trailer.

To analyse the behaviour of a truck/full-trailer combination a dynamic vehicle model has to be made. Using the dynamic vehicle model the truck/full-trailer instability phenomena can

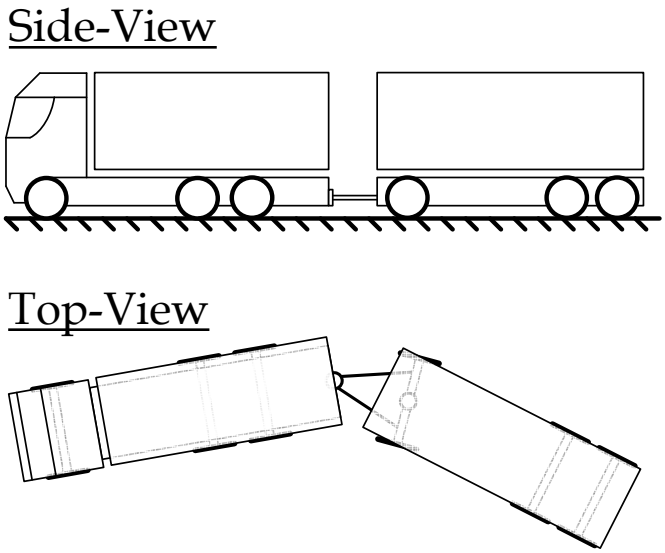


Figure 1.2: Truck/Full-trailer combination

be studied. On the truck/full-trailer combination various sensors and actuators can be placed to study the usage in a controller design. For deriving of the dynamic vehicle model and the design of a controller, a methodology has to be derived which can also be applied on other commercial vehicle configurations, for example a truck/full-trailer combination with another axle configuration.

Summarizing, the problem statement for this research can be given as:

*"Derive a methodology to investigate the dynamic behaviour and instability phenomena, such as the rollover and the yaw-rate instability, of a truck/full-trailer combination which can be used for a controller design. The purpose of the controller design is to influence the dynamics of the truck/full-trailer combination to obtain an acceptable dynamic behaviour. The controller design is restricted by the fact that sensors can only be placed on the truck. Control intervention can be applied by braking on both the truck as well on the full-trailer"*

## 1.3 Organization of the report

In chapter 2, a literature survey will be carried out to get an overview of the vehicle instability phenomena, dynamic vehicle models and vehicle stability control systems. The theory needed for deriving a methodology to analyse the dynamic behaviour and the design of a controller will be discussed in chapter 3. In chapter 4 this methodology will be applied on a truck/full-trailer combination by investigating the dynamic behaviour and instability phenomena. This will be done by performing a vehicle handling study and analyzing the stability of the non-linear equations of motion around various trajectories. A preliminary study for a controller design will be carried out based on the observability and controllability by various sensors and actuators placed on the truck/full-trailer combination. Conclusions and recommendations will be given in chapter 5.

# Chapter 2

# Literature survey

The literature survey has been split into two subjects:

- The explanation of the vehicle instability phenomena
- The methodologies to analyse and control the vehicle instability phenomena

## 2.1 The vehicle instability phenomena

Vehicle instability phenomena can occur on unexpected road changes, during full-braking, obstacle avoidance or severe manoeuvring. Three main instability phenomena can be distinguished: skidding (also called *yaw-rate* instability), *rollover* and the *jack-knife* phenomenon. These instability phenomena will be discussed in the following sections.

### 2.1.1 Yaw-rate instability

Yaw-rate instability has been studied most for passenger cars [Zan03]. Yaw-rate instability is the skidding of a vehicle which occurs through excessive vehicle under/oversteer as shown in figures 2.1 and 2.2. Vehicle under/oversteer arises by a difference of the lateral tyre forces between the front and rear wheels. This difference in the lateral tyre forces can rotate the vehicle in an undesirable direction. The lateral tyre force is a product of the tyre cornering stiffness and the tyre side slip angle. The side slip angle is the angle between the forward and lateral tyre velocity vector. When a wheel lock occurs, for example on a slippery road, the tyre side slip angle decreases and produces a smaller lateral tyre force eventually.

Stability control systems have been developed with the aim to keep the yaw-rate of the vehicle within a stable margin, for example the ESP system [Zan03] and [Gmb]. The ESP system calculates the desired driving direction of the driver by measuring the steering angle and the rotational-speed of each wheel. From the information of the yaw-rate sensor and the lateral acceleration sensor the ESP system recognize if the vehicle is going to skid. If so, the ESP system actuates by selective braking of the individual wheels and/or by reducing the engine torque. By selective braking of the individual wheels, the vehicle can be steered in the desired driving direction of the driver. With this control system excessive under/oversteer

can be prevented, as shown in figure 2.1 and figure 2.2, and the steerability of the vehicle can be maintained during an obstacle avoidance manoeuvre, as shown in figure 2.3.

Skidding of the vehicle can also caused by driving on slippery roads, such as a low-$\mu$ road or a $\mu$-split road. If the driver brakes on these kinds of roads a wheel-lock can occur by which the total brake-force cannot be transferred to the road. When wheel-lock occurs it is possible the vehicle skids and doesn't react on the drivers steering input. The ABS system measures the rotational-speed of each wheel continuously. When wheel-lock or excessive brake slip has been detected, the ABS system reduces temporarily the braking pressure at the wheel in question, which maintains steerability during braking [Gmb].

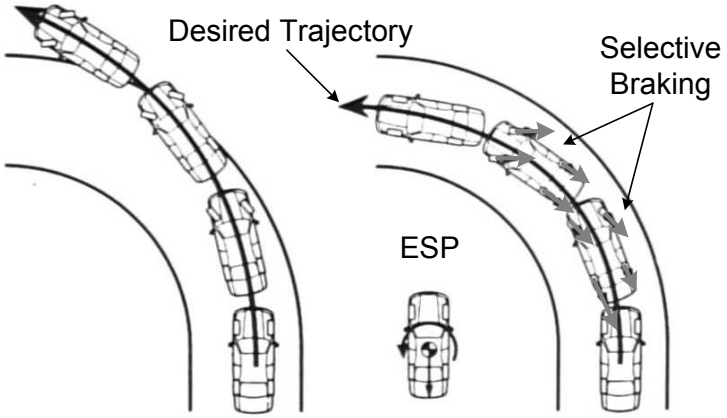


Figure 2.1: Vehicle understeer without (left) and with (right) the ESP system [Zan03]

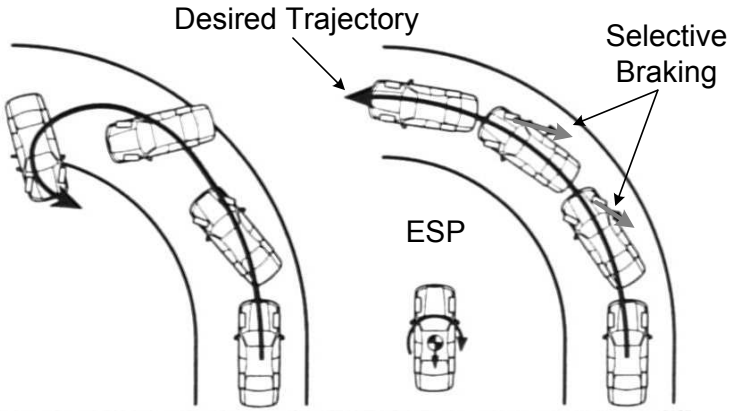


Figure 2.2: Vehicle oversteer without (left) and with (right) the ESP system [Zan03]

### 2.1.2 Jack-knife

The jack-knife phenomenon only occurs on vehicle combinations, such as a tractor/semi-trailer combination. Jack-knife is possible when the tractor or trailer skids [oMVAA06], as shown in figure 2.4. The most common situation is that the rear wheels of the tractor lose traction through excessive braking or acceleration on a low-$\mu$ road. While braking on a low-$\mu$ road it is possible that the tractor rear wheels lock-up and lose traction with the road.

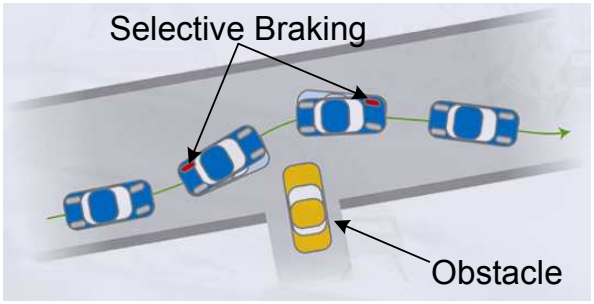


Figure 2.3: Obstacle avoidance with the ESP system [Zan03]

When the tractor skids it is possible the trailer push the tractor sideways which results in the jack-knife phenomenon. When a jack-knife occurs the vehicle combination is difficult to control by the driver. An ABS system placed on the truck and/or trailer prevents the jack-knife phenomenon indirectly by anti-lock control of the wheels. The ESC system prevents the jack-knife phenomenon directly by braking on the rear wheels of the trailer and/or reducing the engine torque.

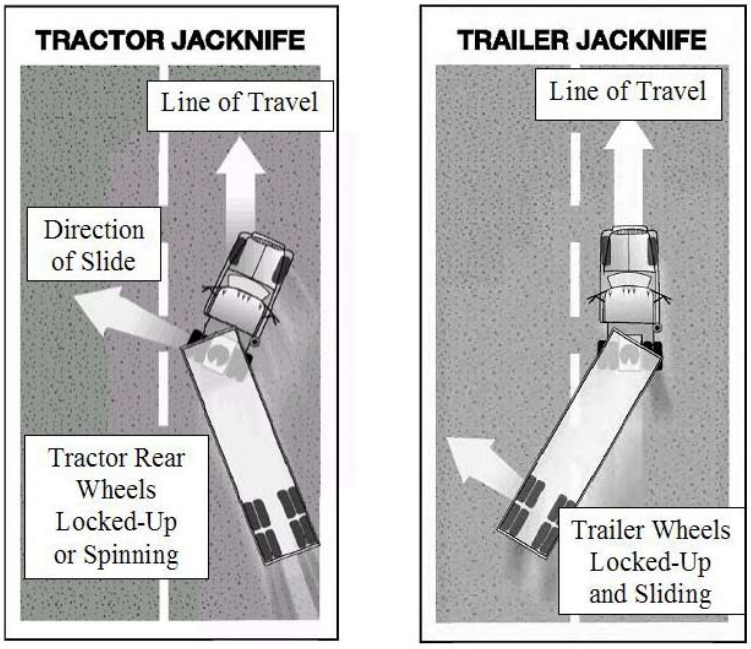


Figure 2.4: Examples of the jack-knife phenomenon [oMVAA06]

### 2.1.3 Rollover

An increase in research on the rollover phenomenon is noticeable with the increasing popularity of Sport Utility Vehicles (SUV's). SUV's contains a high centre of gravity (c.o.g.) and therefore have a higher risk to roll over. Data of NHTSA [fSN04a] shows that SUV's experienced the highest rollover rates compared with other vehicle types: 36.2 percent in fatal crashes, 9.6 percent in injury crashes, and 2.4 percent in property-damage-only crashes.

The data shows that of all crashes in the year 2004 2.3 percent occurred due to the rollover phenomenon. Nevertheless, vehicle rollover crashes have a much higher fatality rate, 20.5 percent, compared to other types of crashes in the year 2004.

Rollover is the state at which the overall c.o.g. of the vehicle has moved laterally passed the vehicle's 'balance point' [Gol01]. An example of a vehicle rollover has been shown in figure 2.5. Factors which play a significant role in the rollover phenomenon are the vehicle type (such as the height of the c.o.g. and track width of the vehicle), driver behaviour and the environmental conditions (such as the condition of the road). Rollover of a vehicle occurs in two ways: *tripped* or *untripped*. NHTSA data show that 95 percent of single-vehicle rollovers are of the tripped form [NHT]. A tripped rollover of a vehicle happens when a vehicle leaves the road and slides sideways, digging its tires into soft soil or hit an object such as a curb or guardrail. The best way to avoid a tripped rollover is to stay on the road. Untripped rollovers occur during high-speed collision/obstacle avoidance manoeuvres.

The NHTSA [(NH02] distinguish two categories to indicate the state at which the vehicle is willing to rollover:

- **Static rollover indicators:** used to indicate *tripped* rollover of a vehicle. Common static rollover indicators are the Tilt Table Ratio, Critical Sliding Velocity (CSV), Static Stability Factor (SSF) and the Track Width Ratio (TWR). These indicators determine the static rollover using the vehicle parameters only. The SSF is the ratio between the track width $T$ and the height of the centre of gravity $h$ of the vehicle. The lower the SSF ratio, the more likely the vehicle is willing to rollover in a single-vehicle crash. This ratio is used by NHTSA to indicate the chance of rollover of all kinds of vehicles. Ervin [Erv87] derived the TWR threshold which is the maximum allowable lateral acceleration of a vehicle's c.o.g. when it will rollover:

  $$a_{y,\max} = \frac{T}{h} \; [m/s^2]$$

  Ervin continues his static analysis for a vehicle model with suspension springs and compliant tyres which results in a smaller maximum allowable lateral acceleration. To study the rollover phenomenon Ervin divided the vehicle mass in an unsprung mass of the chassis and an elevated sprung mass of the body. Winkler [Win00] used this threshold to indicate the maximum lateral acceleration, expressed in gravitational units, at which the vehicle will rollover. For heavy loaded trucks the threshold lies often below 0.5 $[g]$ and sometimes it drops to 0.25 $[g]$. DAF Trucks [Hen04], a manufacturer of commercial vehicles, used the approach of Ervin to determine the maximum allowable lateral acceleration at which a commercial vehicle will rollover, as shown in detail in appendix A.

- **Dynamic rollover indicators:** used to indicate *untripped* rollover of a vehicle. In practice, common tests to indicate an untripped rollover are various "double lane-change" manoeuvres and "fishhook" manoeuvres, as shown in figure 2.6. These tests are "path following" and "defined steering angle" respectively. Dahlberg [Dah01] studied the rollover phenomenon and has determined a dynamic (quasi-static) approach to indicate rollover. This analysis is based on kinetic and potential energy of the dynamic vehicle model.

Figure 2.5: Rollover of a Mercedes A-class ["Der Spiegel", Nr. 45, 1997]

## 2.2 Methodologies to analyse and control vehicle instability phenomena

A common way to analyse the dynamic behaviour, including the stability phenomena, of a vehicle is with the use of a simulation model. The advantages of vehicle simulation studies are the cost and effort benefit compared with testing of a real vehicle. To detect and prevent vehicle instability phenomena a controller can be designed. The set-up and analysis methods of a dynamic vehicle model and the stability controller design are studied in literature and will be discussed in the following sections.

### 2.2.1 Dynamic vehicle models

In literature, different kind of dynamic vehicle models have been presented such as car models, tractor/semi-trailer combinations and a truck/full-trailer combination (by Zegwaard [Zeg88]). Dynamic vehicle models are presented by Pacejka [Pac02] which are used during the graduate courses of Besselink [BV03] and [BC04]. A basic vehicle model is the bicycle model which exists of a single mass, one-track and two wheels, as shown in figure 2.7. The corresponding equations of motion have been derived with the Lagrange formulation. This model is used to explain the basic vehicle handling, such as vehicle under/oversteer. The transfer between steering angle input and vehicle characteristic outputs, such as vehicle side slip angle, yaw-rate and lateral acceleration, at different forward velocities have been studied. The linear equations of motion have been written into the state space formulation and eigenvalue analyses have been carried out to indicate the vehicle stability for different vehicle parameters.

The main focus of Pacejka [Pac02] is to study the complex characteristics and simulation of the tyre behaviour. To study the tyre forces, Pacejka extended the bicycle model into a two-track dynamic vehicle model with an elevated c.o.g. which can roll around the longitudinal axis. For the simplicity of the bicycle model it is assumed that the tyres have only lateral and longitudinal stiffness. To get a more realistic tyre model, relaxation effects and the Magic Formula (MF) have been introduced by Pacejka.

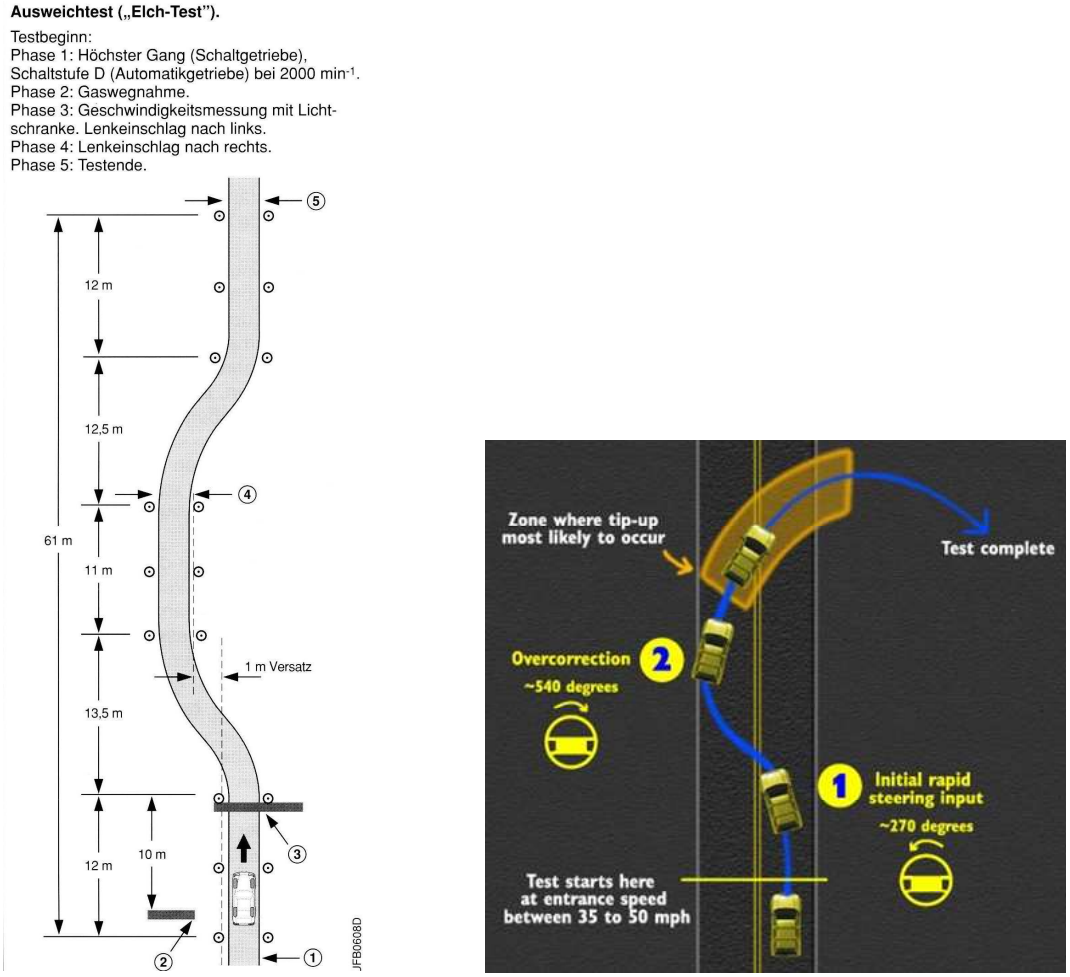


Figure 2.6: Left: Lane-change manoeuvre [Zan03] and Right: fishhook manoeuvre [NHT]

The derived non-linear equations of motion of a dynamic vehicle model which has only tyre cornering stiffness are of the Ordinary Differential Equation (ODE) form. Using more realistic tyres in a dynamic vehicle model, such as the MF-tyres, the tyre parameters are dependent on each other due to the weight transfer in longitudinal and lateral direction. The corresponding non-linear equations of motion are of the Differential Algebraic Equation (DAE) form. DAE's of real-life mechanics have index 3[1] which result that the corresponding stability analysis cannot be performed using standard analysis tools. Authors who analyse vehicle characteristics of complex dynamic vehicle models make the use of multi-body simulation tools, such as SIMPACK, ADAMS and MATLAB SimMechanics.

To analyse the stability of a dynamic vehicle model with the use of the eigenvalue problem the non-linear equations of motion have to be linearized and written into the state space formulation. An eigenvalue analysis is valid when the linearized equations of motion are time-independent. Different approaches are shown in literature to linearize the non-linear

[1]Index is defined as the number of times the constraints must be differentiated to reach a standard form ODE (index 0) system. Most numerical solvers require ODE and it is a non-trivial task to convert DAE systems into ODE systems

equations of motion of the dynamic vehicle model. Pacejka [Pac02] and Zegwaard [Zeg88] applied modifications which results direct in linear equations of motion of the ODE form. Odenthal [Ode02] uses linear tyres and linearize the derived equations of motion by taking a constant forward velocity. Stability of a dynamic vehicle model is shown by using the eigenvalue problem by Pacejka [Pac02], Zegwaard [Zeg88], Besselink [BV03] and [BC04] and Odenthal [Ode02]. Other authors derived non-linear equations of motion and proof stability of the dynamic vehicle model by using the Lyapunov approach, such as [PL99], [AO03], [SS04b] and [SS04a].

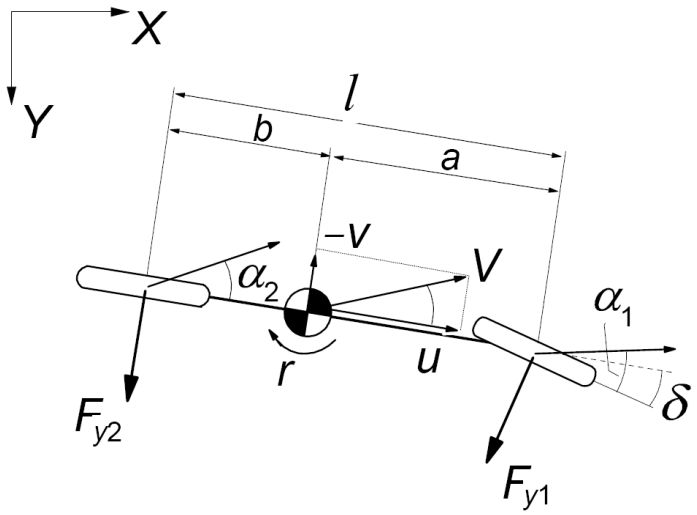


Figure 2.7: Bicycle model [BV03]

### 2.2.2 Vehicle stability controllers

In literature various approaches can be found to prevent vehicle instability phenomena. Examples are steering angle control (also called active steering) with or without braking control ([Ode02], [AO88], [AB98] and [TH02]) or braking control with or without engine control ([Zan03], [HS97] and [HB00]). The control intervention (inputs) can be done by selective braking, engine torque and steering angle input. The system sensors (outputs) are based on lateral acceleration, yaw-rate, roll-rate, steering wheel angle and individual wheel slip information. The studied literature shows different control theories like adaptive learning control [SS04b] and [SS04a], Sliding Mode Control (SMC) [PL99] and [AO03] and linear feedback control [Ode02], [AO88] and [AB98].

### 2.2.3 Connection between dynamic vehicle model and controller

Most authors connect the dynamic vehicle model (plant) and the vehicle stability controller in a closed-loop system, as shown in figure 2.8. With the closed-loop system the designed controller can be tested on the prevention of vehicle instability phenomena. Numerical simulations have been carried out using the mathematical tool MATLAB/Simulink or with the us of a multi-body simulation tool.

Other authors use the dynamic vehicle model only as a reference to predict specified vehicle behaviour, such as the maximum allowable lateral acceleration when a vehicle will roll over.

Some authors carried out real vehicle tests and compared the measurement results with the numerical simulation results. In these experiments the stability controller, sensors and actuators are build in a vehicle. In the stability controller the dynamic vehicle model is embedded in an ECU to use it as a reference model, as shown in [HS97] and [LA97].

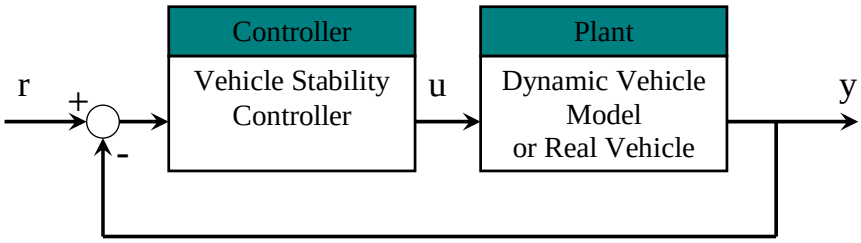


Figure 2.8: Closed-loop system of a dynamic vehicle model and a vehicle stability controller

## 2.3 Conclusions of the literature survey

Important vehicle instability phenomena are the yaw-rate instability, the jack-knife phenomenon and the rollover instability. Based on a dynamic vehicle model the dynamic behaviour, i.e. vehicle handling, can be studied. With a one-track vehicle model it is possible to study the yaw-rate instability based on the side slip angles which can produce a difference in the corresponding lateral tyre forces resulting in under/oversteer of the vehicle. To study the rollover of a vehicle the mass in the dynamic vehicle model can be divided into an unsprung chassis mass and an elevated sprung mass. Using a Static Rollover Criterium, as shown in appendix A, the tripped rollover can be indicated. For indication of the untripped rollover phenomenon a lane-change manoeuvre can be carried out.

Another way to analyse the vehicle stability is by performing an eigenvalue analysis. Unfortunately, in the studied literature an eigenvalue analysis has not been found of a vehicle around a lane-change trajectory. Rajamani [Raj06] shows how to utilize a dynamic vehicle model in which the state variables are in terms of position and orientation errors with respect to a trajectory which can be used to analyse the stability around this trajectory. For this approach the non-linear equations of motion have to be linearized with respect to a trajectory. In the studied literature most authors get rid of the linearization process by applying modifications which results direct in linear equations of motion.

For the stability controller design, most common sensors are the yaw-rate sensor and lateral acceleration sensor. Common control intervention is by braking and/or by reducing of the engine torque. Braking intervention can be done by selective braking of the individual wheels of the tractor or simultaneous braking on wheels of the trailer.

# Chapter 3

# The Dynamic Behaviour and Stability Control of a vehicle

## 3.1 Introduction

This chapter describes a methodology to investigate the dynamic behaviour and controller design of a dynamic vehicle model.

A dynamic vehicle model can be described using non-linear equations of motion, which can be derived using the Lagrange formulation. To analyse the stability of the dynamic vehicle model a simulation study or a stability analysis, based on the linearized equations of motion, can be carried out. In this research an analytic approach is chosen by which the non-linear equations of motion will be linearized around a specified trajectory. For this approach the *tracking error dynamics* will be introduced and the corresponding linearized equations will be written in the state space form.

To achieve a desired dynamic behaviour and velocity tracking of the dynamic vehicle model around a specified trajectory, a controller will be designed. Different combinations of sensors and actuators will be placed on the dynamic vehicle model to compute the observability and controllability of the system (the linearized tracking error dynamics).

## 3.2 Dynamic vehicle model

In this section a dynamic vehicle model will be made of the bicycle model. The bicycle model is a two-dimensional one-track dynamic model which exists of a single mass and two wheels, as shown in figure 3.1. The tyre model has only lateral cornering stiffness. With the absence of an elevated roll mass and a trailer, this dynamic vehicle model cannot be used to study the rollover and the jack-knife phenomena. However, with the exception of the wheel-slip, the yaw-rate instability can be analyzed with the lateral tyre forces. Table 3.1 and table 3.2 show respectively the corresponding parameters and characteristics of the bicycle model.

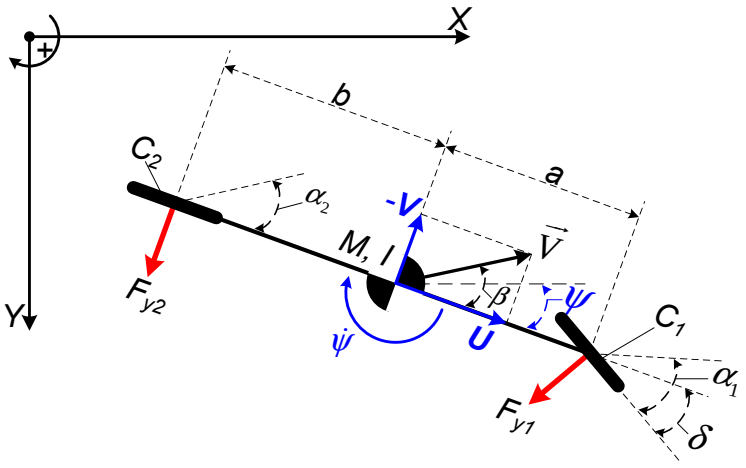


Figure 3.1: Dynamic representation of the bicycle model

| Symbol | Description | Value | Unit |
|---|---|---|---|
| $M$ | mass | 1600 | $[kg]$ |
| $I$ | mass inertia | 3600 | $[kgm^2]$ |
| $a$ | distance c.o.g. to front axis | 1.4 | $[m]$ |
| $b$ | distance c.o.g. to rear axis | 1.6 | $[m]$ |
| $C_1$ | lateral tyre cornering stiffness front wheel | $6 \cdot 10^4$ | $[N/m]$ |
| $C_2$ | lateral tyre cornering stiffness rear wheel | $6 \cdot 10^4$ | $[N/m]$ |

Table 3.1: The bicycle parameters

| Symbol | Description | Unit |
|---|---|---|
| $U$ | forward velocity | $[m/s]$ |
| $V$ | lateral velocity | $[m/s]$ |
| $\psi$ | yaw-angle | $[rad]$ |
| $\dot{\psi}$ | yaw-rate | $[rad/s]$ |
| $\beta$ | vehicle side slip angle | $[rad]$ |
| $\alpha_1$ | side slip angle front wheel | $[rad]$ |
| $\alpha_2$ | side slip angle rear wheel | $[rad]$ |
| $F_{y1}$ | lateral tyre force front wheel | $[N]$ |
| $F_{y2}$ | lateral tyre force rear wheel | $[N]$ |

Table 3.2: The bicycle characteristics

### 3.2.1 Non-linear equations of motion

To derive the non-linear equations of motion of complex dynamic systems, such as the bicycle model, the Lagrange formulation can be used, shown in [KdCv01], [Pac02] and in appendix B. The formulation is based on the kinetic energy ($T_{kin}$), potential energy ($U_{pot}$), dissipation energy ($D_{diss}$) and the generalized external applied forces $Q_{ex}$. For the Lagrange formulation the generalized coordinates $q_i$ have to be chosen.

For the standard Lagrange formulation, as shown in chapter 2 of [KdCv01] and in appendix B (B.1), the generalized coordinates $q_{SL}$ are based on spatial positions expressed in a fixed world

coordinate system with respect to the bicycle mass (the c.o.g.):

$$q_{SL} = \left[ \begin{array}{ccc} X, & Y, & \psi \end{array} \right]^T$$

$$\dot{q}_{SL} = \left[ \begin{array}{ccc} \dot{X}, & \dot{Y}, & \dot{\psi} \end{array} \right]^T$$

$$\ddot{q}_{SL} = \left[ \begin{array}{ccc} \ddot{X}, & \ddot{Y}, & \ddot{\psi} \end{array} \right]^T$$

For the modified Lagrange formulation, as shown in [Pac02] pages 18-19 and in appendix B (B.2), the generalized coordinates $q$ are based on the velocities expressed in moving coordinates of the bicycle mass:

$$q = \left[ \begin{array}{ccc} \int_0^t U \ dt, & \int_0^t V \ dt, & \psi \end{array} \right]^T$$

$$\dot{q} = \left[ \begin{array}{ccc} U, & V, & \dot{\psi} \end{array} \right]^T$$

$$\ddot{q} = \left[ \begin{array}{ccc} \dot{U}, & \dot{V}, & \ddot{\psi} \end{array} \right]^T$$

In further steps the modified Lagrange formulation is used.

### Energy formulation

The bicycle model contains no potential and no dissipation energy which results in only kinetic energy of the system, which can be expressed as:

$$T_{kin} = 1/2 \ M \ \left( U^2 + V^2 \right) + 1/2 \ I \ \dot{\psi}^2 \tag{3.1}$$

Substitution of the kinetic energy in the left-side of the modified Lagrange equation (B.2) results in:

$$\begin{aligned} M \ (\dot{U} - \dot{\psi} \ V) &= Q_U^{ex} \\ M \ (\dot{V} + \dot{\psi} \ U) &= Q_V^{ex} \\ I \ \ddot{\psi} &= Q_{\dot{\psi}}^{ex} \end{aligned} \tag{3.2}$$

### Generalized external forces

The generalized external forces $Q_{ex}$, as shown in (B.3), are introduced with the lateral tyre forces $F_{yi}$. In (B.3) the velocity vectors $r_i$ of the generalized external forces are expressed in

the moving generalized coordinates. First the velocities at the front ($U_1$, $V_1$) and rear ($U_2$, $V_2$) axles have to be determined and expressed in $U$ and $V$:

$$\begin{aligned} U_1 &= U \\ V_1 &= V + a\ \dot{\psi} \\ U_2 &= U \\ V_2 &= V - b\ \dot{\psi} \end{aligned} \tag{3.3}$$

The corresponding velocity vectors $r_i$ are:

$$\begin{aligned} r_1 &= \begin{bmatrix} U \\ V + a\ \dot{\psi} \end{bmatrix} \\ r_2 &= \begin{bmatrix} U \\ V - b\ \dot{\psi} \end{bmatrix} \end{aligned} \tag{3.4}$$

The corresponding generalized external forces $F_i$ in the $U/V$-direction are:

$$\begin{aligned} F_1 &= \begin{bmatrix} -F_{y1}\ \sin(\delta) \\ F_{y1}\ \cos(\delta) \end{bmatrix} \\ F_2 &= \begin{bmatrix} 0 \\ F_{y2} \end{bmatrix} \end{aligned} \tag{3.5}$$

Substitution in (B.3) gives:

$$Q^{ex} = \begin{bmatrix} -F_{y1}\ \sin(\delta) \\ F_{y1}\ \cos(\delta) + F_{y2} \\ a\ F_{y1}\ \cos(\delta) - b\ F_{y2} \end{bmatrix} \tag{3.6}$$

The lateral tyre forces are dependent on the side slip angles ($\alpha_i$), steering angle ($\delta$), tyre

cornering stiffness ($C_i$) and the corresponding velocities ($U_i/V_i$):

$$\begin{aligned} F_{y1} &= C_1 \ (\delta + \alpha_1) \\ F_{y2} &= C_2 \ (\alpha_2) \\ with \quad \alpha_1 &= \arctan\left(\tfrac{-V_1}{U_1}\right) \\ \alpha_2 &= \arctan\left(\tfrac{-V_2}{U_2}\right) \end{aligned} \tag{3.7}$$

**Ordinary differential equation**
Substitution of the generalized external forces (3.6) and the lateral tyre forces (3.7) into the modified Lagrange equations (3.2) results in non-linear equations of motion of the Ordinary Differential Equation (ODE) form. The non-linear equations of motion can be written as:

$$\ddot{q} = f(q, \dot{q}, u) \tag{3.8}$$

*with*

$$f(q,\dot{q},u) = \begin{bmatrix} -\frac{C_1}{M}\left[u + \arctan\left(\frac{-\dot{q}(2)-a\dot{q}(3)}{\dot{q}(1)}\right)\right]\sin(u) + \dot{q}(2)\dot{q}(3) \\ \frac{C_1}{M}\left[u + \arctan\left(\frac{-\dot{q}(2)-a\dot{q}(3)}{\dot{q}(1)}\right)\right]\cos(u) + \frac{C_2}{M}\arctan\left(\frac{-\dot{q}(2)+b\dot{q}(3)}{\dot{q}(1)}\right) - \dot{q}(1)\dot{q}(3) \\ \frac{aC_1}{I}\left[u + \arctan\left(\frac{-\dot{q}(2)-a\dot{q}(3)}{\dot{q}(1)}\right)\right]\cos(u) - \frac{bC_2}{I}\arctan\left(\frac{-\dot{q}(2)+b\dot{q}(3)}{\dot{q}(1)}\right) \end{bmatrix}$$

where $u$ is the input vector: $u = \delta$.

### 3.2.2 Validation of the derived non-linear equations of motion

To check the correctness of the derived non-linear equations of motion (3.8) a validation can be carried out by using a simulation model. Therefore the bicycle model has been created in the Simulink environment using the SimMechanics toolbox[1].
For simulation of the derived non-linear equations of motion the MATLAB *ode45* solver has been used. This solver integrates ODE's, such as (3.8), with specified initial conditions (IC's). The settings for the *ode45* solver and the Simulink/SimMechanics model are given in table 3.3. The simulation results are shown in figure 3.2, which shows a similarity of responses (vehicle characteristics) between the derived non-linear equations of motions and the SimMechanics model for the given steering input and IC's.

**Dynamic behaviour analysis**
By simulation of the non-linear equations of motion, i.e. the dynamic system, the dynamic

[1]MATLAB 7.1.0 (R14) SP3, Simulink 6.3 and SimMechanics 2.3

| **Input** | **Value** | **Unit** |
|---|---|---|
| $\delta$ | $5 \cdot \pi/180$ | $[rad]$ |
| **Initial condition IC at** $t = 0$ $[s]$ | **Value** | **Unit** |
| $U$ | 25 | $[m/s]$ |
| $V$ | 0 | $[m/s]$ |
| $\dot{\psi}$ | 0 | $[rad/s]$ |

Table 3.3: Settings for simulation of the non-linear equations of motion and the Simulink/SimMechanics model

behaviour can be analyzed. With the simulation results the stability of the dynamic system can be evaluated for the given inputs and IC's. The dynamic behaviour is local stable for the given inputs and IC's if the responses does not diverge in time, as shown in figure 3.2. Unfortunately to analyse the stability of the dynamic system various simulations, with different inputs and IC's, have to be carried out. As mentioned in the introduction of this chapter, another approach to evaluate the stability of a dynamic system can be done by considering the linearization of the non-linear equations of motion around a specified trajectory.

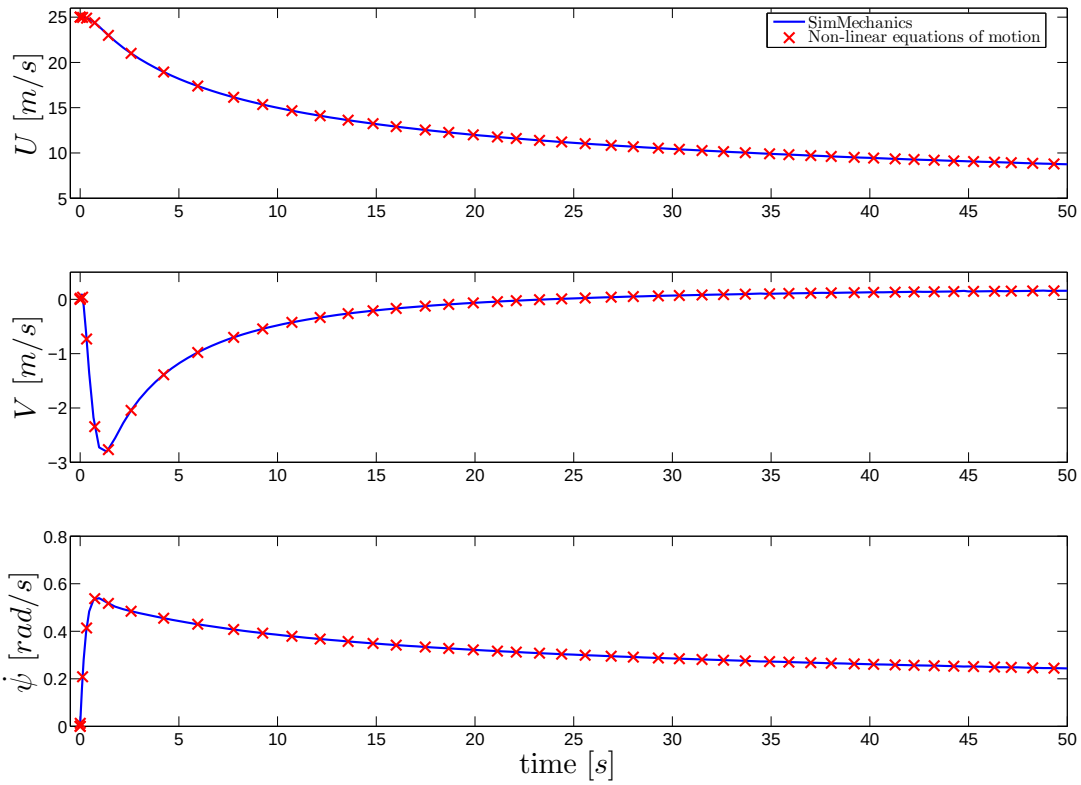


Figure 3.2: Simulation results of the derived non-linear equations of motion and the Simulink/SimMechanics model

## 3.3 Stability analysis of the bicycle model

### 3.3.1 Introduction

In practice, a common test to verify different vehicle instability phenomena, such as the yaw-rate instability and the rollover instability, is by driving a lane-change manoeuvre. The purpose of this research is to analyse the stability of the non-linear equations of motion around this trajectory.

As written in the previous section the stability of the non-linear equations of motion can be evaluated by considering the linearized equations of motion around a specified trajectory. When these linearized equations of motion are time-independent the stability can be evaluated with the corresponding eigenvalues. However, the lane-change manoeuvre is a complex manoeuvre and to make the linearization process easier the lane-change manoeuvre has been split up into two trajectories; a *straight-line trajectory* and a *circle trajectory*, as shown in figure 3.3.

To analyse the stability of the non-linear equations of motion around a specified trajectory the non-linear *tracking error dynamics* have to be defined. With the linearized tracking error dynamics it is possible to analyse the stability around the specified trajectory. A requirement for a valid stability analysis is that the specified trajectory is a solution of the non-linear equations of motion, also called the *nominal trajectory*.

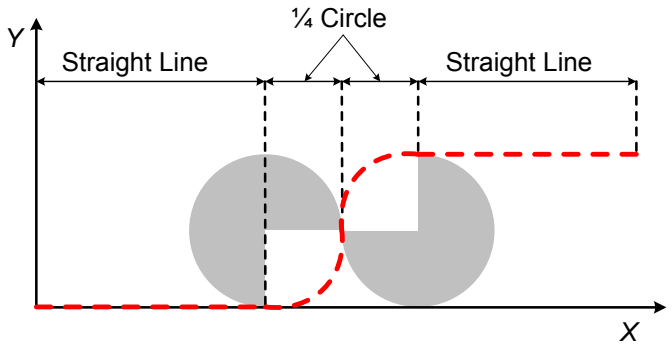


Figure 3.3: Vehicle position during a lane-change manoeuvre (−−). The lane-change manoeuvre has been split up in a straight-line trajectory and a circle trajectory

### 3.3.2 Tracking error dynamics (general formulation)

Derivation of the tracking error dynamics for trajectory linearization has been shown by [LZ04] and will be explained in this section.

A general non-linear dynamic system can be written as:

$$\begin{aligned} \dot{x} &= f(x, u, \theta) \\ y &= h(x, u, \theta) \end{aligned} \tag{3.9}$$

where $x$, $u$, $y$ and $\theta$ are the state, input, output and parameter vectors respectively.

The nominal trajectory dynamics can be written as:

$$\begin{aligned} \dot{x}_{traj} &= f\left(x_{traj}, u_{traj}, \theta\right) \\ y_{traj} &= h\left(x_{traj}, u_{traj}, \theta\right) \end{aligned} \tag{3.10}$$

where $x_{traj}$, $u_{traj}$ and $y_{traj}$ are the nominal state, nominal input and nominal output vectors respectively.

The state, input and output tracking errors can be defined by:

$$e = x - x_{traj},\ v = u - u_{traj} \quad and \quad w = y - y_{traj} \tag{3.11}$$

The non-linear tracking error dynamics can be derived with (3.9), (3.10) and (3.11) and can be written as:

$$\begin{aligned} \dot{e} &= F\left(e, v, \theta, x_{traj}, u_{traj}\right) \\ w &= H\left(e, v, \theta, x_{traj}, u_{traj}\right) \end{aligned} \tag{3.12}$$

Linearization of the non-linear tracking error dynamics (3.12) around $e = 0$ results in the linearized tracking error dynamics around the nominal trajectory $x_{traj}$. If the linearized tracking error dynamics are time-invariant these equations can be expressed in the state space formulation as:

$$\begin{aligned} &\dot{e} = \mathbf{A}\ e + \mathbf{B}\ v \\ &w = \mathbf{C}\ e + \mathbf{D}\ v \\ &with \\ &\mathbf{A} = \left.\frac{\partial F}{\partial e}\right|_{(e=0,\ v=0,\ \theta,\ x_{traj},\ u_{traj})},\ \mathbf{B} = \left.\frac{\partial F}{\partial v}\right|_{(e=0,\ v=0,\ \theta,\ x_{traj},\ u_{traj})} \\ &\mathbf{C} = \left.\frac{\partial H}{\partial e}\right|_{(e=0,\ v=0,\ \theta,\ x_{traj},\ u_{traj})},\ \mathbf{D} = \left.\frac{\partial H}{\partial v}\right|_{(e=0,\ v=0,\ \theta,\ x_{traj},\ u_{traj})} \end{aligned} \tag{3.13}$$

Where **A**, **B**, **C** and **D** are the system, input, output and feedthrough matrices respectively.

### 3.3.3 Nominal trajectory (general formulation)

A stability analysis, by considering the linearized equations of motion around a specified trajectory (also called *system*), is valid if the displacements of the system around this trajectory are small. A sensible choice for such a trajectory is that the trajectory is a solution of the non-linear equations of motion, i.e. the nominal trajectory $x_{traj}$. To find a nominal trajectory, the nominal state dynamics (3.10) have to be solved:

$$\dot{x}_{traj} = f\left(x_{traj}, u_{traj}, \theta\right) \tag{3.14}$$

There are various ways for solving (3.14). One of the possibilities is to set the left-side of the state dynamics to constant values. With a set of known variables of $x_{traj}$ and $u_{traj}$ the corresponding set of unknown variables can be derived. Still, this option for deriving a nominal trajectory can be difficult because of the complex state dynamics. With the use of a numerical approach, such as the MATLAB function *fsolve.m*, the unknown set of variables can be derived. This will be explained in a later stage and an example is given in appendix C.

### 3.3.4 Tracking error dynamics of the bicycle model

The non-linear equations of motion of the bicycle model (3.8) have been derived in a previous section. No sensors have been placed on the bicycle model, which results in a zero output vector $y = 0$. The non-linear equations of motion can be expressed in the general state dynamics of (3.9):

$$\begin{bmatrix} \dot{q} \\ \\ \ddot{q} \end{bmatrix} = \begin{bmatrix} \dot{q} \\ \\ f\left(q, \dot{q}, u, \theta\right) \end{bmatrix} \tag{3.15}$$

The state vector corresponds with $x = [q,\ \dot{q}]^T$.

The nominal state dynamics for the bicycle model can be written with the nominal state vector $x_{traj} = [q_{traj},\ \dot{q}_{traj}]^T$.

Second, the state tracking error vector $E$ can be defined as:

$$\begin{aligned} &E = x - x_{traj} \Leftrightarrow \begin{bmatrix} e \\ \\ \dot{e} \end{bmatrix} = \begin{bmatrix} q - q_{traj} \\ \\ \dot{q} - \dot{q}_{traj} \end{bmatrix} \\ &with \\ &e = \begin{bmatrix} e_1 \\ \\ e_2 \\ \\ e_3 \end{bmatrix} = \begin{bmatrix} \int_0^t U dt - \int_0^t U_{traj} dt \\ \\ \int_0^t V dt - \int_0^t V_{traj} dt \\ \\ \psi - \psi_{traj} \end{bmatrix} \end{aligned} \tag{3.16}$$

Where $e_1$ is the longitudinal displacement error, $e_2$ the lateral displacement error and $e_3$ the yaw angle error around the nominal trajectory.

Using (3.15) and (3.16) the non-linear state tracking error dynamics for the bicycle model can be written as:

$$\begin{bmatrix} \dot{e} \\ \\ \ddot{e} \end{bmatrix} = \begin{bmatrix} \dot{e} \\ \\ F\left(e, \dot{e}, v, \theta, x_{traj}, u_{traj}\right) \end{bmatrix} \tag{3.17}$$

*with*

$$F\left(e,\dot{e},v,\theta,x_{traj},u_{traj}\right)=\begin{bmatrix} -\frac{C_1}{M}\left[u_{traj}+\arctan\left(\frac{-(\dot{e}_2+V_{traj})-a\left(\dot{e}_3+\dot{\psi}_{traj}\right)}{\dot{e}_1+U_{traj}}\right)\right]\sin\left(u_{traj}\right)+\cdots \\ \left(\dot{e}_2+V_{traj}\right)\left(\dot{e}_3+\dot{\psi}_{traj}\right) \\ \\ \frac{C_1}{M}\left[u_{traj}+\arctan\left(\frac{-(\dot{e}_2+V_{traj})-a\left(\dot{e}_3+\dot{\psi}_{traj}\right)}{\dot{e}_1+U_{traj}}\right)\right]\cos\left(u_{traj}\right)+\cdots \\ \frac{C_2}{M}\arctan\left(\frac{-(\dot{e}_2+V_{traj})+b\left(\dot{e}_3+\dot{\psi}_{traj}\right)}{\dot{e}_1+U_{traj}}\right)-\cdots \\ \left(\dot{e}_1+U_{traj}\right)\left(\dot{e}_3+\dot{\psi}_{traj}\right) \\ \\ \frac{aC_1}{I}\left[u_{traj}+\arctan\left(\frac{-(\dot{e}_2+V_{traj})-a\left(\dot{e}_3+\dot{\psi}_{traj}\right)}{\dot{e}_1+U_{traj}}\right)\right]\cos\left(u_{traj}\right)-\cdots \\ \frac{bC_2}{I}\arctan\left(\frac{-(\dot{e}_2+V_{traj})+b\left(\dot{e}_3+\dot{\psi}_{traj}\right)}{\dot{e}_1+U_{traj}}\right) \end{bmatrix}$$

*where* $u_{traj}=\delta$

**Straight-line trajectory**

The derived non-linear tracking error dynamics of the bicycle model (3.17) can be used for the straight-line trajectory (indicated by $_{\mathbf{SL}}$).

**Circle trajectory**

In a later stage, the nominal circle trajectory has been derived based on constant velocities of the bicycle model during the trajectory. For the bicycle model it means that the derivative of the generalized coordinates for a nominal trajectory,
$\underline{\dot{q}}_{traj}=\begin{bmatrix} U_{traj}, & V_{traj}, & \dot{\psi}_{traj} \end{bmatrix}^T$, have to be constant in time.
In practice, when driving the circle trajectory, the steering angle will rotate the front wheel and the corresponding lateral tyre force. This results in a negative longitudinal force on the front axle and will decrease the forward velocity in time. By adding a longitudinal force, $F_{cruise}$, at the rear axle of the bicycle model it is possible to remain a constant forward velocity while driving a circle trajectory. The corresponding non-linear tracking error dynamics for the circle trajectory (indicated by $_{\mathbf{Circle}}$) can be written as:

$$\begin{bmatrix} \dot{e}_{Circle} \\ \\ \ddot{e}_{Circle} \end{bmatrix}=\begin{bmatrix} \frac{de_{Circle}}{dt} \\ \\ F_{Circle}\left(e_{Circle},\dot{e}_{Circle},v_{Circle},\theta,x_{Circle},u_{Circle}\right) \end{bmatrix} \tag{3.18}$$

*with* $\quad u_{Circle}=\begin{bmatrix} \delta, & F_{cruise} \end{bmatrix}^T$

### 3.3.5 Nominal straight-line trajectory

To find the nominal straight-line trajectory the nominal state dynamics (3.14) have to be solved. First assumptions have to be made for deriving the nominal straight-line trajectory,

$x_{SL} = \left[ \; q_{traj}, \quad \dot{q}_{traj} \; \right]^T$:

- The derivatives of the generalized coordinates are chosen to be constant in time: $\ddot{q}_{traj} = \left[ \; \dot{U}_{traj}, \quad \dot{V}_{traj}, \quad \ddot{\psi}_{traj} \; \right]^T = \left[ \; 0, \quad 0, \quad 0 \; \right]^T$
- For a straight-line trajectory the forward velocity is constant, for example $U = 15 \; [m/s]$, and the lateral velocity and yaw-rate are zero, which gives: $\dot{q}_{traj} = \left[ \; U_{traj}, \quad V_{traj}, \quad \dot{\psi}_{traj} \; \right]^T = \left[ \; 15, \quad 0, \quad 0 \; \right]^T$ and

  $q_{traj} = \left[ \; \int_0^t U_{traj} dt \quad \int_0^t V_{traj} dt \quad \psi_{traj} \; \right]^T = \left[ \; 15t \quad 0 \quad 0 \; \right]^T$
- The steering angle is zero: $u_{traj} = \delta = 0$

Substitution of these assumptions into (3.15) results in:

$$\begin{bmatrix} \frac{dq_{traj}}{dt} \\ f\left( q_{traj}, \dot{q}_{traj} = \left[ \; 15 \quad 0 \quad 0 \; \right]^T, u_{traj} = 0, \theta \right) = 0 \end{bmatrix} = \begin{bmatrix} 15 \\ 0 \\ 0 \\ 0 \\ 0 \\ 0 \end{bmatrix} \tag{3.19}$$

Solving (3.19) gives the nominal straight-line trajectory $x_{SL}$:

$$\begin{aligned} &\underline{x}_{SL} = \left[ \; \underline{q}_{traj} \quad \underline{\dot{q}}_{traj} \; \right]^T = \left[ \; 15t \quad 0 \quad 0 \quad 15 \quad 0 \quad 0 \; \right]^T \\ &and \quad \underline{u}_{SL} = 0 \end{aligned} \tag{3.20}$$

### 3.3.6 Stability analysis around the nominal straight-line trajectory

First, the non-linear tracking error dynamics for the nominal straight-line trajectory will be linearized around $\left[ \; e_{SL} \quad \dot{e}_{SL} \; \right]^T = \left[ \; 0 \quad 0 \; \right]^T$. After substitution of the bicycle parameters, as shown in table 3.1, the resulting linearized tracking error dynamics for the straight-line trajectory can be written as:

$$\begin{bmatrix} \dot{e}_{SL} \\ \ddot{e}_{SL} \end{bmatrix} = \mathbf{A}_{SL} \begin{bmatrix} e_{SL} \\ \dot{e}_{SL} \end{bmatrix} \tag{3.21}$$

with the system matrix $\mathbf{A}_{SL} = \begin{bmatrix} 0 & 0 & 0 & 1 & 0 & 0 \\ 0 & 0 & 0 & 0 & 1 & 0 \\ 0 & 0 & 0 & 0 & 0 & 1 \\ 0 & 0 & 0 & 0 & 0 & 0 \\ 0 & 0 & 0 & 0 & -5.0000 & -14.5000 \\ 0 & 0 & 0 & 0 & 0.2222 & -5.0222 \end{bmatrix}$

The linearized tracking error dynamics are time-independent. The stability of the time-invariant autonomous dynamics can be analyzed based on the system matrix $\mathbf{A}_{SL}$ with the use of the corresponding eigenvalues as shown in table 3.4.

| **Number** | **Eigenvalue** $[-]$ | **Damping ratio** $[-]$ | **Frequency** $[Hz]$ |
|---|---|---|---|
| 1, 2, 3 and 4 | 0 | - | - |
| 5 | -5.0111 + 1.7950i | 0.9414 | 0.8472 |
| 6 | -5.0111 - 1.7950i | 0.9414 | 0.8472 |

Table 3.4: Eigenvalues, damping and frequency of the autonomous tracking error dynamics for the straight-line trajectory

Table 3.4 shows that four eigenvalues are zero. Three of these eigenvalues can be explained by the fact that the system matrix $\mathbf{A}_{SL}$ has three zero columns, which is the result that the non-linear tracking error dynamics for the nominal straight-line trajectory is independent of the tracking error state $e$. The $4^{th}$ zero eigenvalue corresponds with the fact that the non-linear tracking error dynamics is independent of the forward velocity error $\dot{e}_1$ around the nominal straight-line trajectory. The fifth and sixth complex eigenvalues have a negative real value which corresponds with stable eigenvalues.

A graphical representation of the stability of the non-linear equations of motion for the nominal straight-line trajectory can be made by using a simulation, as explained in section 3.2.2. The non-linear equations of motion have been simulated with the nominal straight-line trajectory as input and the initial conditions at time $t = 0$ $[s]$. A perturbation has been applied on the initial conditions of $\dot{e}_{SL}$ to show the stability of $\begin{bmatrix} e_{SL}, & \dot{e}_{SL} \end{bmatrix}^T$ around the nominal straight-line trajectory. Figure 3.4 shows that by the perturbation of the initial conditions the lateral velocity and yaw-rate converges to the nominal straight-line trajectory as expected from the eigenvalue analysis.

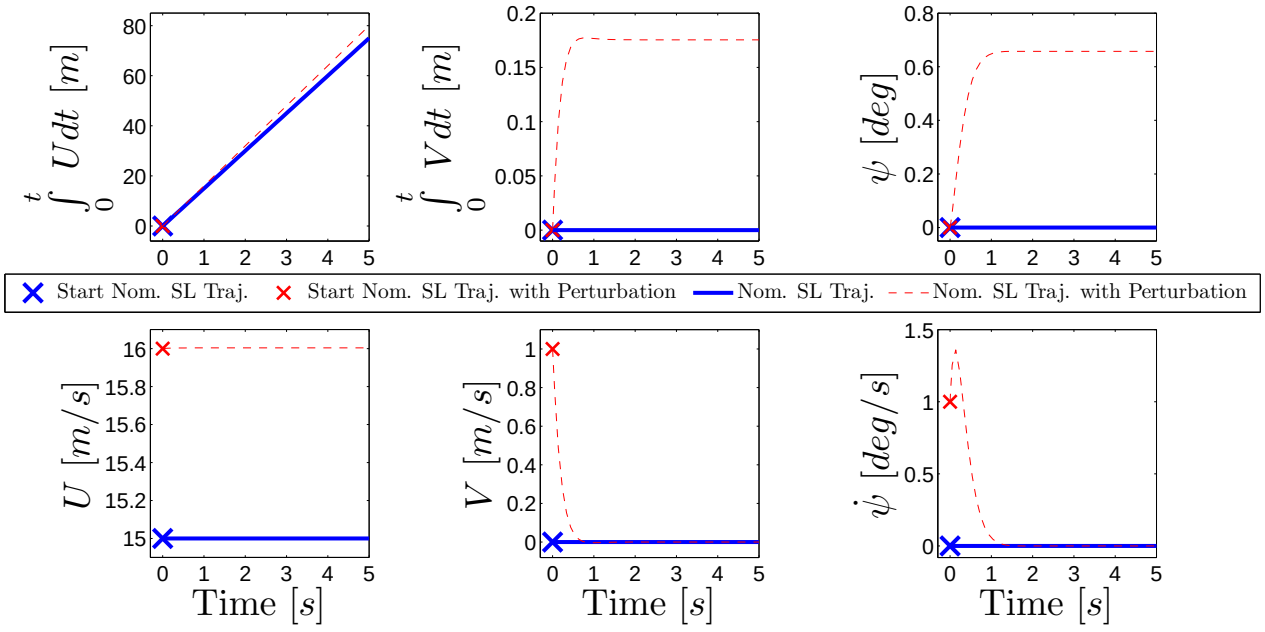


Figure 3.4: Stability of nominal (Nom.) straight-line (SL) trajectory

To obtain a global picture of the straight-line trajectory the simulation results have been written into the spatial velocities expressed in a fixed world coordinate system with respect to the bicycle mass (c.o.g.):

$$\begin{aligned} \dot{x} &= U\cos(\psi) - V\sin(\psi) \\ \dot{y} &= U\sin(\psi) + V\cos(\psi) \\ x &= \int_0^t \dot{x}\ dt \\ y &= \int_0^t \dot{y}\ dt \end{aligned} \tag{3.22}$$

By the fact that only the lateral velocity $V$ and the yaw-rate $\dot{\psi}$ converge to the nominal trajectory, the responses expressed in a fixed world coordinate system does not converge to the nominal trajectory, as shown in figure 3.5.

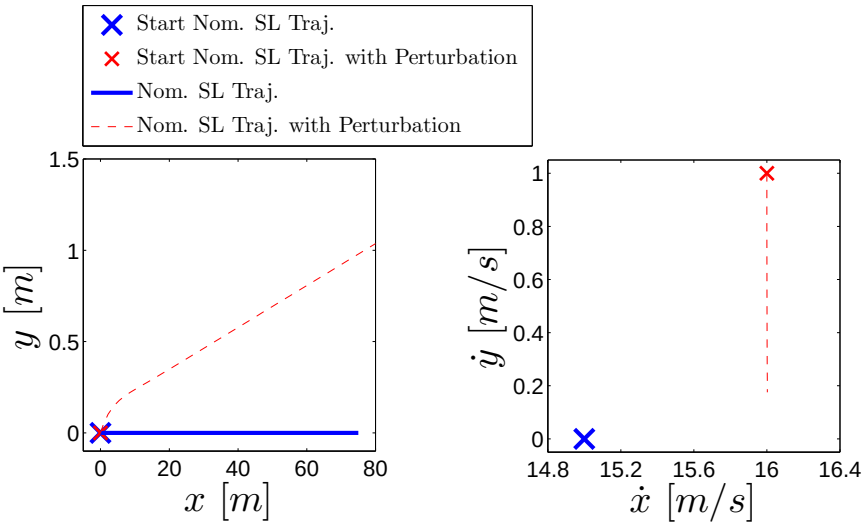


Figure 3.5: Global picture of the stability around a nominal (Nom.) straight-line (SL) trajectory

### 3.3.7 Nominal circle trajectory

To find the nominal circle trajectory the nominal state dynamics (3.14) have to be solved. Therefore the following assumptions are made to derive the nominal circle trajectory, $x_{Circle} = \left[\ q_{traj},\ \ \dot{q}_{traj}\ \right]^T$:

- The derivatives of the generalized coordinates are chosen to be constant in time, i.e. $\ddot{q}_{traj} = \left[\ \dot{U}_{traj},\ \ \dot{V}_{traj},\ \ \ddot{\psi}_{traj}\ \right]^T = \left[\ 0,\ \ 0,\ \ 0\ \right]^T$

- The forward velocity is equal to nominal straight-line trajectory, i.e. $U = 15\ [m/s]$. The lateral velocity is dependent on the forward velocity by the vehicle side slip angle $\beta$:

$$V_{traj} = -U_{traj} \tan(\beta)\ \ [m/s] \tag{3.23}$$

  a realistic side slip angle is 1 $[deg]$ [BV03], this results in $V_{traj} = -0.2618\ [m/s]$

- To maintain a nominal circle trajectory $\delta$ and $F_{cruise}$ have to be constant in time

These assumptions are divided in known and unknown characteristics as shown in table 3.5.

| **Known characteristic** | **Value** | **Unit** |
|---|---|---|
| $\beta$ | $1 \cdot \pi/180$ | $[rad]$ |
| $U_{traj}$ | 15 | $[m/s]$ |
| $V_{traj}$ | -0.2618 | $[m/s]$ |
| **Unknown characteristic** | **Value** | **Unit** |
| $\delta$ | constant | $[rad]$ |
| $F_{cruise}$ | constant | $[N]$ |
| $\dot{\psi}_{traj}$ | constant | $[rad/s]$ |

Table 3.5: Assumptions to derive the nominal circle trajectory

To solve the nominal state dynamics a numerical approach with the MATLAB function *fsolve.m* is used, as shown in appendix C.1. This results in the nominal circle trajectory of:

$$x_{circle} = \begin{bmatrix} q_{traj} \\ \\ \dot{q}_{traj} \end{bmatrix} = \begin{bmatrix} 15.0000\ t \\ -0.2618\ t \\ 0.2179\ t \\ 15.0000 \\ -0.2618 \\ 0.2179 \end{bmatrix} \tag{3.24}$$

with the nominal input vector: $u_{circle} = \begin{bmatrix} \delta, & F_{cruise} \end{bmatrix}^T = \begin{bmatrix} 2.832 \cdot \pi/180, & 229.2608 \end{bmatrix}^T$

The corresponding radius of the nominal circle trajectory is:

$$R_{traj} = \frac{\overrightarrow{V}_{traj}}{\dot{\psi}_{traj}} = \frac{\sqrt{U_{traj}^2 + V_{traj}^2}}{\dot{\psi}_{traj}} = 68.8470\ [m] \tag{3.25}$$

### 3.3.8 Stability analysis around the nominal circle trajectory

To analyze the stability around the nominal circle trajectory the non-linear tracking error dynamics for the nominal circle trajectory is linearized around $e_{Circle} = 0$ . The derived

time-invariant system matrix is:

$$\mathbf{A}_{Circle} = \begin{bmatrix} 0 & 0 & 0 & 1 & 0 & 0 \\ 0 & 0 & 0 & 0 & 1 & 0 \\ 0 & 0 & 0 & 0 & 0 & 1 \\ 0 & 0 & 0 & -0.0004 & 0.3414 & -0.0889 \\ 0 & 0 & 0 & -0.3123 & -4.9928 & -14.5023 \\ 0 & 0 & 0 & 0.0767 & 0.2212 & -5.0148 \end{bmatrix}$$

The corresponding eigenvalues are:

| **Number** | **Eigenvalue** $[-]$ | **Damping ratio** $[-]$ | **Frequency** $[Hz]$ |
|---|---|---|---|
| 1, 2 and 3 | 0 | - | - |
| 4 | -0.0340 | 1 | 0.0054 |
| 5 | -4.9870 + 1.7759i | 0.9421 | 0.8425 |
| 6 | -4.9870 - 1.7759i | 0.9421 | 0.8425 |

Table 3.6: Eigenvalues, damping and frequency of $\mathbf{A}_{Circle}$

Table 3.6 shows that three eigenvalues are zero, which are caused by the independency of the tracking error state $e$. The other three eigenvalues have a negative real part, which corresponds that the derivatives in the tracking error state $\dot{e}$ are stable. The fifth and sixth eigenvalues are nearly identical with the fifth and sixth eigenvalues of the straight-line trajectory (table 3.4).

A graphical representation of the stability of the non-linear equations of motion for the nominal circle trajectory is made using a simulation. For the global picture the simulation results have been written into the spatial velocities expressed in a fixed world coordinate system, as shown in figure 3.6. This figure shows that by a perturbation of the initial conditions the velocities converges to the nominal circle trajectory as expected from the eigenvalue analysis.

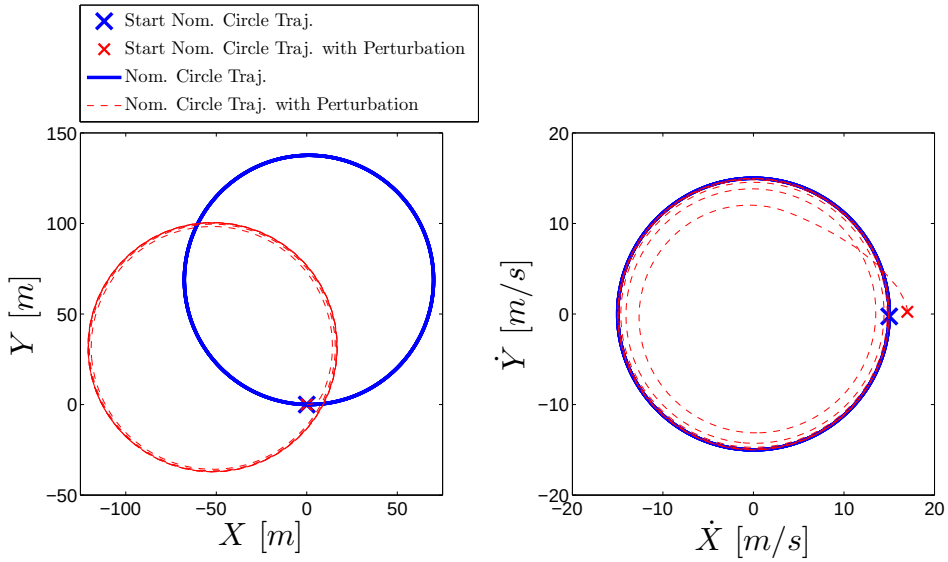


Figure 3.6: Stability of around the nominal (Nom.) circle trajectory

### 3.3.9 Vehicle handling study and stability analysis for various nominal circle trajectories

A vehicle handling study and stability analysis can be made of the bicycle model around various nominal circle trajectories. Different radii $R$ and forward velocities $U$ have been chosen to determine, with the use of *fsolve.m*, the unknown bicycle characteristics and inputs. The assumptions for determination of these nominal circle trajectories are:

- The derivatives of the generalized coordinates are constant in time
- The lateral velocity is dependent on the forward velocity by the vehicle side slip angle $\beta$:

$$V_{traj} = -U_{traj} \tan(\beta_{traj})$$

- The yaw-rate is dependent on the forward velocity, lateral velocity and radius, as shown in (3.25), which results in:

$$\dot{\psi}_{traj} = \frac{\sqrt{U_{traj}^2 + V_{traj}^2}}{R_{traj}}$$

The unknown vehicle characteristics and inputs have been determined, as shown in figure 3.7 and figure 3.8 respectively.

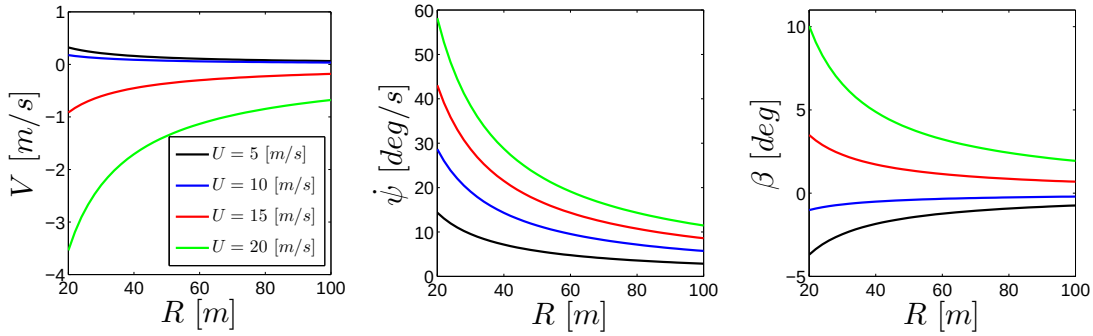


Figure 3.7: Vehicle characteristics for various nominal circle trajectories

The under/oversteer of the bicycle model can be determined by analyzing the yaw-rate instability using a vehicle handling diagram, ([BV03], sheet 3-19). In a vehicle handling diagram the difference between the side slip angles $\alpha_1$ and $\alpha_2$ of the forward and rear tyres respectively are determined and the relation of the "Ackerman steer" $\frac{L}{R} = \frac{(a+b)}{R} = \delta - \alpha_1 + \alpha_2$ is shown in figure 3.9. When a difference between both side slip angles occurs the corresponding difference in lateral tyre force can rotate the vehicle in an undesired direction, i.e. under/oversteer as shown in table 3.7. For the various nominal circle trajectories with $U = 15$ $[m/s]$ the vehicle handling diagram is shown in figure 3.9. Figures 3.9 and 3.10 show that the bicycle is understeered and by increasing the radius $R$ of the nominal circle trajectory or decreasing the forward velocity $U$ the bicycle model is going to neutral steer.

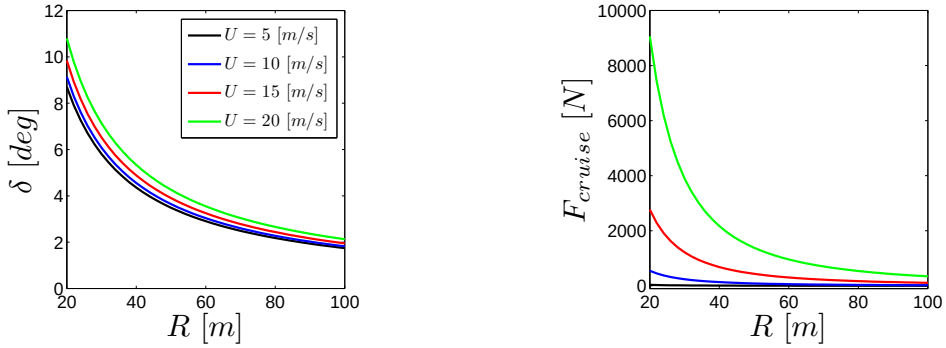


Figure 3.8: Inputs $\delta$ and $F_{cruise}$ for various nominal circle trajectories

| | |
|---|---|
| Neutral steer | $\alpha_1 = \alpha_2$ |
| Understeer | $\alpha_1 > \alpha_2$ |
| Oversteer | $\alpha_1 < \alpha_2$ |

Table 3.7: Neutral-, under- and oversteer of a one-track 2-axle dynamic vehicle model

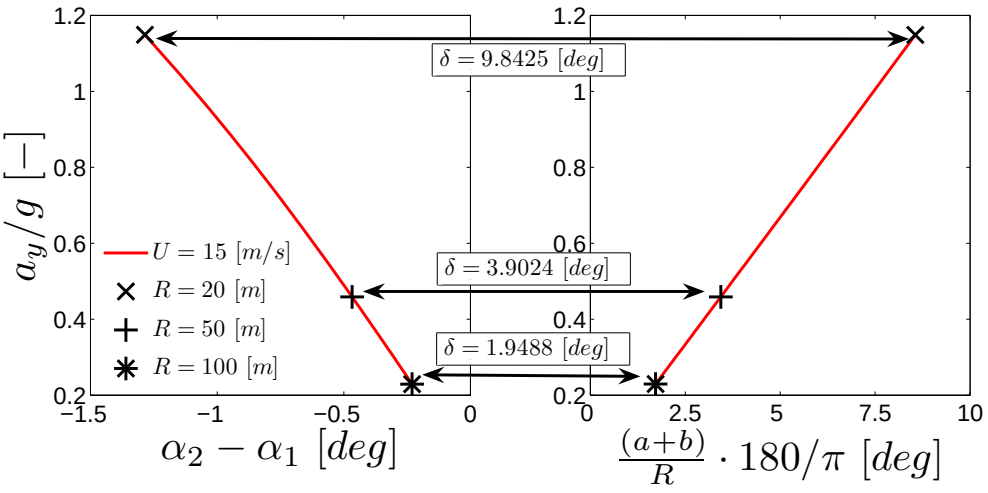


Figure 3.9: Vehicle handling diagram which shows the relation between the side slip angles difference and "Ackerman steer" for the nominal circle trajectories with $U = 15\ [m/s]$

Another important vehicle characteristic is the lateral acceleration of the c.o.g. of the bicycle model, which can be determined with:

$$a_{y,traj} = \dot{V}_{traj} + U_{traj}\dot{\psi}_{traj} \tag{3.26}$$

with $\dot{V}_{traj} = 0$ (one of the assumptions) for the nominal circle trajectories.

Figure 3.11 shows the lateral acceleration for the various nominal circle trajectories. From this figure it can be seen that the lateral acceleration increases by increasing the forward

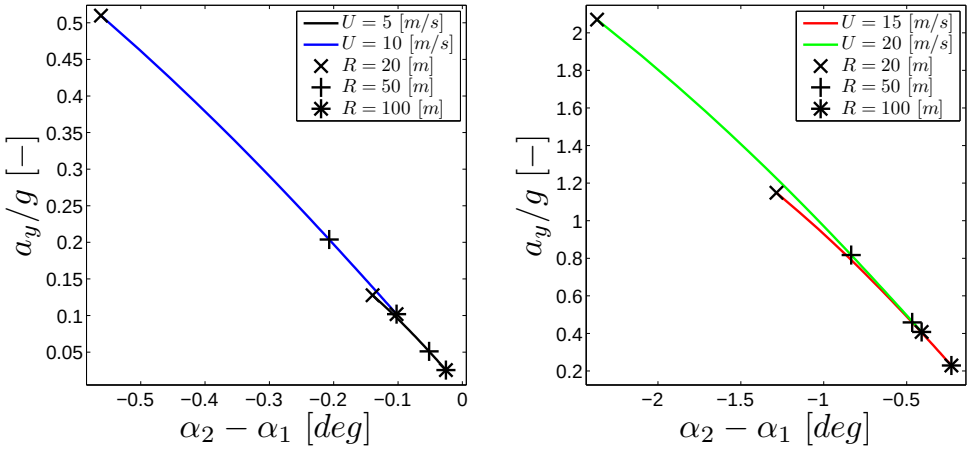


Figure 3.10: Vehicle handling diagram for various nominal circle trajectories

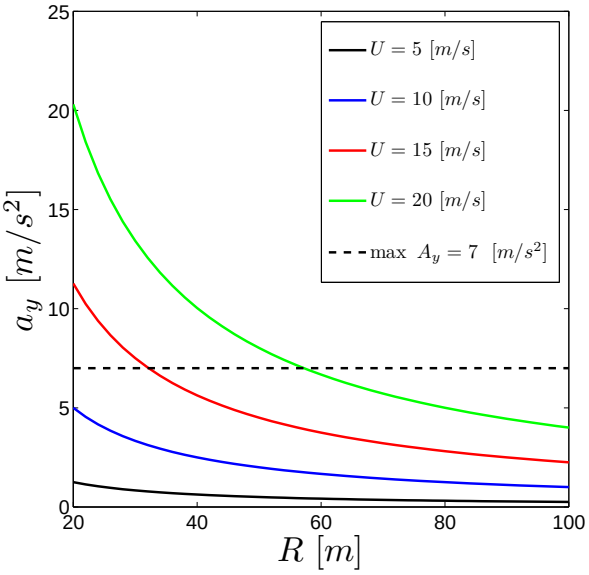


Figure 3.11: Lateral acceleration for various nominal circle trajectories

velocity $U$ or decreasing the radius $R$ of the nominal circle trajectory.

From passenger car tests an average lateral acceleration of 7 $[m/s^2]$ has been measured ([BV03], sheets 3-5 and 3-6) which the tested vehicle has become uncontrollable by the driver, such as skidding of the vehicle. Nevertheless, the bicycle model is a simplistic dynamic representation of a passenger car (absence of a suspension, a realistic tyre model and an elevated roll mass), this critical lateral acceleration is used as a reference for the maximum allowable lateral acceleration of the bicycle model. In figure 3.11 this critical lateral acceleration is shown and for the forward velocities $U = 15$ $[m/s]$ and $U = 20$ $[m/s]$ the corresponding radii have been determined as shown in table 3.8.

| Symbol | Value | Value | Unit |
|---|---|---|---|
| $U_{traj}$ | 15 | 20 | $[m/s]$ |
| $R_{traj}$ | 32.18 | 57.26 | $[m]$ |
| $a_{y,traj}$ | 6.996 | 6.998 | $[m/s^2]$ |

Table 3.8: Maximum lateral acceleration for different forward velocities

### Stability analysis

To perform a valid stability analysis of the bicycle model around different nominal circle trajectories, these trajectories have to determined at which the lateral acceleration is under 7 $[m/s^2]$ as discussed before. For all situations the linearized tracking error dynamics are time-invariant and the stability of the autonomous dynamics can be analyzed with the corresponding eigenvalues, as shown in figure 3.12. This figure shows that by increasing the forward velocity the eigenvalues are moving to the imaginary axis which results in a decrease of the stability margins of the bicycle model around the nominal circle trajectory.
Figure 3.13 shows the eigenvalues near the imaginary axis. As expected from section 3.3.8 this figure shows that for all situations three eigenvalues are at the origin. This corresponds with the independency of the generalized coordinates $\int_0^t U\ dt$, $\int_0^t V\ dt$ and $\psi$ of the bicycle non-linear equations of motion.
In contrast with a previous observation the eigenvalues corresponding to the nominal circle trajectories with a radius of $R = 100$ $[m]$ shows that by *decreasing* the forward velocity these eigenvalues are moving to the imaginary axis. This phenomenon can be explained by the fact that by decreasing the forward velocity of the nominal circle trajectories with a large radius the linearized tracking error dynamics corresponds near to the linearized tracking error dynamics around a nominal straight-line trajectory which is independent of the generalized coordinate $U$, as shown in section 3.3.6.

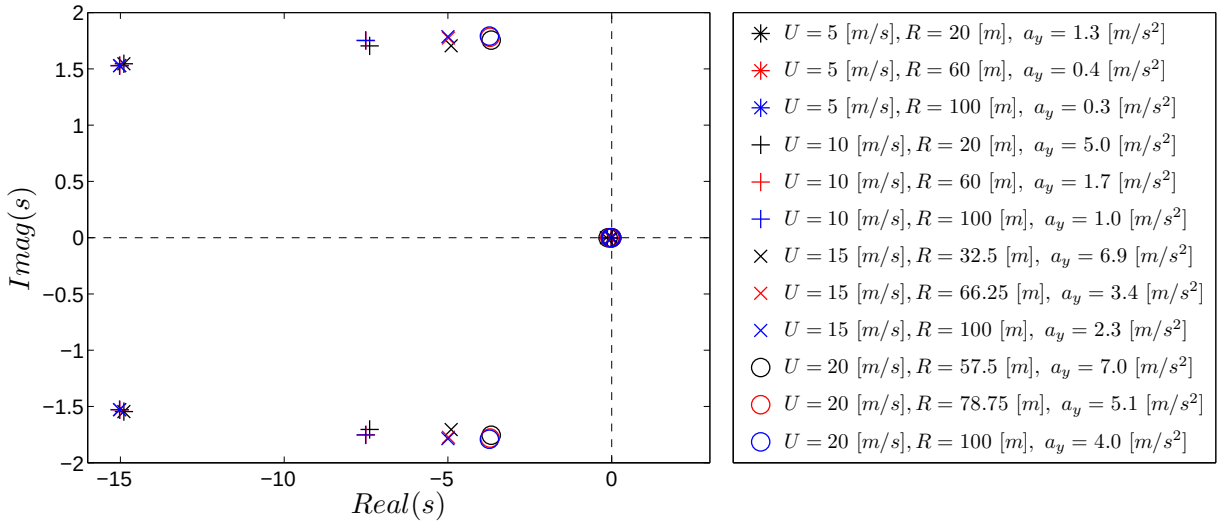


Figure 3.12: Eigenvalues for various nominal circle trajectories

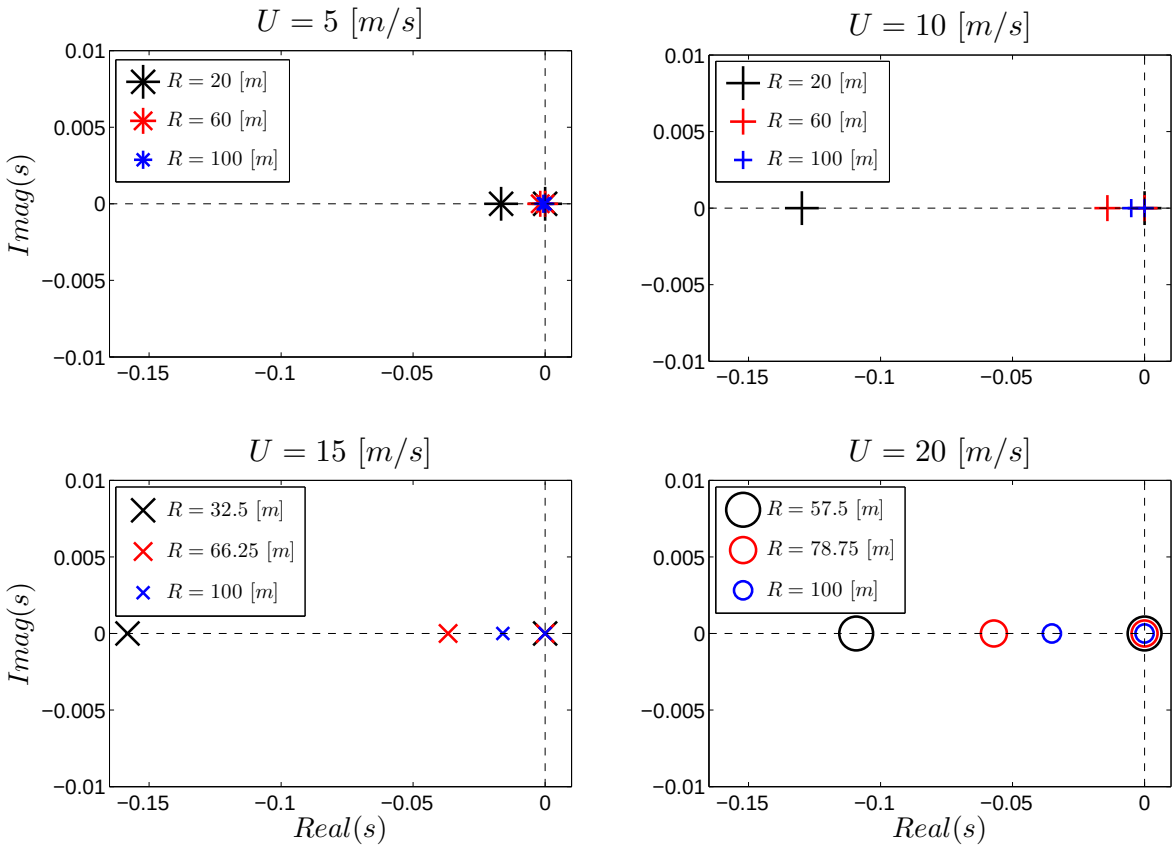


Figure 3.13: Eigenvalues for various nominal circle trajectories near the imaginary axis

### 3.3.10 Transition from circle trajectory to straight-line trajectory

The purpose of this research is to analyze the stability of a dynamic vehicle model around a lane-change trajectory. The lane-change trajectory has been divided into two trajectories to make the linearization process easier. However the stability around the transition between both trajectories is unknown.
To analyse the stability around this transition a function $F_{trans}\,(t_2 - t_1)$ has to be derived which makes the transition possible from the nominal straight-line trajectory to the nominal circle trajectory in a specified time-period, for example:

$$\begin{bmatrix} x_{SL}(t_1) \\ \\ u_{SL}(t_1) \end{bmatrix} \Rightarrow F_{trans}\,(t_2 - t_1) \Rightarrow \begin{bmatrix} x_{Circle}(t_2) \\ \\ u_{Circle}(t_2) \end{bmatrix} \tag{3.27}$$

The derivation of the transition function will be complex and a non-linear time-dependent function will be expected.

The derivation of the transition function will not be performed in this research because critical vehicle characteristics can already be achieved by driving a nominal circle trajectory. These critical vehicle characteristics will result in vehicle instability eventually.

## 3.4 Controller design (general formulation)

The controller design is based on the state-space method presented by [FEN94]. This controller design has the aim to achieve a desired dynamic behaviour of a system. The method of the controller design is to find a dynamic compensation $D_c(s)$ by working direct with the state space description of the general linearized dynamic system (3.28), as shown in figure 3.14. The state-space method can be used for **SISO** as well for **MIMO** systems.

$$\begin{aligned} \dot{x} &= \mathbf{A}x + \mathbf{B}u \\ y &= \mathbf{C}x + \mathbf{D}u \end{aligned} \tag{3.28}$$

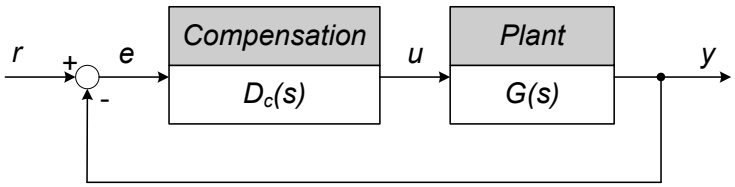


Figure 3.14: Controller design

To find the compensation $D_c(s)$ the next steps have to be carried out:

1. Develop a **Control law** for the closed-loop system by selecting desired pole locations
2. Designing a **State estimator**, because not all states can be measured
3. Combining the control law and the state estimator in a **closed-loop system**
4. Introduction of a **reference input**

In this research, a controller will be designed for the bicycle model around a nominal straight-line trajectory and a nominal circle trajectory. Therefore the state space representation of the linearized tracking error dynamics, as described in previous section, will be used.

### 3.4.1 Design of the control law

The purpose of the control law is to assign a set of desired (control) pole locations of the closed-loop system which corresponds with a satisfactory dynamic behaviour. An assumption of designing the control law is that all states are available for feedback, i.e. full state feedback as shown in figure 3.15. This results in a state feedback law where the input is linear dependent on the states of the system:

$$u = -\mathbf{K}\ x \tag{3.29}$$

where $\mathbf{K}$ is the state feedback gain matrix and $x$ is the state vector.

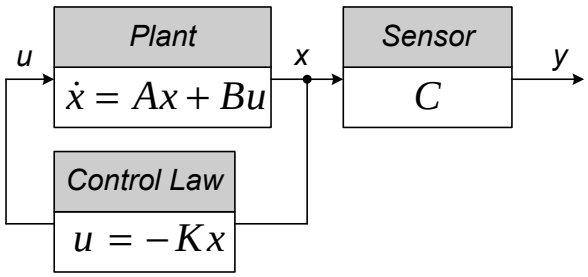


Figure 3.15: Control law

Substitution of the state feedback law (3.29) into the general linearized dynamic system (3.28) gives:

$$\dot{x} = (\mathbf{A} - \mathbf{B}\ \mathbf{K})\, x \tag{3.30}$$

The corresponding characteristic equation of this closed-loop system is:

$$\det\left[s\ \mathbf{I} - (\mathbf{A} - \mathbf{B}\ \mathbf{K})\right] = 0 \tag{3.31}$$

The control-law design is to find the state feedback gains $K_{11}, \cdots, K_{mn}$ so that the eigenvalues of (3.31) are at desirable locations $s_n$. This requirement results in the corresponding desired characteristic equation:

$$\alpha_c(s) = (s - s_1)\,(s - s_2) \cdots (s - s_n) = 0 \tag{3.32}$$

The state feedback gains $K_{11}, \cdots, K_{mn}$ can be found by solving the combination of (3.31) and (3.32). Numeric determination of the state feedback gains can be done with the use of the MATLAB function *place.m*[2], which can also be used for more complex cases, such as **MIMO** systems. The function assumes that all the inputs of the system are control inputs, i.e. full state feedback. More solutions are possible for the state feedback gain matrix that achieves the desired locations $s_n$.

### Controllability

Uncontrollable systems have certain modes that are unaffected by the control law feedback. This means that parts of the systems are physically disconnected from the input. A mathematical test to deduce information about the number of states of the system ($\mathbf{A}$, $\mathbf{B}$) which can be controlled by the inputs, i.e. controllability, is the rank of the controllability matrix, **CM**. The controllability matrix has been found as:

$$\mathbf{CM} = \left[\ \mathbf{B} \quad \mathbf{A}\ \mathbf{B} \quad \mathbf{A}^2\ \mathbf{B} \quad \cdots \quad \mathbf{A}^{n-1}\ \mathbf{B}\ \right] \tag{3.33}$$

The system ($\mathbf{A}$, $\mathbf{B}$) is controllable if the rank of **CM** is equal to the number of states. With this mathematical test it is possible to indicate the controllability of a system with the placed actuators (inputs) on the system.

[2]The MATLAB function *place.m* computes a solution that minimizes the sensitivity of the closed-loop poles with respect to perturbations in $\mathbf{A}$ or $\mathbf{B}$. More information about the function *place.m* can be found with [Matb]

### 3.4.2 Design of a state estimator

The control law assumed that all states are available for feedback. In most cases, not all the state variables are measured. With the use of a state estimator it is possible to reconstruct all the states of a system from a few measurements. The estimate of a state is denoted by $\hat{x}$. To study the dynamics of this estimate an error in the state estimates has been defined as:

$$\tilde{x} = x - \hat{x} \tag{3.34}$$

With the general state dynamics $\dot{x} = \mathbf{A}\, x + \mathbf{B}\, u$ and the state estimate dynamics $\dot{\hat{x}} = \mathbf{A}\, \hat{x} + \mathbf{B}\, u$ the dynamics of the error in state estimates can be derived:

$$\dot{x} - \dot{\hat{x}} = \mathbf{A}\ (x - \hat{x}) \ \Leftrightarrow\ \dot{\tilde{x}} = \mathbf{A}\ \tilde{x} \tag{3.35}$$

The error converges to zero if the system ($\mathbf{A}$) is stable. However, there is no ability to influence the rate at which the state estimate $\hat{x}$ converges to the true state $x$, therefore feedback has been introduced. By feedback of the output error the state estimate equation can be continuously corrected:

$$\dot{\hat{x}} = \mathbf{A}\ \hat{x} + \mathbf{B}\ u + \mathbf{L}\ (y - \mathbf{C}\ \hat{x}) \tag{3.36}$$

where $\mathbf{L}$ is the proportional gain defined as $\mathbf{L} = L_{11}, \cdots, L_{mn}$.

Subtracting the state estimate equation from the state equation gives the error in the state estimate equation:

$$\dot{\tilde{x}} = (\mathbf{A} - \mathbf{L}\ \mathbf{C})\ \tilde{x} \tag{3.37}$$

The characteristic equation of the dynamics of the error in the state estimate is:

$$\det\left[s\ \mathbf{I} - (\mathbf{A} - \mathbf{L}\ \mathbf{C})\right] = 0 \tag{3.38}$$

The dynamics of the error in the state estimate (3.38) can be chosen to be stable as well as much faster than the open-loop dynamics. As a rule of thumb, the state estimator error poles should be chosen to be faster than the controller poles by a factor of 2 to 6. This ensures a faster decay of the state estimator errors compared with the desired dynamics, which results that the controller poles will dominate the total response. However, increasing the speed of response of the state estimator, the bandwidth of the state estimator will increase. When sensor noise is a major concern the bandwidth has to be small, otherwise the sensor noise will be passing on to the control law. The choice of the locations of the state estimator error poles is a balance between a fast decay of the state estimator errors and a low-enough bandwidth that sensor noise does not significant impair actuator activity. The corresponding desired state estimator characteristic equation is:

$$\alpha_e(s) = (s - \beta_1)\,(s - \beta_2) \cdots (s - \beta_n) \tag{3.39}$$

The proportional gains $L_{11} \cdots L_{mn}$ can be found by solving the combination of (3.38), (3.39) and with the desired locations of the state estimator error poles, $\beta_n$. Numeric determination of the proportional gain $\mathbf{L}$ can be done, like the same approach as the determination of the state feedback gain $\mathbf{K}$, using the MATLAB function *place.m*.

**Observability**

Observability refers to the ability to deduce information about all the states of the system $(\mathbf{A}, \mathbf{C})$ by monitoring only the sensed outputs. The observability matrix has been found as:

$$\mathbf{OM} = \left[\mathbf{C},\ \mathbf{CA},\ \mathbf{CA}^2,\ \cdots,\ \mathbf{CA}^{n-1}\right]^T \tag{3.40}$$

The system $(\mathbf{A}, \mathbf{C})$ is observable if the rank of $\mathbf{OM}$ is equal to the number of the states. A requirement for designing the compensation $D_c(s)$ is full state estimation, the system is observable, because the control law has been designed for full state feedback.

### 3.4.3 Combining the control law and the state estimator in a closed-loop

The closed-loop within the control law, the state estimator and the plant is shown in figure 3.16. The transfer function of the compensator $D_c(s)$ is:

$$D_c(s) = \frac{U(s)}{Y(s)} = -\mathbf{K}\left(s\,\mathbf{I} - \mathbf{A} + \mathbf{B}\,\mathbf{K} + \mathbf{L}\,\mathbf{C}\right)^{-1}\mathbf{L} \tag{3.41}$$

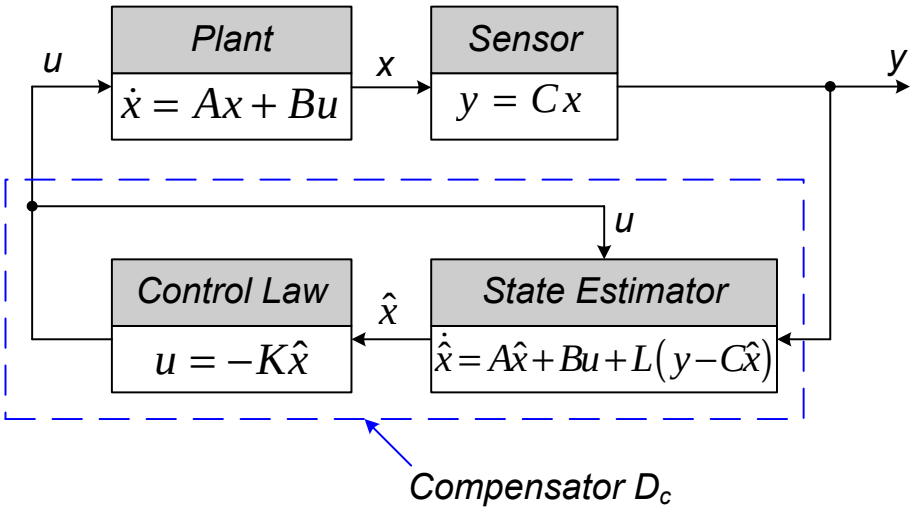


Figure 3.16: Combining the control law and the state estimator [FEN94]

### 3.4.4 Reference input in the closed-loop system

In general, a *good disturbance rejection* and *good command following* both need to be taken into account in designing a controller. The obtained controller, which exists of combining

the control law and the state estimator, has been chosen for good disturbance rejection. Good command following is done by properly introducing the reference input into the system equations. There are different possibilities for introducing the reference input $r$ into the closed-loop system, as shown in [FEN94]. The reference has been introduced as shown in figure 3.17:

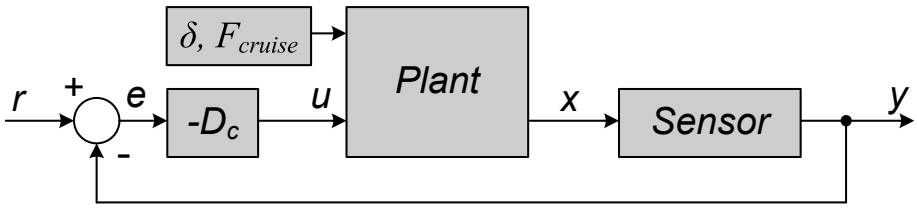


Figure 3.17: Reference input

## 3.5 Controller design for the straight-line trajectory

Sensors and actuators have been placed on the bicycle model for designing a controller. Figure 3.18 and table 3.9 show the available sensors and actuators which can be used.

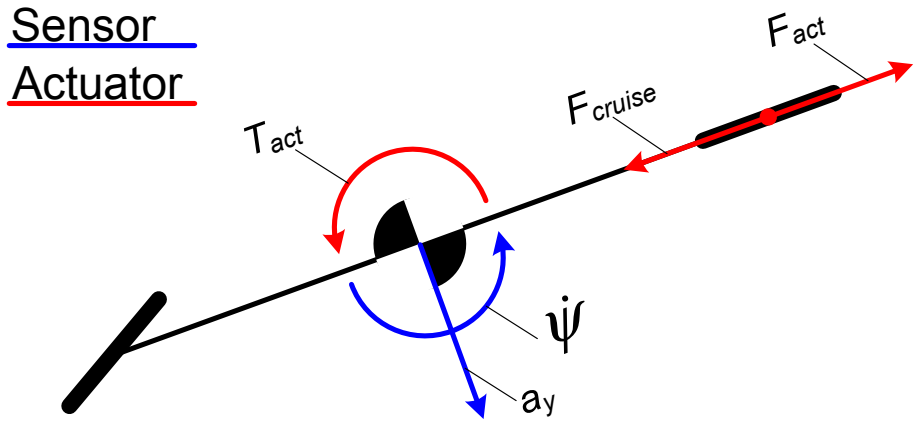


Figure 3.18: Sensors and actuators placed on the bicycle model

| **Sensor** | **Description** | **Unit** |
|---|---|---|
| $\dot{\psi}$ | Yaw-rate sensor placed on bicycle mass | $[rad/s]$ |
| $a_y = \dot{V} + U\ \dot{\psi}$ | Lateral acceleration sensor placed on bicycle mass | $[m/s^2]$ |
| **Actuator** | **Description** | **Unit** |
| $F_{cruise}$ | Maintain a constant forward velocity $U$ during a nominal circle trajectory | $[N]$ |
| $F_{act}$ | Force actuator placed at the rear wheel | $[N]$ |
| $T_{act}$ | Torque actuator at the bicycle mass | $[Nm]$ |

Table 3.9: Available sensors and actuators for the bicycle model

All sensors and actuators have been placed on the bicycle model and the corresponding non-linear equations of the state dynamics and output dynamics have been derived. Second, the non-linear tracking error dynamics have been derived for the specified nominal straight-line trajectory (3.20). The non-linear tracking error dynamics are linearized around this trajectory and can be written in the time-invariant state space form:

$$\begin{aligned} \dot{E} &= \mathbf{A}\ E + \mathbf{B}\ v \\ w &= \mathbf{C}\ E + \mathbf{D}\ v \end{aligned} \tag{3.42}$$

where:

- The state tracking error defined as: $E = \begin{bmatrix} e \\ \dot{e} \end{bmatrix} = \begin{bmatrix} q - q_{traj} \\ \dot{q} - \dot{q}_{traj} \end{bmatrix}$
- The input defined as: $v = u - u_{traj} = \begin{bmatrix} F_{act} - F_{act,\ traj} \\ T_{act} - T_{act,\ traj} \end{bmatrix}$
- The output defined as: $w = y - y_{traj} = \begin{bmatrix} \dot{\psi} - \dot{\psi}_{traj} \\ a_y - a_{y,\ traj} \end{bmatrix}$
- The system matrix defined as:

$$\mathbf{A} = \mathbf{A_{SL}} = \frac{\partial F}{\partial E}\Big|_{(E=0,\ v=0,\ \theta,\ \delta=0,\ q_{traj},\ \dot{q}_{traj},\ u_{traj})} = \begin{bmatrix} 0 & 0 & 0 & 1 & 0 & 0 \\ 0 & 0 & 0 & 0 & 1 & 0 \\ 0 & 0 & 0 & 0 & 0 & 1 \\ 0 & 0 & 0 & 0 & 0 & 0 \\ 0 & 0 & 0 & 0 & -5.0000 & -14.5000 \\ 0 & 0 & 0 & 0 & 0.2222 & -5.0222 \end{bmatrix}$$

- The input matrix defined as:

$$\mathbf{B} = \frac{\partial F}{\partial v}\Big|_{(E=0,\ v=0,\ \theta,\ \delta=0,\ q_{traj},\ \dot{q}_{traj},\ u_{traj})} = \begin{bmatrix} 0 & 0 \\ 0 & 0 \\ 0 & 0 \\ -6.2500 & 0 \\ 0 & 0 \\ 0 & 2.7778 \end{bmatrix} \cdot 10^{-4}$$

- The output matrix defined as:

$$\mathbf{C} = \frac{\partial H}{\partial E}\Big|_{(E=0,\ v=0,\ \theta,\ \delta=0,\ q_{traj},\ \dot{q}_{traj},\ u_{traj})} = \begin{bmatrix} 0 & 0 & 0 & 0 & 0 & 1 \\ 0 & 0 & 0 & 0 & -5.0000 & 0.50000 \end{bmatrix}$$

- The feedthrough matrix defined as:

$$\mathbf{D} = \frac{\partial H}{\partial v}\Big|_{(E=0,v=0,\theta,\delta=0,q_{traj},\dot{q}_{traj},u_{traj})} = \begin{bmatrix} 0 & 0 \\ 0 & 0 \end{bmatrix}$$

### 3.5.1 Observability and controllability

To design a controller the observability and controllability have to be determined. The system is observable and controllable if the rank of the **OM** and **CM** is 6 (the length of the state tracking error vector $E$). With the derived system matrix $\mathbf{A}$, the input matrix $\mathbf{B}$ and the output matrix $\mathbf{C}$ the observability and controllability are determined for different sensor and actuator combinations, as shown in table 3.10.

| **Sensor(s)** | $\dot{\psi}$ | $a_y$ | $\dot{\psi} + a_y$ |
|---|---|---|---|
| Rank of **OM** | 2 | 2 | 2 |
| **Actuator(s)** | $F_{act}$ | $T_{act}$ | $F_{act} + T_{act}$ |
| Rank of **CM** | 2 | 3 | 5 |

Table 3.10: Observability and controllability for different sensor and actuator combinations

Table 3.10 shows that for each combination of sensor placement the rank of the observability matrix is 2 (< full rank 6), which means that not all information of the state tracking error vector $E$ can be reconstructed with a state estimator. Also, for each combination of actuator placement the rank of the controllability matrix is smaller than the full rank of 6, so not all state tracking errors can be physically influenced.

#### Modification of state space form

The objective is to develop a stability control system for *velocity tracking*. To achieve velocity tracking, modifications have to be applied. As described in previous sections the tracking error dynamics of the bicycle model is independent of the displacement error vector $e$, as shown in (3.17). With the independency of the displacement error vector $e$ the state space form can be written with respect to the velocities of the error vector $\dot{e}$ only. This modification results in 'the modified state space form':

$$\begin{aligned} \ddot{e} &= \mathbf{A}\ \dot{e} + \mathbf{B}\ v \\ w &= \mathbf{C}\ \dot{e} + \mathbf{D}\ v \end{aligned} \tag{3.43}$$

where:

- The system matrix defined as:

$$\mathbf{A} = \mathbf{A_{SL}} = \frac{\partial F}{\partial \dot{e}}\Big|_{(\dot{e}=0,\ v=0,\ \theta,\ \delta=0,\ \dot{q}_{traj},\ \ u_{traj})} = \begin{bmatrix} 0 & 0 & 0 \\ 0 & -5.0000 & -14.5000 \\ 0 & 0.2222 & -5.0222 \end{bmatrix}$$

- The input matrix defined as:

$$\mathbf{B} = \frac{\partial F}{\partial v}\Big|_{(\dot{e}=0,\ v=0,\ \theta,\ \delta=0,\ \dot{q}_{traj},\ u_{traj})} = \begin{bmatrix} -6.2500 & 0 \\ 0 & 0 \\ 0 & 2.7778 \end{bmatrix} \cdot 10^{-4}$$

- The output matrix defined as:

$$\mathbf{C} = \frac{\partial H}{\partial \dot{e}}\Big|_{(\dot{e}=0,\ v=0,\ \theta,\ \delta=0,\ \dot{q}_{traj},\ u_{traj})} = \begin{bmatrix} 0 & 0 & 1 \\ 0 & -5.0000 & 0.50000 \end{bmatrix}$$

- The feedthrough matrix **D** does not change

This system is maximal observable and controllable if the rank of the **OM** and **CM** is 3 (the length of the state tracking error vector $\dot{e}$). For the derived **A**, **B** and **C** the observability and controllability can be determined for different sensor and actuator combinations, as shown in table 3.11.

| **Sensor(s)** | $\dot{\psi}$ | $a_y$ | $\dot{\psi} + a_y$ |
|---|---|---|---|
| Rank of **OM** | 2 | 2 | 2 |
| **Actuator(s)** | $F_{act}$ | $T_{act}$ | $F_{act} + T_{act}$ |
| Rank of **CM** | 1 | 2 | **3** |

Table 3.11: Observability and controllability for the modified state space form

Table 3.11 shows that the system is not maximal observable, because for each combination of sensor placement the rank of the observability is 2 (< full rank 3). With the available sensors information about the forward velocity error $\dot{e}_1$ cannot be reconstructed around the nominal straight-line trajectory.
However with the use of both actuators, $F_{act}$ and $T_{act}$, the system is maximal controllable. With the force actuator $F_{act}$ the forward velocity error can be influenced only. Using the torque actuator $T_{act}$ the lateral velocity error and yaw-rate error can be influenced. Combination of both actuators results that all state tracking errors $\dot{e}$ can be influenced.

### Driver model

To develop a stability control system for *velocity tracking* full (maximal) observability of the system is desired. To achieve full observability a driver model is introduced. In practice, the driver of a vehicle can be seen as a 'cruise control'. The driver observes with his eyes the forward velocity of the speedometer and actuates the desirable forward velocity by a throttle/braking input. The driver model is introduced by a forward velocity $U$ sensor. Next, the corresponding state space form has been derived (3.44) and the corresponding observability, as shown in table 3.12. This table shows that the system is maximal observable with a sensor combination within the forward velocity sensor $U$.

$$\begin{aligned} \ddot{e} &= \mathbf{A}\ \dot{e} + \mathbf{B}\ v \\ w &= \mathbf{C}\ \dot{e} + \mathbf{D}\ v \end{aligned} \tag{3.44}$$

where:

- The system matrix **A** does not change w.r.t. (3.43)
- The input matrix **B** does not change w.r.t. (3.43)

- The output defined as: $w = y - y_{traj} = \begin{bmatrix} U - U_{traj} \\ \dot{\psi} - \dot{\psi}_{traj} \\ a_y - a_{y,\ traj} \end{bmatrix}$
- The output matrix defined as:

$$\mathbf{C} = \frac{\partial H}{\partial \dot{e}}\Big|_{(\dot{e}=0,\ v=0,\ \theta,\ \delta=0,\ q_{traj},\ \dot{q}_{traj},\ u_{traj})} = \begin{bmatrix} 1 & 0 & 0 \\ 0 & 0 & 1 \\ 0 & -5.0000 & 0.50000 \end{bmatrix}$$

- The feedthrough matrix defined as:

$$\mathbf{D} = \frac{\partial H}{\partial v}\Big|_{(\dot{e}=0,v=0,\theta,\delta=0,q_{traj},\dot{q}_{traj},u_{traj})} = \begin{bmatrix} 0 & 0 \\ 0 & 0 \\ 0 & 0 \end{bmatrix}$$

| **Sensor(s)** | $U$ | $U + \dot{\psi}$ | $U + a_y$ | $U + \dot{\psi} + a_y$ |
|---|---|---|---|---|
| Rank of **OM** | 1 | **3** | **3** | **3** |

Table 3.12: Observability of the modified state space form within a Driver model

### 3.5.2 Designing the controller

The cost of the required sensors and actuators is decisive, therefore a minimal set of sensors and actuators has been chosen for designing the controller. To reconstruct all information of the tracking error states $\dot{e}$ with a minimal set of sensors the forward velocity and yaw-rate sensors ($U$ and $\dot{\psi}$) are chosen. To place all eigenvalues of the system on desired eigenvalue locations both actuators ($F_{act}$ and $T_{act}$) are necessary. The placed sensors and actuators are shown in figure 3.19. This choice of sensor and actuator combination results in the state space form as written in (3.45).

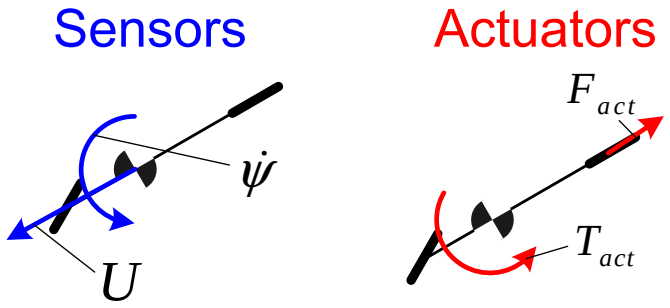


Figure 3.19: Sensor and actuator placement on the bicycle model for the controller design around the nominal straight-line trajectory

$$\begin{aligned} \ddot{e} &= \mathbf{A}\ \dot{e} + \mathbf{B}\ v \\ w &= \mathbf{C}\ \dot{e} + \mathbf{D}\ v \end{aligned} \tag{3.45}$$

where:

- The state tracking error defined as: $\dot{e} = \left[ \begin{array}{c} \dot{q} - \dot{q}_{traj} \end{array} \right]$
- The input defined as: $v = u - u_{traj} = \left[ \begin{array}{c} F_{act} - F_{act,\ traj} \\ T_{act} - T_{act,\ traj} \end{array} \right]$
- The output defined as: $w = y - y_{traj} = \left[ \begin{array}{c} U - U_{traj} \\ \dot{\psi} - \dot{\psi}_{traj} \end{array} \right]$
- The system matrix defined as:

$$\mathbf{A} = \mathbf{A_{SL}} = \left. \frac{\partial F}{\partial \dot{e}} \right|_{(\dot{e}=0,\ v=0,\ \theta,\ \delta=0,\ \dot{q}_{traj},\ \ u_{traj})} = \left[ \begin{array}{ccc} 0 & 0 & 0 \\ 0 & -5.0000 & -14.5000 \\ 0 & 0.2222 & -5.0222 \end{array} \right]$$

- The input matrix defined as:

$$\mathbf{B} = \left. \frac{\partial F}{\partial v} \right|_{(\dot{e}=0,\ v=0,\ \theta,\ \delta=0,\ \dot{q}_{traj},\ u_{traj})} = \left[ \begin{array}{cc} -6.2500 & 0 \\ 0 & 0 \\ 0 & 2.7778 \end{array} \right] \cdot 10^{-4}$$

- The output matrix defined as:

$$\mathbf{C} = \left. \frac{\partial H}{\partial \dot{e}} \right|_{(\dot{e}=0,\ v=0,\ \theta,\ \delta=0,\ q_{traj},\ \dot{q}_{traj},\ u_{traj})} = \left[ \begin{array}{ccc} 1 & 0 & 0 \\ 0 & 0 & 1 \end{array} \right]$$

- The feedthrough matrix defined as:

$$\mathbf{D} = \left. \frac{\partial H}{\partial v} \right|_{(\dot{e}=0,v=0,\theta,\delta=0,q_{traj},\dot{q}_{traj},u_{traj})} = \left[ \begin{array}{cc} 0 & 0 \\ 0 & 0 \end{array} \right]$$

The objectives of the controller design are velocity tracking around the nominal straight-line trajectory and to achieve a specified dynamic behaviour by choosing the eigenvalues of the autonomous dynamic at desired locations.

### Control law

For the control law the control eigenvalues $p_c$ have to be chosen. The autonomous dynamics show that the first eigenvalue (table 3.13) is at the imaginary axis and for a stable dynamic behaviour a negative real part is required. The other desired control eigenvalue locations are arbitrary chosen, as shown in table 3.19.

| | **Eigenvalue** [−] |
|---|---|
| 1 | 0 |
| 2 | -5.0111 + 1.7950i |
| 3 | -5.0111 - 1.7950i |

Table 3.13: Eigenvalues autonomous dynamics around nominal straight-line trajectory

| | **Eigenvalue** [−] |
|---|---|
| 1 | -2 |
| 2 | -7 + 1.5i |
| 3 | -7 - 1.5i |

Table 3.14: Desired control eigenvalues $p_c$

The corresponding state feedback gain **K** is determined with the use of the MATLAB function *place.m*:

$$\mathbf{K} = \begin{bmatrix} -9.9610 & -2.0581 & -0.8951 \\ -2.2418 & 2.2454 & -0.8923 \end{bmatrix} \cdot 10^3 \tag{3.46}$$

The derived feedback gain **K** matrix is verified by determining the eigenvalues $s$ of the characteristic equation $det\,[s\ I - (\mathbf{A} - \mathbf{B}\ \mathbf{K})] = 0$, which results in $s = p_c$. The state feedback gains $K_{11}, \cdots, K_{mn}$ are large, however physically possible by selective braking of the individual wheels of the vehicle.

### State estimator design

For the state estimator design the desired state estimate error poles $p_e$ are chosen to be four times faster than the desired control poles, which gives:

| | **Eigenvalue** [−] |
|---|---|
| 1 | -8 |
| 2 | -28 |
| 3 | -28 |

Table 3.15: Desired state estimate error poles $p_e$

The corresponding proportional gain **L** is:

$$\mathbf{L} = \begin{bmatrix} 28.0000 & 0.0000 \\ 0.0000 & 296.0000 \\ 0.0000 & 25.9778 \end{bmatrix} \tag{3.47}$$

## 3.5.3 Verification of the stability performance

After deriving the state feedback gain **K** and the proportional gain **L** the next step is to verify the designed controller with the use of a simulation.

The controller design objectives are; a specified dynamic behaviour and a stable velocity tracking around a nominal trajectory. However, this section will only verify a stable velocity tracking, because the specified dynamic behaviour has been arbitrarily chosen with the desired control $p_c$ and state estimator poles $p_e$.

To verify the stability performance of the velocity tracking around the nominal straight-line trajectory, simulations have been carried out. First, a simulation has been performed of the non-linear equations of motion with the nominal straight-line trajectory as input and used for

the IC's, i.e. an open-loop simulation. To verify the stability of the non-linear equations of motion around this nominal trajectory a perturbation of 3 $[rad/s]$ has been given on the IC of the yaw-rate $\dot{\psi}$. The simulation results of the open-loop system are shown in figure 3.20. As expected from the eigenvalue analysis of the autonomous dynamics, table 3.13, two signals will converge to a zero error in time, i.e. the lateral velocity and the yaw-rate. The forward velocity converges to another nominal value corresponding to the zero eigenvalue.

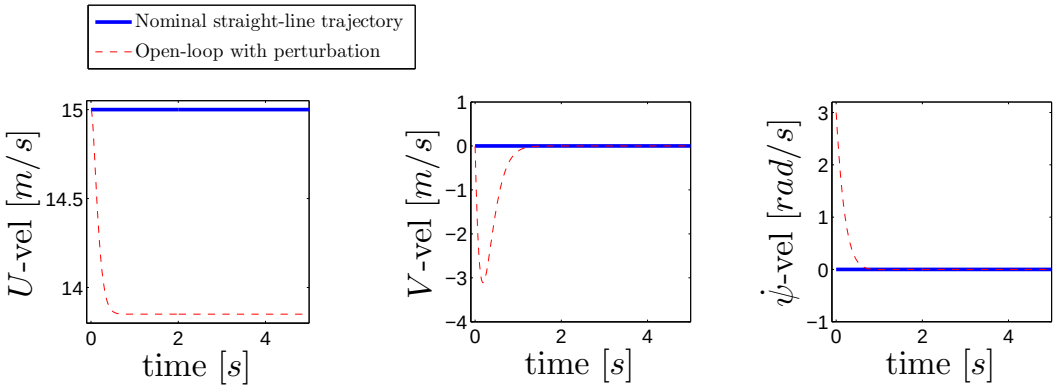


Figure 3.20: Open-loop Simulation with and without perturbation on the IC at $t = 0$ $[s]$

Second, a simulation has been performed of the non-linear equations of motion combined with the designed controller, i.e. a closed-loop simulation. The same perturbation has been given on the IC of the yaw-rate to analyse the stability around the nominal straight-line trajectory. The corresponding simulation results are shown in figure 3.21 and show that all signals converge to the nominal trajectory in time. The corresponding inputs are shown in figure 3.22. This figure shows large values for $F_{act}$ and $T_{act}$ in a short time period to achieve a stable velocity tracking around the nominal trajectory. In practice, these kind of inputs are physically not possible by fast braking of the individual wheels and is not comfortable for the passengers. A feasible control intervention has to be done in a larger time-period.

## 3.6 Controller design for the circle trajectory

For designing the controller for the nominal circle trajectory, the same approach will be carried out as described in previous section. All sensors ($U$, $\dot{\psi}$ and $a_y$) and all actuators ($F_{act}$ and $T_{act}$) have been placed on the bicycle model. The corresponing linear tracking error dynamics have been derived for the specified nominal circle trajectory (3.24) and written into the state space form (3.42), where:

- The state tracking error defined as: $E = \begin{bmatrix} e \\ \dot{e} \end{bmatrix} = \begin{bmatrix} q - q_{traj} \\ \dot{q} - \dot{q}_{traj} \end{bmatrix}$
- The input defined as: $v = u - u_{traj} = \begin{bmatrix} F_{act} - F_{act,\ traj} \\ T_{act} - T_{act,\ traj} \end{bmatrix}$

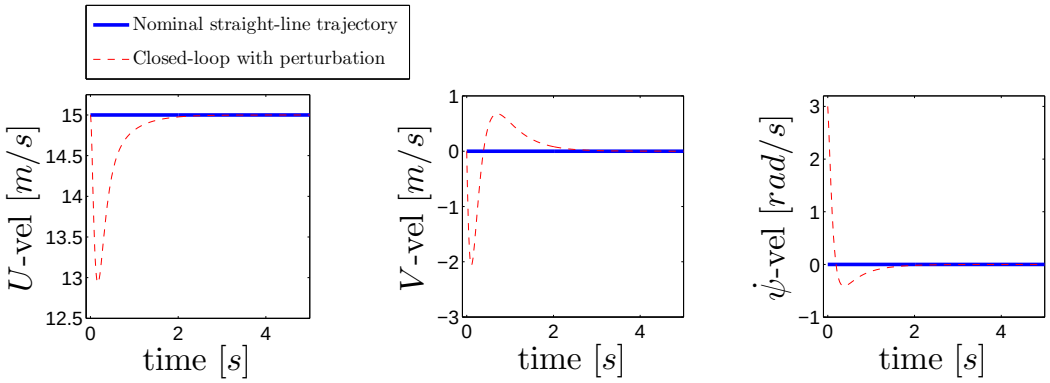


Figure 3.21: Closed-loop Simulation with and without perturbation on the IC at $t = 0$ $[s]$

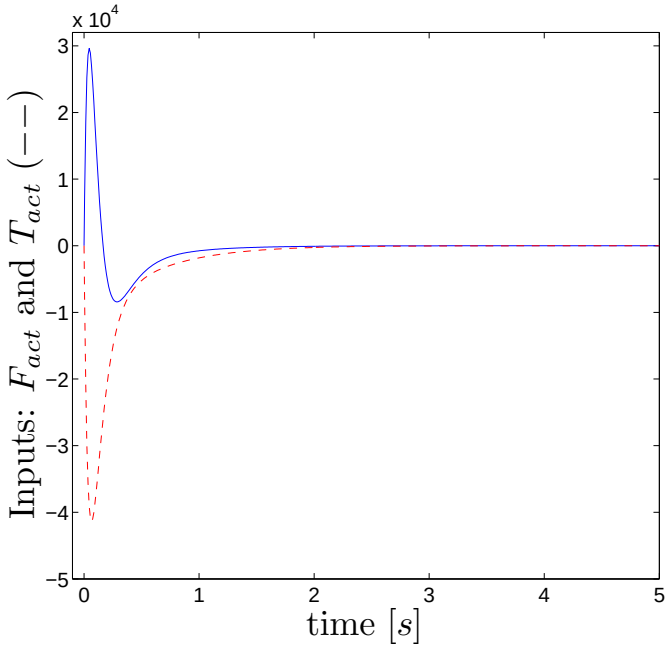


Figure 3.22: Inputs of the closed-loop simulation with perturbation on the IC at $t = 0$ $[s]$

- The output defined as: $w = y - y_{traj} = \begin{bmatrix} U - U_{traj} \\ \dot{\psi} - \dot{\psi}_{traj} \\ a_y - a_{y,\,traj} \end{bmatrix}$

- The system matrix defined as:

$$\mathbf{A} = \left.\frac{\partial F}{\partial E}\right|_{(E=0,\ v=0,\ \theta,\ \delta=2.8319\cdot\pi/180,\ F_{cruise}=229.2608,\ q_{traj},\ \dot{q}_{traj},\ u_{traj})} =$$

$$\mathbf{A_{Circle}} = \begin{bmatrix} 0 & 0 & 0 & 1 & 0 & 0 \\ 0 & 0 & 0 & 0 & 1 & 0 \\ 0 & 0 & 0 & 0 & 0 & 1 \\ 0 & 0 & 0 & -0.0004 & 0.3414 & -0.0889 \\ 0 & 0 & 0 & -0.3123 & -4.9928 & -14.5023 \\ 0 & 0 & 0 & 0.0767 & 0.2212 & -5.0148 \end{bmatrix}$$

- The input matrix defined as:

$$\mathbf{B} = \frac{\partial F}{\partial v}\Big|_{(E=0,\ v=0,\ \theta,\ \delta=2.8319\cdot\pi/180,\ F_{cruise}=229.2608,\ q_{traj},\ \dot{q}_{traj},\ u_{traj})}$$
$$= \begin{bmatrix} 0 & 0 \\ 0 & 0 \\ 0 & 0 \\ -6.2500 & 0 \\ 0 & 0 \\ 0 & 2.7778 \end{bmatrix} \cdot 10^{-4}$$

- The output matrix defined as:

$$\mathbf{C} = \frac{\partial H}{\partial E}\Big|_{(E=0,\ v=0,\ \theta,\ \delta=2.8319\cdot\pi/180,\ F_{cruise}=229.2608,\ q_{traj},\ \dot{q}_{traj},\ u_{traj})}$$
$$= \begin{bmatrix} 0 & 0 & 0 & 1 & 0 & 0 \\ 0 & 0 & 0 & 0 & 0 & 1 \\ 0 & 0 & 0 & -0.0944 & -4.9928 & 0.4977 \end{bmatrix}$$

- The feedthrough matrix defined as:

$$\mathbf{D} = \frac{\partial H}{\partial v}\Big|_{(E=0,\ v=0,\ \theta,\ \delta=2.8319\cdot\pi/180,\ F_{cruise}=229.2608,\ q_{traj},\ \dot{q}_{traj},\ u_{traj})}$$
$$= \begin{bmatrix} 0 & 0 \\ 0 & 0 \\ 0 & 0 \end{bmatrix}$$

### 3.6.1 Observability and controllability

The system is observable and controllable if the rank of the **OM** and **CM** is 6. With the derived system matrix **A**, the input matrix **B** and the output matrix **C** the observability and controllability is computed for different sensor and actuator combinations, as shown in table 3.16.

| **Sensor(s)** | $U$ | $\dot{\psi}$ | $a_y$ | $U+\dot{\psi}$ | $U+a_y$ | $\dot{\psi}+a_y$ | $U+\dot{\psi}+a_y$ |
|---|---|---|---|---|---|---|---|
| Rank of **OM** | 3 | 3 | 3 | 3 | 3 | 3 | 3 |

| **Actuator(s)** | $F_{act}$ | $T_{act}$ | $F_{act}+T_{act}$ |
|---|---|---|---|
| Rank of **CM** | 4 | 4 | 5 |

Table 3.16: Observability and controllability for different sensor and actuator combinations

Table 3.16 shows that for each combination of sensor placement the rank of the observability matrix is 3 (< full rank 6). With the available sensors the velocities of the error vector $\dot{e}$ can be reconstructed only. For each combination of actuator placement the rank of the controllability matrix is smaller than the full rank of 6, because with the available actuators the lateral displacement error $e_2$ cannot be influenced.

### Modification of state space form

The objective is to develop a stability control system for *velocity tracking* around the nominal circle trajectory. With the independency of the displacement error vector $e$ the state space form can be rewritten with respect to the velocities of the error vector $\dot{e}$ only (3.43), where:

- The system matrix defined as:

$$\mathbf{A} = \frac{\partial F}{\partial \dot{e}}\Big|_{(\dot{e}=0,\ v=0,\ \theta,\ \delta=2.8319\cdot\pi/180,\ F_{cruise}=229.2608,\ q_{traj},\ \dot{q}_{traj},\ u_{traj})} =$$

$$\mathbf{A_{Circle}} = \begin{bmatrix} -0.0004 & 0.3414 & -0.0889 \\ -0.3123 & -4.9928 & -14.5023 \\ 0.0767 & 0.2212 & -5.0148 \end{bmatrix}$$

- The input matrix defined as:

$$\mathbf{B} = \frac{\partial F}{\partial v}\Big|_{(\dot{e}=0,\ v=0,\ \theta,\ \delta=2.8319\cdot\pi/180,\ F_{cruise}=229.2608,\ q_{traj},\ \dot{q}_{traj},\ u_{traj})}$$

$$= \begin{bmatrix} -6.2500 & 0 \\ 0 & 0 \\ 0 & 2.7778 \end{bmatrix} \cdot 10^{-4}$$

- The output matrix defined as:

$$\mathbf{C} = \frac{\partial H}{\partial \dot{e}}\Big|_{(\dot{e}=0,\ v=0,\ \theta,\ \delta=2.8319\cdot\pi/180,\ F_{cruise}=229.2608,\ q_{traj},\ \dot{q}_{traj},\ u_{traj})}$$

$$= \begin{bmatrix} 1 & 0 & 0 \\ 0 & 0 & 1 \\ -0.0944 & -4.9928 & 0.4977 \end{bmatrix}$$

- The feedthrough matrix $\mathbf{D}$ does not change

For the derived $\mathbf{A}$, $\mathbf{B}$ and $\mathbf{C}$ the observability and controllability can be determined for different sensor and actuator combinations, as shown in table 3.17. This table shows that the system is maximal observable and controllable for all sensor and actuator combinations.

| **Sensor(s)** | $U$ | $\dot{\psi}$ | $a_y$ | $U+\dot{\psi}$ | $U+a_y$ | $\dot{\psi}+a_y$ | $U+\dot{\psi}+a_y$ |
|---|---|---|---|---|---|---|---|
| Rank of **OM** | 3 | 3 | 3 | 3 | 3 | 3 | 3 |

| **Actuator(s)** | $F_{act}$ | $T_{act}$ | $F_{act}+T_{act}$ |
|---|---|---|---|
| Rank of **CM** | 3 | 3 | 3 |

Table 3.17: Observability and controllability for the modified state space form

### 3.6.2 Designing the controller

Designing a controller for stable velocity tracking around the nominal circle trajectory is unnecessary because section 3.3.8 shows that the system is already stable for $\dot{e}$ (all eigenvalue are in the LHP as shown in table 3.18). However with the described controller design a desired dynamic behaviour can be achieved, such as a faster convergence to the nominal circle trajectory.
A minimal set of sensors and actuators has been chosen for designing the controller. To reconstruct all information of the tracking error states $\dot{e}$, the yaw-rate sensor ($\dot{\psi}$) has been chosen. To place all eigenvalues of the system on desired eigenvalue locations, the force actuator ($F_{act}$) has been chosen.

#### Control law

The eigenvalues of the autonomous dynamics are:

| | **Eigenvalue** [−] |
|---|---|
| 1 | -0.0340 |
| 2 | -4.9870 + 1.7759i |
| 3 | -4.9870 - 1.7759i |

Table 3.18: Eigenvalues autonomous dynamics around the nominal circle trajectory

The desired control eigenvalues $p_c$ locations are arbitrary chosen:

| | **Eigenvalue** [−] |
|---|---|
| 1 | -2 |
| 2 | -7 + 1.5i |
| 3 | -7 - 1.5i |

Table 3.19: Desired control eigenvalues $p_c$

The corresponding state feedback gain $K_{F_{act}}$ is determined with the use of the MATLAB function *place.m*:

$$K_{F_{act}} = \begin{bmatrix} -0.9587 & -3.4898 & 4.7290 \end{bmatrix} \cdot 10^4 \tag{3.48}$$

The state feedback gains of $K_{F_{act}}$ are large. To reduce the feedback gains the torque actuator $T_{act}$ is also used, which results in the state feedback gain $\mathbf{K}$ of:

$$\mathbf{K} = \begin{bmatrix} -1.0117 & 0.1638 & 0.0818 \\ 0.2213 & 0.2280 & -0.1191 \end{bmatrix} \cdot 10^4 \tag{3.49}$$

The state feedback gains of $\mathbf{K}$ are smaller than the derived $K_{F_{act}}$ and are physically possible by selective braking of the individual wheels.

#### State estimator design

For the state estimator design the desired state estimate error poles $p_e$ are chosen to be four times faster than the desired control poles, as shown in table 3.20.

| | **Eigenvalue** $[-]$ |
|---|---|
| 1 | -8 |
| 2 | -28 |
| 3 | -28 |

Table 3.20: Desired state estimate error poles $p_e$

The corresponding proportional gain $L_{\dot{\psi}}$ is:

$$L_{\dot{\psi}} = [2.0248,\ -0.2789,\ 0.0054]^T \cdot 10^4 \tag{3.50}$$

To reduce the proportional gains of $L_{\dot{\psi}}$ the lateral acceleration sensor $a_y$ is also used. This results in the corresponding proportional gain $\mathbf{L}$:

$$\mathbf{L} = \begin{bmatrix} 215.4749 & 184.9771 \\ -17.9619 & -9.5473 \\ 23.5657 & 0.4352 \end{bmatrix} \tag{3.51}$$

### 3.6.3 Verification of the stability performance

This section will verify the stable velocity tracking around the nominal circle trajectory. An open-loop simulation and a closed-loop simulation with a perturbation on the IC's are performed for a time period of 100 $[s]$. As expected from the eigenvalue analysis the open-loop simulation shows a stable convergence to the velocities of the nominal circle trajectory, as shown in figure 3.23. In combination with the designed controller a faster convergence to the velocities of the nominal circle trajectory is achieved, as shown in figure 3.24. The corresponding inputs are large in a short time-period, as shown in figure 3.25.

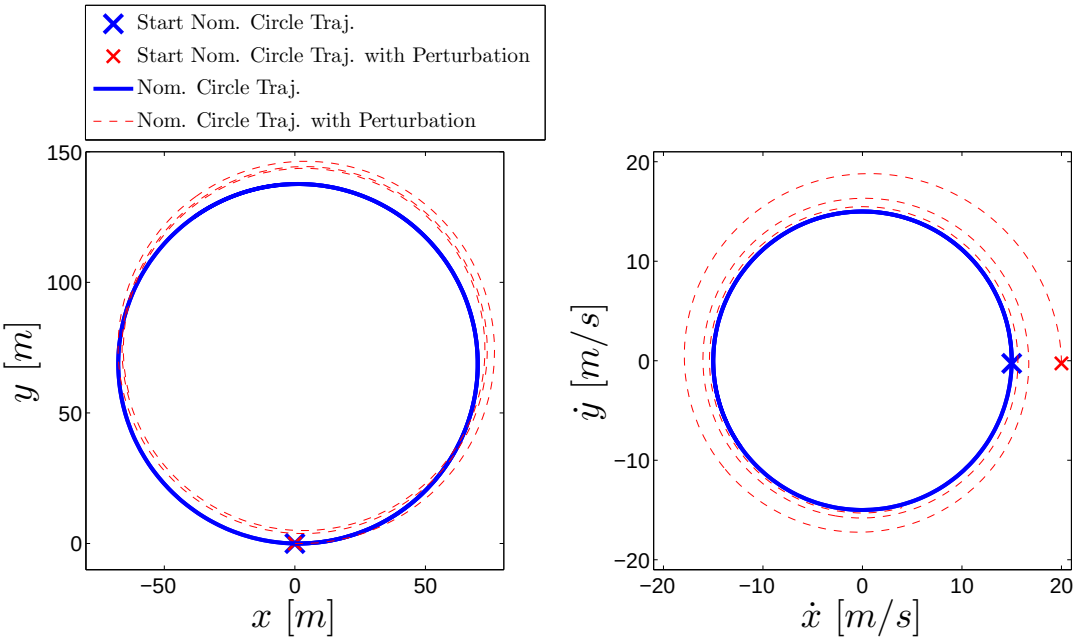


Figure 3.23: Open-loop simulation with and without perturbation on the IC's at $t = 0$ $[s]$

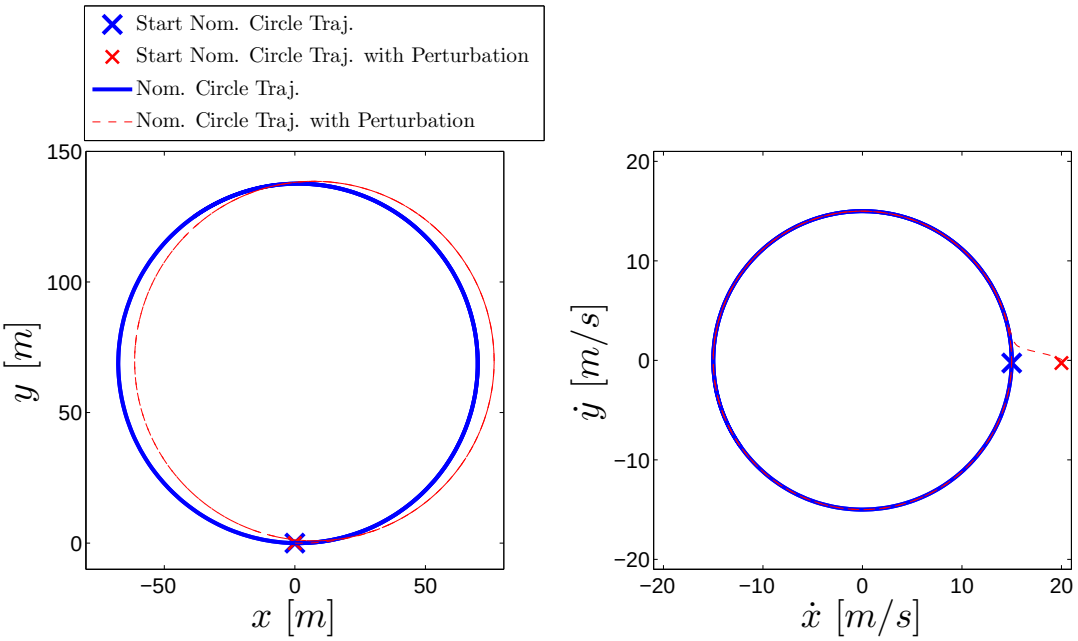


Figure 3.24: Closed-loop simulation with and without perturbation on the IC's at $t = 0$ $[s]$

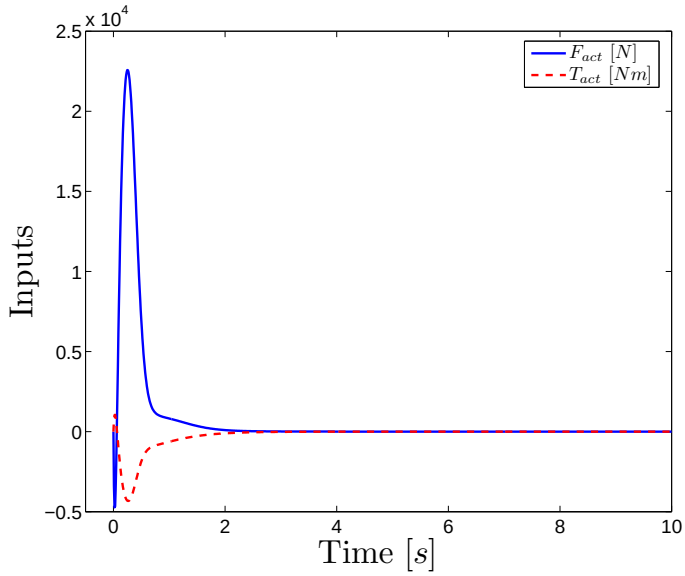


Figure 3.25: Inputs of the closed-loop simulation with perturbation on the IC's at $t = 0$ $[s]$

## 3.7 Conclusions

A commonly used test to analyse various vehicle instability phenomena is driving a so-called lane-change manoeuvre. However, linearizing the non-linear equations of motion of the bicycle model around a lane-change trajectory is difficult and therefore this manoeuvre has been split up into a straight-line and circle trajectory.

For maintaining a constant forward velocity during a circle trajectory an extra longitudinal force $F_{cruise}$ has been added to the bicycle model. Moreover, a numerical approach has been used to determine the nominal trajectory due to the non-linear characteristics of the underlying dynamic bicycle model.

Cause of the complex non-linear dynamics of the bicycle model, a numerical approach is used to determine a nominal circle trajectory.

By analyzing the linearized tracking error dynamics of the bicycle model around a nominal straight-line and a nominal circle trajectory, it shows three eigenvalues at the imaginary axis. These eigenvalues are the result that the bicycle non-linear equations of motion are independent of three generalized displacement coordinates. The linearized tracking error dynamics around a nominal straight-line trajectory shows an extra eigenvalue at the imaginary axis due to its independency of the forward velocity error around this trajectory. The remaining eigenvalues are stable due to its negative real part.

A vehicle handling study shows a decrease in stability margins around a nominal circle trajectory by increasing the forward velocity. For various nominal circle trajectories a vehicle handling diagram has been made to analyse the yaw-rate instability and shows that the bicycle model is understeered.

Second part of this chapter is the controller design based on the state-space method to control the states in a more desirable manner. For a nominal straight-line and a nominal circle trajectory the observability and controllability are analyzed for various sensor and actuator

combinations.
To reconstruct all information of the tracking error states $\dot{e}$ around a nominal straight-line trajectory the forward velocity $U$ and yaw-rate $\dot{\psi}$ sensors are chosen. For the control intervention the force $F_{act}$ and torque $T_{act}$ actuators are used.
The controller design around a nominal circle trajectory needs one sensor and one actuator less to achieve a desired dynamic behaviour in theory. However, the resulting controller gains are large and physical impossible. To decrease those gains a set of two sensors ($\dot{\psi}$ and $a_y$) and two actuators ($F_{act}$ and $T_{act}$) is used.
A verification of both controller designs around a nominal straight-line and a nominal circle trajectory shows a stable velocity tracking.

# Chapter 4

# The Dynamic Behaviour and Stability Control of a Truck/full-trailer combination

## 4.1 Introduction

In this chapter the dynamic behaviour and stability control will be studied of a truck/full-trailer combination. A dynamic vehicle model will be made and the corresponding non-linear equations of motion will be derived. With the non-linear equations of motion the dynamic behaviour and stability will be analyzed around nominal straight-line and nominal circle trajectories. A vehicle handling study will be carried out to analyse the yaw-rate instability and rollover phenomenon around various circle trajectories. Also the stability of the dynamic vehicle model will be analyzed based on the eigenvalues of the linearized tracking error dynamics.

Final part of this chapter is a preliminary study of controller design based on the observability and controllability of the linearized tracking error dynamics of the truck/full-trailer combination with the use of various sensor and actuator combinations.

## 4.2 Dynamic vehicle model

The dynamic vehicle model and vehicle parameters of the truck/full-trailer combination, as shown in figure 4.1, are based on the report of Zegwaard [Zeg88]. The dynamic vehicle model is a 3-dimensional one-track model which exists of a truck, a drawbar and a trailer part as shown in figure 4.2. The truck has one steerable front axle and a double rear axle, to support the truck cargo. The drawbar has one axle and the trailer has a double rear axle. The vehicle combination has two articulation points which can rotate around its vertical axis. The used tyre model has only lateral cornering stiffness which produces the lateral tyre forces $F_{yi}$. The chassis of the truck, drawbar and trailer have a point mass $M_i$. To study the rollover of the vehicle combination, elevated roll masses $M_{\varphi i}$ have been attached on the chassis masses of the truck and trailer. These roll masses are suspended with springs and dampers as shown

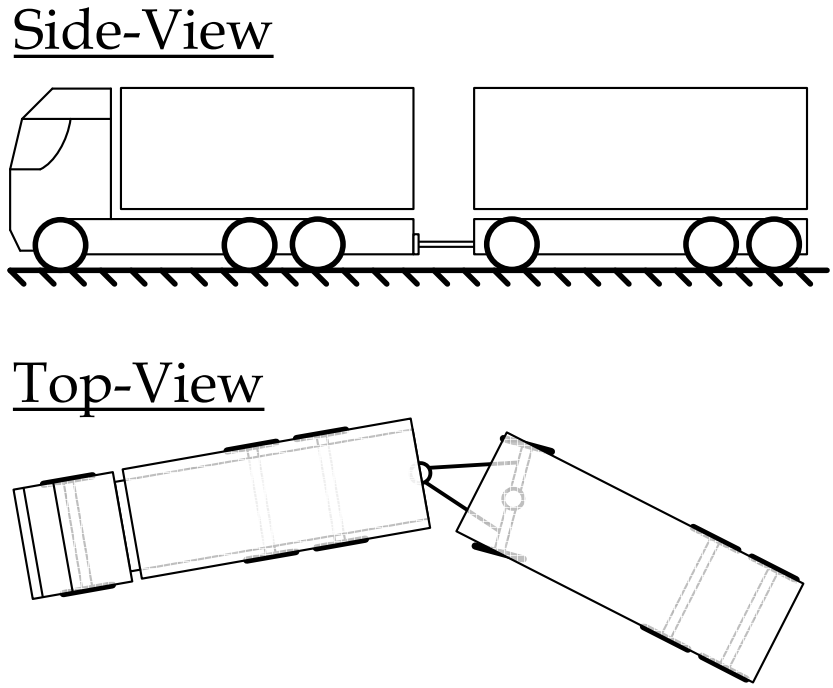


Figure 4.1: Truck/Full-trailer combination

in the front view of figure 4.2. The corresponding vehicle characteristics and parameters are shown in table 4.1 and appendix D respectively. The dynamic vehicle model can be used to study the following vehicle instability phenomena:

- **Yaw-rate instability**, by a difference in the lateral tyre forces of the truck, or of the trailer, the vehicle combination can steer in an undesirable direction, i.e. exhibit under/oversteer.

- **Jack-knife phenomenon**, the dynamic vehicle model contains articulation points between the drawbar & truck and between the drawbar & trailer. By these articulation points the jack-knife phenomenon can be studied when the truck or trailer skids. For example, when the truck skids it is possible that the trailer push the truck sideways which results in the jack-knife phenomenon.

- **Rollover**, the vehicle combination can rollover by the forces which are produced by the elevated roll masses. However the dynamic vehicle model is a one-track model in which rollover can not occur. Nevertheless, by the use of the static rollover indicator, presented in appendix A, the rollover of the vehicle combination can be analyzed.

In this chapter only the yaw-rate instability and the rollover phenomenon will be studied.

| **Symbol** | **Description** | **Unit** |
|---|---|---|
| $U$ | forward velocity of the truck chassis mass | $[m/s]$ |
| $V$ | lateral velocity of the truck chassis mass | $[m/s]$ |
| $\psi_1$ | yaw angle of the truck w.r.t. the fixed world coordinate system | $[rad]$ |
| $\psi_2$ | yaw angle of the drawbar w.r.t. the truck | $[rad]$ |
| $\psi_3$ | yaw angle of the trailer w.r.t. the drawbar | $[rad]$ |
| $\varphi_1$ | roll angle of the truck roll mass w.r.t. the truck chassis mass | $[rad]$ |
| $\varphi_3$ | roll angle of the trailer roll mass w.r.t. the trailer chassis mass | $[rad]$ |
| $\delta$ | steering angle of the truck | $[rad]$ |
| $\alpha_1$ | side slip angle of the truck front wheel | $[rad]$ |
| $\alpha_2$ | side slip angle of the truck first rear wheel | $[rad]$ |
| $\alpha_3$ | side slip angle of the truck second rear wheel | $[rad]$ |
| $\alpha_4$ | side slip angle of the drawbar wheel | $[rad]$ |
| $\alpha_5$ | side slip angle of the trailer first rear wheel | $[rad]$ |
| $\alpha_6$ | side slip angle of the trailer second rear wheel | $[rad]$ |
| $F_{y1}$ | lateral tyre force of the truck front wheel | $[N]$ |
| $F_{y2}$ | lateral tyre force of the truck first rear wheel | $[N]$ |
| $F_{y3}$ | lateral tyre force of the truck second rear wheel | $[N]$ |
| $F_{y4}$ | lateral tyre force of the drawbar wheel | $[N]$ |
| $F_{y5}$ | lateral tyre force of the trailer first rear wheel | $[N]$ |
| $F_{y6}$ | lateral tyre force of the trailer second rear wheel | $[N]$ |

Table 4.1: Truck/full-trailer characteristics

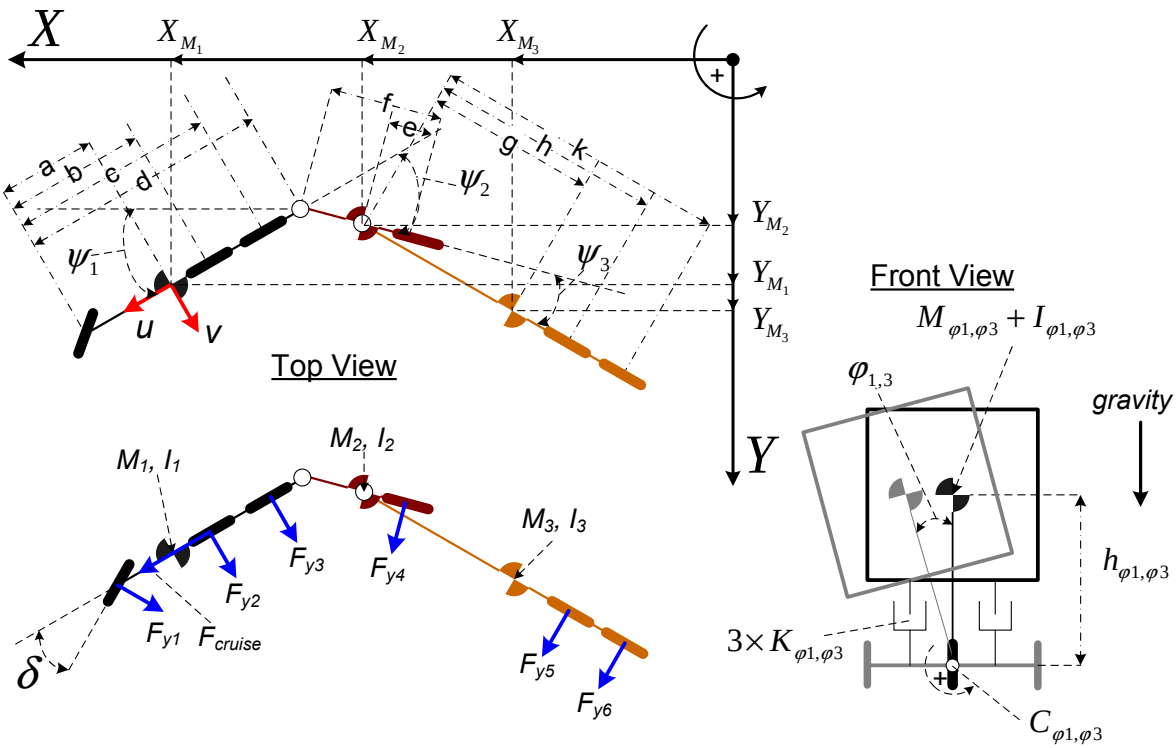


Figure 4.2: Dynamic model of a truck/full-trailer combination

### 4.2.1 Non-linear equations of motion

For the derivation of the non-linear equations of motion of the dynamic vehicle model the Lagrange formulation is used. The generalized coordinates are:

$$
\begin{aligned}
q &= \left[ \int_o^t U\ dt,\quad \int_o^t V\ dt,\quad \psi_1,\quad \psi_2,\quad \psi_3,\quad \varphi_1,\quad \varphi_3 \right]^T \\
\dot{q} &= \left[ U,\quad V,\quad \dot{\psi}_1,\quad \dot{\psi}_2,\quad \dot{\psi}_3,\quad \dot{\varphi}_1,\quad \dot{\varphi}_3 \right]^T \\
\ddot{q} &= \left[ \dot{U},\quad \dot{V},\quad \ddot{\psi}_1,\quad \ddot{\psi}_2,\quad \ddot{\psi}_3,\quad \ddot{\varphi}_1,\quad \ddot{\varphi}_3 \right]^T
\end{aligned}
\tag{4.1}
$$

The first two generalized displacement coordinates, $\int_o^t U\ dt$ and $\int_o^t V\ dt$, are expressed in a moving coordinate system with respect to the truck chassis mass. The third generalized coordinate ($\psi_1$) is expressed with respect to the fixed coordinate system. This implies that for these three generalized coordinates the modified Lagrange formulation has to be used (B.2). The other generalized coordinates ($\psi_2$, $\psi_3$, $\varphi_1$, $\varphi_3$) are expressed in the moving coordinate system at which the normal Lagrange formulation can be used. For the derivation of the non-linear equations of motion a combination of the two Lagrange formulations, as shown in appendix B (B.4), is used.

### Velocities in the dynamic vehicle model

For the energy formulations and the generalized external forces various velocities of the dynamic vehicle model have to be known. Therefore the forward and lateral velocities of the masses and tyres in the dynamic vehicle model, as shown (numbered) in figure 4.3, will be determined.

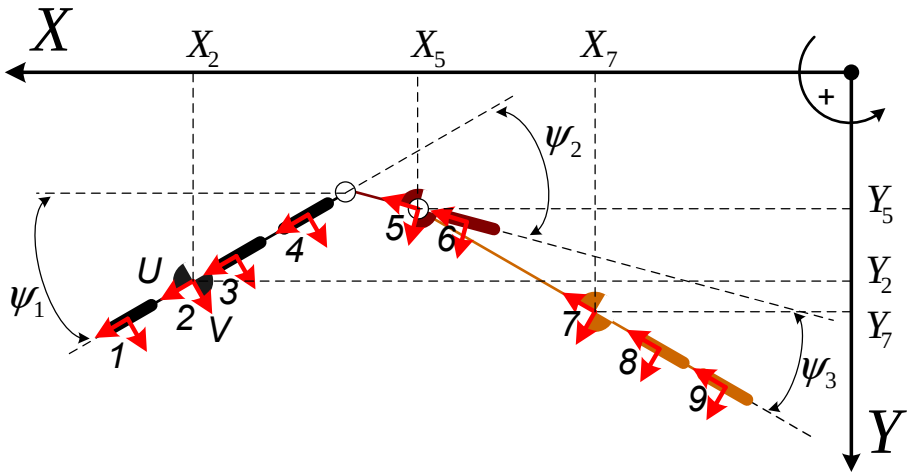


Figure 4.3: The velocities of chassis masses and tyres

Using figures 4.2 and 4.3 the velocities of the truck can be simply determined:

$$
\begin{aligned}
&U_1 = U \\
&V_1 = V + a\ \dot{\psi}_1 \\
&\\
&U_2 = U \\
&V_2 = V \\
&\\
&U_3 = U \\
&V_3 = V - (b-a)\ \dot{\psi}_1 \\
&\\
&U_4 = U \\
&V_4 = V - (c-a)\ \dot{\psi}_1
\end{aligned}
\tag{4.2}
$$

It is more difficult to determine the velocities of the drawbar and trailer. First the velocities of the drawbar chassis mass will be determined. The spatial positions of the drawbar chassis mass are expressed in the fixed coordinate system:

$$
\begin{aligned}
&X_5 = X_2 - (d-a)\cos(\psi_1) - (f-e)\cos(\psi_2 - \psi_1) \\
&\\
&Y_5 = Y_2 - (d-a)\sin(\psi_1) + (f-e)\sin(\psi_2 - \psi_1)
\end{aligned}
\tag{4.3}
$$

These equations have to be differentiate with respect to time $t$ for the corresponding velocities:

$$\begin{aligned}\dot{X}_5 &= \tfrac{dX_5}{dt} = \dot{X}_2 + (d-a)\dot{\psi}_1 \sin(\psi_1) + (f-e)(\dot{\psi}_2 - \dot{\psi}_1)\sin(\psi_2 - \psi_1) \\ \dot{Y}_5 &= \tfrac{dY_5}{dt} = \dot{Y}_2 - (d-a)\dot{\psi}_1 \cos(\psi_1) + (f-e)(\dot{\psi}_2 - \dot{\psi}_1)\cos(\psi_2 - \psi_1)\end{aligned} \tag{4.4}$$

Conversion from the fixed coordinate system in the moving coordinate system, with respect to the truck chassis mass in the $U/V$-direction, gives:

$$\begin{aligned}U_i &= \dot{X}_i \cos(\psi_1) + \dot{Y}_i \sin(\psi_1) \\ V_i &= -\dot{X}_i \sin(\psi_1) + \dot{Y}_i \cos(\psi_1)\end{aligned} \tag{4.5}$$

and vice versa:

$$\begin{aligned}\dot{X}_i &= U_i \cos(\psi_1) - V_i \sin(\psi_1) \\ \dot{Y}_i &= U_i \sin(\psi_1) + V_i \cos(\psi_1)\end{aligned} \tag{4.6}$$

Substitution of (4.6) in (4.4) gives:

$$\begin{aligned}U_5^* \cos(\psi_1) - V_5^* \sin(\psi_1) &= U_2 \cos(\psi_1) - V_2 \sin(\psi_1) + (d-a)\dot{\psi}_1 \sin(\dot{\psi}_1) + \ldots \\ &\qquad (f-e)(\dot{\psi}_2 - \dot{\psi}_1)\sin(\psi_2 - \psi_1) \\ U_5^* \sin(\psi_1) + V_5^* \cos(\psi_1) &= U_2 \sin(\psi_1) + V_2 \cos(\psi_1) - (d-a)\dot{\psi}_1 \cos(\dot{\psi}_1) + \ldots \\ &\qquad (f-e)(\dot{\psi}_2 - \dot{\psi}_1)\cos(\psi_2 - \psi_1)\end{aligned} \tag{4.7}$$

where $U_5^*$ and $V_5^*$ are the velocities of the drawbar chassis mass in the $U/V$-direction.

Multiplying the first and second part of (4.7) with $cos(\psi_1)$ and $sin(\psi_1)$ respectively and adding the resulting equations results in the forward velocity expressed in the moving coordinate system with respect to the truck mass in the $U/V$-direction:

$$U_5^* = U_2 + (f-e)(\dot{\psi}_2 - \dot{\psi}_1)\sin(\psi_2) \tag{4.8}$$

Multiplying the first and second part of (4.7) with $sin(\psi_1)$ and $cos(\psi_1)$ respectively and subtract the resulting equations gives the lateral velocity of the drawbar in the $U/V$-direction:

$$V_5^* = V_2 - (d-a)\dot{\psi}_1 + (f-e)(\dot{\psi}_2 - \dot{\psi}_1)\cos(\psi_2) \tag{4.9}$$

The final step is to rotate the velocities with the yaw angle between the truck and drawbar, $\psi_2$, and substitute the velocities $U_2 = U$ and $V_2 = V$ (4.2) which gives the forward and the lateral velocity of the drawbar chassis mass:

$$\begin{aligned}U_5 &= U_5^* \cos(\psi_2) - V_5^* \sin(\psi_2) \\ &= U\cos(\psi_2) - V\sin(\psi_2) + (d-a)\dot{\psi}_1 \sin(\psi_2) \\ V_5 &= U_5^* \sin(\psi_2) + V_5^* \cos(\psi_2) \\ &= U\sin(\psi_2) + V\cos(\psi_2) - (d-a)\dot{\psi}_1 \cos(\psi_2) + (f-e)(\dot{\psi}_2 - \dot{\psi}_1)\end{aligned} \tag{4.10}$$

With the shown method for deriving the drawbar chassis mass velocities (4.3 - 4.10), the remaining velocities of the masses and tyres can be determined as shown in appendix E.1.

### Energy formulations

The dynamic vehicle model of the truck/full-trailer combination contains kinetic energy $T_{kin}$, potential energy $U_{pot}$ and dissipation energy $D_{diss}$ which can be expressed as:

$$\begin{aligned} T_{kin} = {} & 1/2\ M_1\ (U_2^2 + V_2^2) + 1/2\ I_1\ \dot{\psi}_1^2 + \dots \\ & 1/2\ M_2\ (U_5^2 + V_5^2) + 1/2\ I_2\ \left(\dot{\psi}_2 - \dot{\psi}_1\right)^2 + \dots \\ & 1/2\ M_3\ (U_7^2 + V_7^2) + 1/2\ I_3\ \left(\dot{\psi}_3 + \dot{\psi}_2 - \dot{\psi}_1\right)^2 + \dots \\ & 1/2\ M_{\varphi 1}\left(U_{\varphi 1}^2 + V_{\varphi 1}^2\right) + 1/2\ I_{\varphi 1}\ \dot{\varphi}_1^2 + \dots \\ & 1/2\ M_{\varphi 3}\left(U_{\varphi 3}^2 + V_{\varphi 3}^2\right) + 1/2\ I_{\varphi 3}\ \dot{\varphi}_3^2 \end{aligned} \tag{4.11}$$

$$\begin{aligned} U_{pot} = {} & 1/2\ C_{\varphi 1}\ \varphi_1^2 - M_{\varphi 1}\ gravity\ h_{\varphi 1} \cos(\varphi_1) + \dots \\ & 1/2\ C_{\varphi 3}\ \varphi_3^2 - M_{\varphi 3}\ gravity\ h_{\varphi 3} \cos(\varphi_3) \end{aligned} \tag{4.12}$$

$$D_{diss} = 1/2\,(3\ K_1\ L_1)\,\dot{\varphi}_1^2 + 1/2\,(3\ K_3\ L_3)\,\dot{\varphi}_3^2 \tag{4.13}$$

### Generalized external forces

The generalized external forces $Q_i^{ex}$ are introduced with the lateral tyre forces $F_{yi}$. The velocity vectors $r_i$ of the generalized external forces are expressed in the moving generalized coordinates in the $U/V$-direction. The corresponding velocity vectors $r_i$, the external forces $F_i$ and the lateral tyre forces $F_{yi}$ are shown in appendix E.2.

### Ordinary differential equation

All components of the Lagrange formulation have been derived. The determination of the non-linear equations of motion by hand will be difficult next to impossible by the large size of the velocity equations. Therefore the non-linear equations of motion will be derived using MATLAB. The approach of the used *m-file*, as shown in appendix F, is to calculate the second-order derivatives of the generalized coordinates, expressed as:

$$\ddot{q} = \mathbf{M}(q,\ \theta)^{-1}\ \ f(q,\ \dot{q},\ u,\ \theta) \qquad [7 \times 1] \tag{4.14}$$

where $\mathbf{M}(q,\ \theta)$ is the mass matrix, $u = [\delta,\ F_{cruise}]^T$ the input vector and $\theta$ the vehicle parameters.

The *m-file* calculates the mass matrix $\mathbf{M}(q,\ \theta)$ and $f(q,\ \dot{q},\ u,\ \theta)$. The resulting $\mathbf{M}(q,\ \theta)$ and $f(q,\ \dot{q},\ u,\ \theta)$ are too large to present in this report and it is left to the reader to run the *m-file*.

### 4.2.2 Validation of the non-linear equations of motion

As in the previous chapter a SimMechanics model has been made to verify the correctness of the derived non-linear equations of motion. The graphical representation of the truck/full-trailer SimMechanics model is shown in figure 4.4. Simulation of the derived non-linear equations is done using the MATLAB *ode45* integrator. The inputs and initial conditions of the *ode45* solver and the SimMechanics model are given in table 4.2. The simulation results are shown in figure 4.5 and 4.6, which shows a similarity of the responses (vehicle characteristics) between the derived non-linear equations of motions and the SimMechanics model for the given steering input and IC's.

*Note:* Figure 4.5 shows that the yaw-sensor $\psi_1$ in the SimMechanics model has a measurement range of $-180 \leq \psi_1 \leq 180$ $[deg]$.

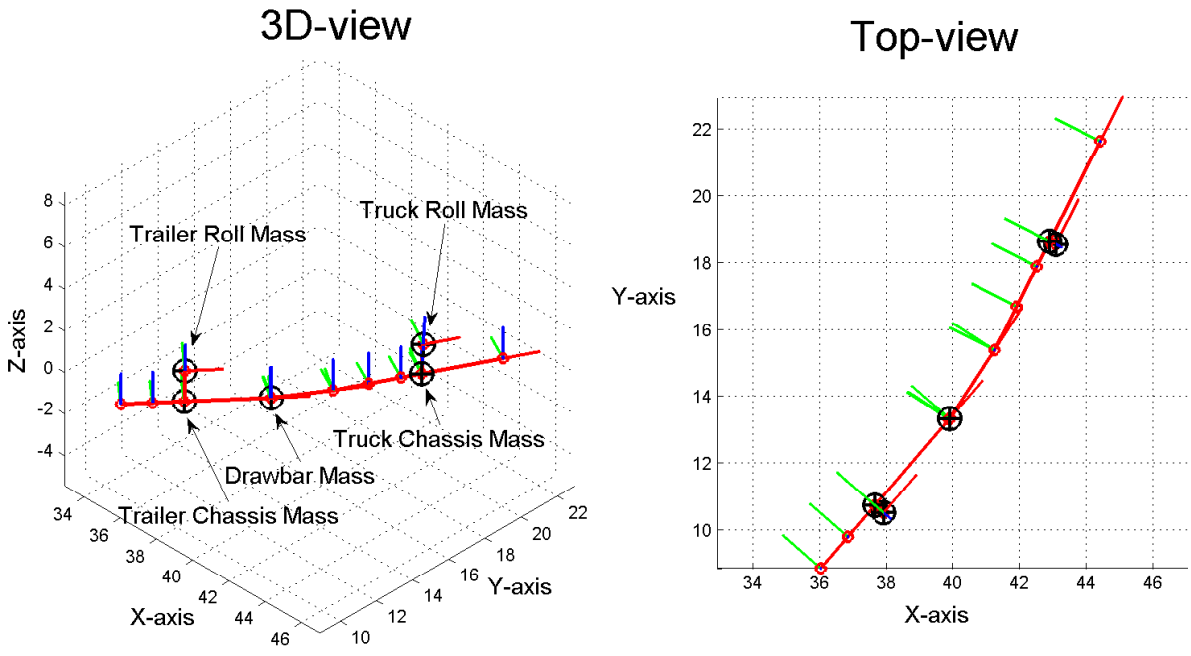


Figure 4.4: Truck/full-trailer SimMechanics model

| **Input** | **Value** | **Unit** |
|---|---|---|
| $\delta$ | $5 \cdot \pi/180$ | $[rad]$ |
| $F_{cruise}$ | 0 | $[N]$ |
| **IC at** $t = 0$ $[s]$ | **Value** | **Unit** |
| $U$ | 20 | $[m/s]$ |

Table 4.2: Settings for simulation of the non-linear equations of motion and the SimMechanics model of the truck/full-trailer combination

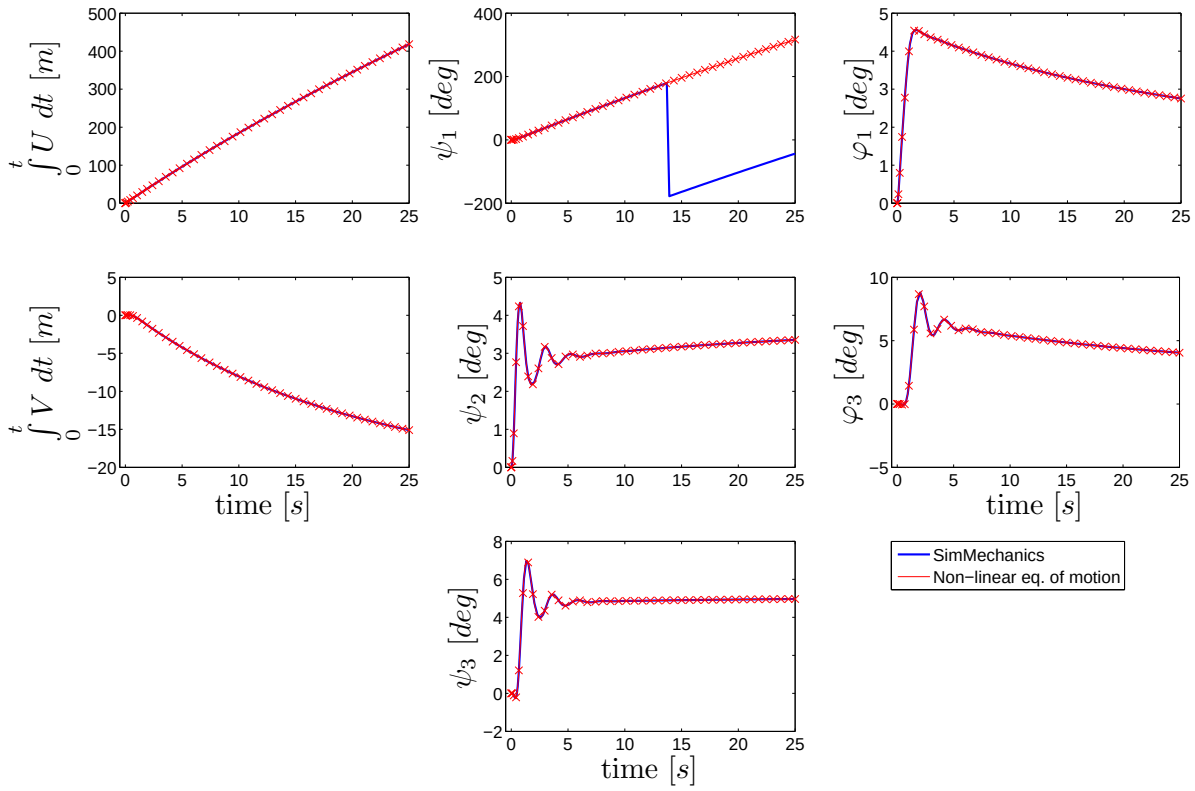


Figure 4.5: Responses of the generalized displacement coordinates $q$ of the non-linear equations of motion and the SimMechanics model of the truck/full-trailer dynamic model

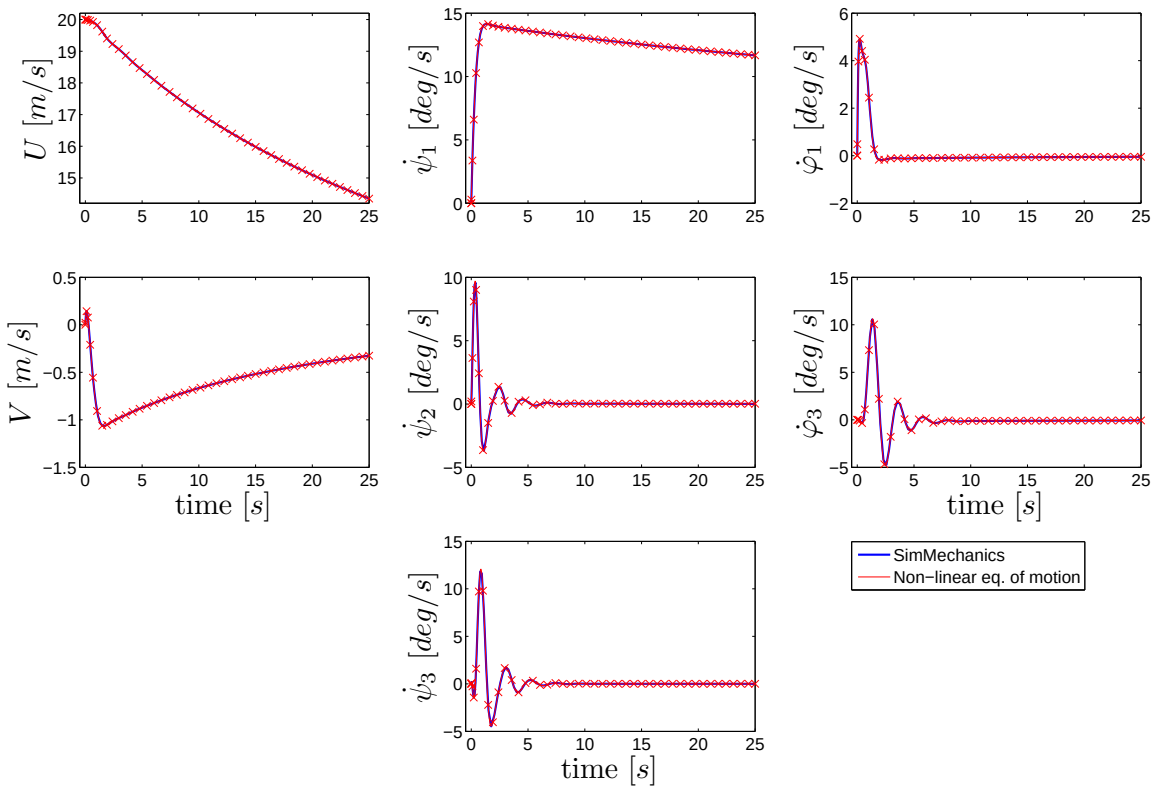


Figure 4.6: Responses of the generalized velocity coordinates $\dot{q}$ of the non-linear equations of motion and the SimMechanics model of the truck/full-trailer dynamic model

## 4.3 Stability analysis of the truck/full trailer combination

To analyse the stability of the dynamic truck/full-trailer model around a specified trajectory, the nominal trajectories have to be found. Using these nominal trajectories the non-linear tracking error dynamics can be derived. Based on the linearized tracking error dynamics the stability of the truck/full-trailer combination can be analyzed around those nominal trajectories.

The purpose is to analyse the stability around a lane-change trajectory, however to make the linearization process easier the stability will be studied around nominal straight-line and nominal circle trajectories.

### 4.3.1 Nominal straight-line trajectory

With the numerical MATLAB *fsolve.m* procedure, as shown in previous chapter and appendix C, a nominal trajectory can be found. The assumptions for a straight-line trajectory $x_{SL} = [q_{traj}, \dot{q}_{traj}]^T$ are:

- The second-order derivatives of the generalized coordinates are chosen to be constant in time:
  $\ddot{q}_{traj} = \left[ \begin{array}{ccccccc} \dot{U}_{traj}, & \dot{V}_{traj}, & \ddot{\psi}_{1,\,traj}, & \ddot{\psi}_{2,\,traj}, & \ddot{\psi}_{3,\,traj}, & \ddot{\varphi}_{1,\,traj}, & \ddot{\varphi}_{3,\,traj} \end{array} \right]^T = 0$

- A constant forward velocity, for example $U_{traj} = 20\ [m/s]$

- A constant yaw-rate of the drawbar and trailer in time and a constant roll-rate in time:
  $\left[ \begin{array}{cccc} \dot{\psi}_{2,\,traj}, & \dot{\psi}_{3,\,traj}, & \dot{\varphi}_{1,\,traj}, & \dot{\varphi}_{3,\,traj} \end{array} \right]^T = 0$

- The lateral velocity of the truck depends on the truck side slip angle $\beta_{traj}$ via:
  $V_{traj} = -U_{traj} \tan(\beta_{traj})$

- The inputs are zero for a straight-line trajectory:
  $\left[ \begin{array}{cc} \delta_{traj}, & F_{cruise,\,traj} \end{array} \right]^T = \left[ \begin{array}{cc} 0, & 0 \end{array} \right]^T$

  In practice a constant forward velocity can maintained by an engine torque ($F_{cruise,\,traj} \neq 0$) to counterbalance the vehicle resistances, such as the aerodynamic drag and the tyre roll resistance. These resistances are neglected in the dynamic vehicle model and therefore $F_{cruise,\,traj} = 0$.

- The vehicle characteristics which have to be determined are:
  $\beta_{traj},\ \psi_{2,\,traj},\ \psi_{3,\,traj},\ \varphi_{1,\,traj},\ \varphi_{3,\,traj}$ *and* $\dot{\psi}_{1,\,traj}$

Solving the non-linear equations of motion with these assumptions, the generalized coordinates and inputs of the nominal straight-line trajectory are:

$$\begin{aligned} x_{SL} &= \begin{bmatrix} \int_0^t U_{traj}\, dt & \int_0^t V_{traj}\, dt & \psi_{1,\,traj} & \psi_{2,\,traj} & \psi_{3,\,traj} & \varphi_{1,\,traj} & \varphi_{3,\,traj} \\ U_{traj} & V_{traj} & \dot{\psi}_{1,\,traj} & \dot{\psi}_{2,\,traj} & \dot{\psi}_{3,\,traj} & \dot{\varphi}_{1,\,traj} & \dot{\varphi}_{3,\,traj} \end{bmatrix} \\ &= \begin{bmatrix} 20t & 0 & 0 & 0 & 0 & 0 & 0 \\ 20 & 0 & 0 & 0 & 0 & 0 & 0 \end{bmatrix} \\ u_{SL} &= \begin{bmatrix} \delta_{traj}, & F_{cruise,\,traj} \end{bmatrix}^T = \begin{bmatrix} 0, & 0 \end{bmatrix}^T \end{aligned} \tag{4.15}$$

### Non-linear tracking error dynamics around a nominal trajectory

Using the nominal straight-line trajectory the non-linear tracking error dynamics of the truck/full-trailer combination can be derived and written in the following state space form:

$$\begin{bmatrix} \dot{e} \\ \ddot{e} \end{bmatrix} = \begin{bmatrix} \dot{e} \\ \mathbf{M}\,(e,\ q_{traj},\ \theta)^{-1}\ f\,(e,\ \dot{e},\ q_{traj},\ \dot{q}_{traj},\ \theta) \end{bmatrix} \quad (14 \times 1) \tag{4.16}$$

### Linearizing by using MATLAB

The size of the non-linear equations corresponding to the tracking error dynamics are large which makes the linearization by hand too difficult. Therefore, a MATLAB procedure has been written to compute the linearized tracking error dynamics:

- The non-linear tracking error dynamics are determined and for that purpose the inverse of the $\mathbf{M}\,(e,\ q_{traj},\ \theta)$ has to be calculated. The computation of this matrix inverse is not possible using the MATLAB function *inv* because this matrix contains too many symbols. To reduce the complexity of the computation of the non-linear tracking error dynamics, Cramer's rule has been used by which the size of the matrix $\mathbf{M}$ decreases in multiple matrices at which the function *inv* can be applied without computer memory problems or an increase of the calculation time.
- The derived non-linear tracking error dynamics will be linearized around: $\begin{bmatrix} e_{SL}, & \dot{e}_{SL} \end{bmatrix}^T = 0$.

### Stability analysis around the nominal straight-line trajectory

Using the nominal straight-line trajectory (4.15) the non-linear tracking error dynamics of the truck/full-trailer combination are derived. For the stability analysis around this nominal trajectory the corresponding linearized tracking error dynamics can be written as:

$$\begin{bmatrix} \dot{e}_{SL} \\ \ddot{e}_{SL} \end{bmatrix} = \mathbf{A}_{SL} \begin{bmatrix} e_{SL} \\ \dot{e}_{SL} \end{bmatrix} \tag{4.17}$$

with

$$\mathbf{A}_{SL}\,(14\times 14) = \begin{bmatrix} \mathbf{0} & \mathbf{I} \\ \mathbf{A}^{e}_{SL} & \mathbf{A}^{\dot{e}}_{SL} \end{bmatrix}$$

$$\mathbf{A}^{e}_{SL}\,(7\times 7) = \begin{bmatrix} 0 & 0 & 0 & 0 & 0 & 0 & 0 \\ 0 & 0 & 0 & -1.0668 & -0.8544 & -71.7607 & -0.6510 \\ 0 & 0 & 0 & 0.2555 & 0.2046 & -0.1895 & 0.1559 \\ 0 & 0 & 0 & -63.7691 & -30.5038 & 28.2466 & -23.2438 \\ 0 & 0 & 0 & 60.0239 & 18.1606 & -28.3203 & 22.3888 \\ 0 & 0 & 0 & -0.4135 & -0.3312 & -51.5222 & -0.2524 \\ 0 & 0 & 0 & -64.6364 & -44.8089 & -0.2687 & -38.7665 \end{bmatrix}$$

$$\mathbf{A}^{\dot{e}}_{SL}\,(7\times 7) = \begin{bmatrix} 0 & 0 & 0 & 0 & 0 & 0 & 0 \\ 0 & -6.6871 & -17.7017 & -0.3533 & -0.2217 & -4.6231 & -0.0447 \\ 0 & 0.1157 & -2.1971 & 0.0846 & 0.0531 & -0.0122 & 0.0107 \\ 0 & -0.2809 & 21.6650 & -15.8105 & -7.9170 & 1.8198 & -1.5946 \\ 0 & 0.2080 & -19.2457 & 11.9936 & 4.5479 & -1.8245 & 1.5359 \\ 0 & -2.5922 & 0.8909 & -0.1369 & -0.0860 & -3.3193 & -0.0173 \\ 0 & -3.2583 & 31.6524 & -19.8211 & -11.8411 & -0.0173 & -2.6594 \end{bmatrix}$$

The stability of the time invariant autonomous dynamics can be analyzed using the eigenvalues of the system matrix $\mathbf{A}_{SL}$, as shown in table 4.3. This table shows that four eigenvalues are at the imaginary axis. Three of these eigenvalues can be explained by the fact that the tracking error dynamics is independent of the generalized displacement coordinates $\int_0^t U\ dt$, $\int_0^t V\ dt$ and $\psi_1$. The fourth zero eigenvalue is caused by the fact that the tracking error dynamics around the nominal straight-line trajectory is independent of the forward velocity error $\dot{e}_1 = U - U_{traj}$. The remaining eigenvalues are stable by the negative real values.

| **Number** | **Eigenvalue** $[-]$ | **Damping ratio** $[-]$ | **Frequency** $[Hz]$ |
|---|---|---|---|
| 1, 2, 3 and 4 | 0 | - | - |
| 5 and 6 | -0.6797 ± 2.8535i | 0.2317 | 0.4669 |
| 7 and 8 | -1.1927 ± 4.8996i | 0.2365 | 0.8026 |
| 9 and 10 | -2.9669 ± 5.2438i | 0.4924 | 0.9589 |
| 11 and 12 | -3.0459 ± 1.7050i | 0.8726 | 0.5556 |
| 13 and 14 | -5.1775 ± 4.6178i | 0.7463 | 1.1042 |

Table 4.3: Eigenvalues, damping and frequency of the autonomous tracking error dynamics of the truck/full-trailer around the nominal straight-line trajectory

A graphical representation of the stability of the non-linear equations of motion around the nominal straight-line trajectory is made. The simulation results have been written in the spatial velocities expressed in a fixed world coordinate system, as shown in figure 4.7. This figure shows that by a perturbation on the initial conditions the velocities do not converge to the nominal straight-line trajectory as a result of the zero eigenvalue corresponding to the independency of the forward velocity error. Nevertheless, the figure shows by the displacements $x$ and $y$ that the vehicle combination drives a straight-line trajectory with a specified

offset caused by the perturbation. Figure 4.8 shows that the yaw angles $\psi_2$ & $\psi_3$ and the roll angles $\varphi_1$ & $\varphi_3$ converge to the nominal trajectory in time, as expected from the stable eigenvalues.

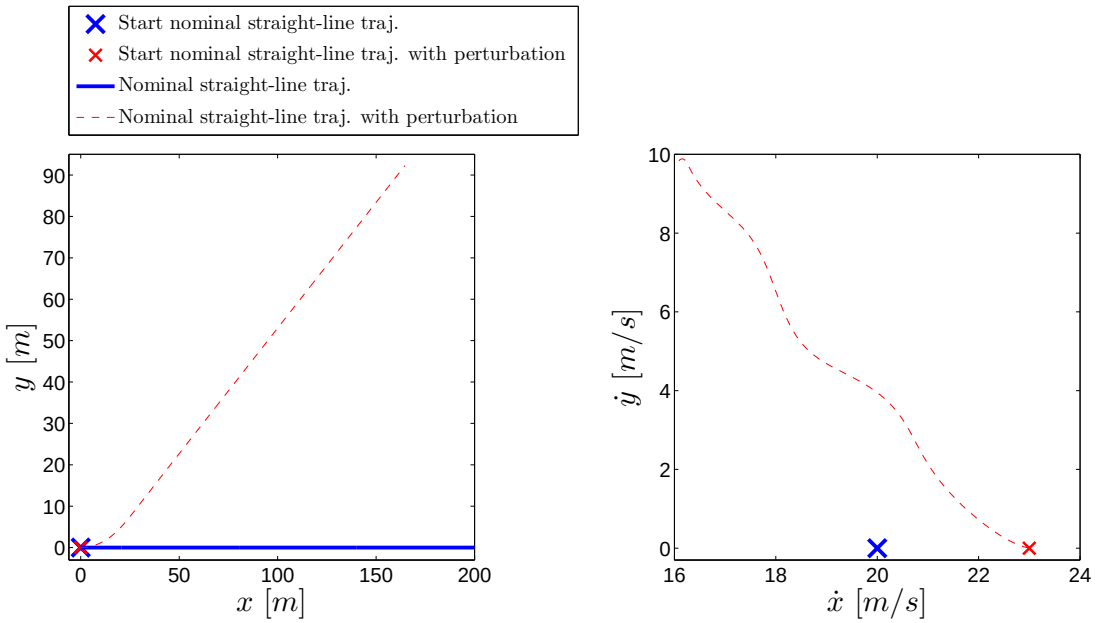


Figure 4.7: Global picture of the stability of the non-linear equations of motion around the nominal straight-line trajectory

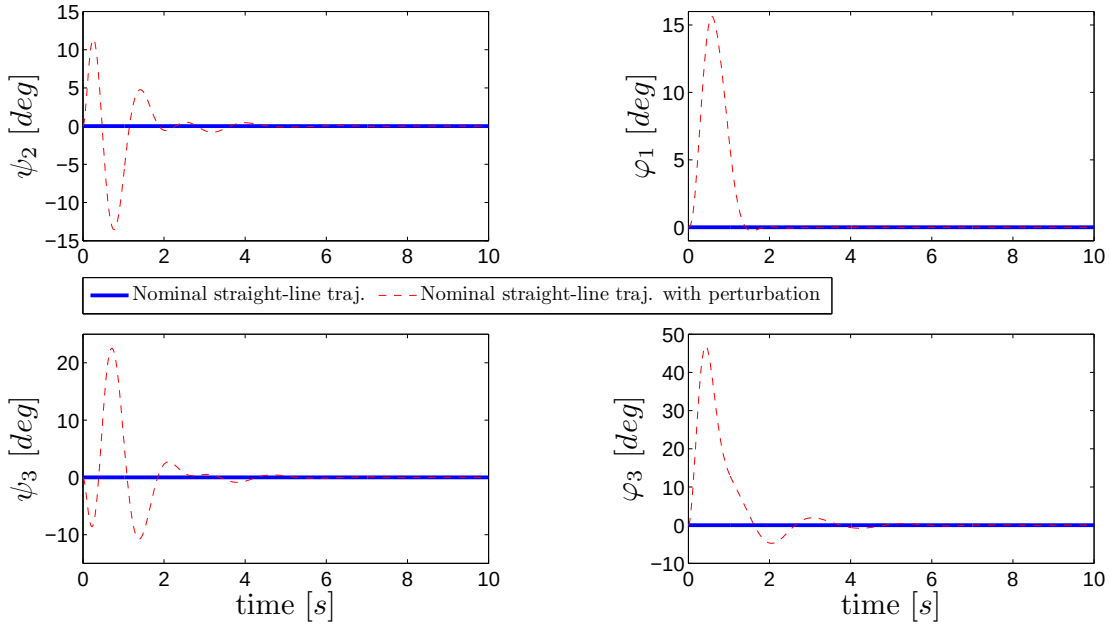


Figure 4.8: Global picture of the stability of yaw and roll angles around the nominal straight-line trajectory

### 4.3.2 Nominal circle trajectory

The assumptions for a nominal circle trajectory $x_{Circle} = [q_{traj}, \dot{q}_{traj}]^T$ are the same as for the nominal straight-line trajectory except for the inputs. Possible assumptions for the inputs can be $\delta_{traj} = 5$ $[deg]$ and $F_{cruise,traj} \neq 0$ $[N]$. Solving the non-linear equations of motion results in the generalized coordinates and inputs as shown in table 4.4.

| $\mathbf{q_{traj}}$ | **Value** | **Unit** | $\mathbf{\dot{q}_{traj}}$ | **Value** | **Unit** |
|---|---|---|---|---|---|
| $\int_0^t U_{traj}\ dt$ | $20t$ | $[m]$ | $U_{traj}$ | 20 | $[m/s]$ |
| $\int_0^t V_{traj}\ dt$ | $-1.0841t$ | $[m]$ | $V_{traj}$ | -1.0841 | $[m/s]$ |
| $\psi_{1,\ traj}$ | $13.8550t$ | $[deg]$ | $\dot{\psi}_{1,\ traj}$ | 13.8550 | $[deg/s]$ |
| $\psi_{2,\ traj}$ | 2.6254 | $[deg]$ | $\dot{\psi}_{2,\ traj}$ | 0 | $[deg/s]$ |
| $\psi_{3,\ traj}$ | 4.6309 | $[deg]$ | $\dot{\psi}_{3,\ traj}$ | 0 | $[deg/s]$ |
| $\varphi_{1,\ traj}$ | 4.5233 | $[deg]$ | $\dot{\varphi}_{1,\ traj}$ | 0 | $[deg/s]$ |
| $\varphi_{3,\ traj}$ | 6.6694 | $[deg]$ | $\dot{\varphi}_{3,\ traj}$ | 0 | $[deg/s]$ |
| **Input** | **Value** | **Unit** | **Symbol** | **Value** | **Unit** |
| $\delta_{traj}$ | 5 | $[deg]$ | $\beta_{traj}$ | 3.1026 | $[deg]$ |
| $F_{cruise,traj}$ | 19524.8725 | $[N]$ | $R_{traj}$ | 82.8290 | $[m]$ |

Table 4.4: Generalized coordinates ($q_{traj},\ \dot{q}_{traj}$), inputs ($\delta_{traj},\ F_{cruise,traj}$) and characteristics ($\beta_{traj},\ R_{traj}$) of a nominal circle trajectory of the truck/full-trailer combination

**Stability analysis around the nominal circle trajectory**

With the derived nominal circle trajectory the non-linear error dynamics can be determined and linearized with respect to this trajectory. The stability of the autonomous dynamics can be analyzed based on the time-invariant system matrix $\mathbf{A}_{Circle}$ as shown in appendix G. The corresponding eigenvalues are shown in table 4.5. This table shows that three eigenvalues are at the imaginary axis which corresponds, same observation as for stability analysis around the nominal straight-line trajectory, that the linearized tracking error dynamics is independent of the generalized coordinates $\int_0^t U\ dt$, $\int_0^t V\ dt$ and $\psi_1$. The remaining eigenvalues have a negative real part which corresponds with stable dynamics.

A graphical representation of the stability of the non-linear equations of motion around the nominal circle trajectory is made as shown in figures 4.9 and 4.10. These figures show that the generalized coordinates converge to the nominal circle trajectory in time, as expected from the eigenvalues around this nominal circle trajectory.

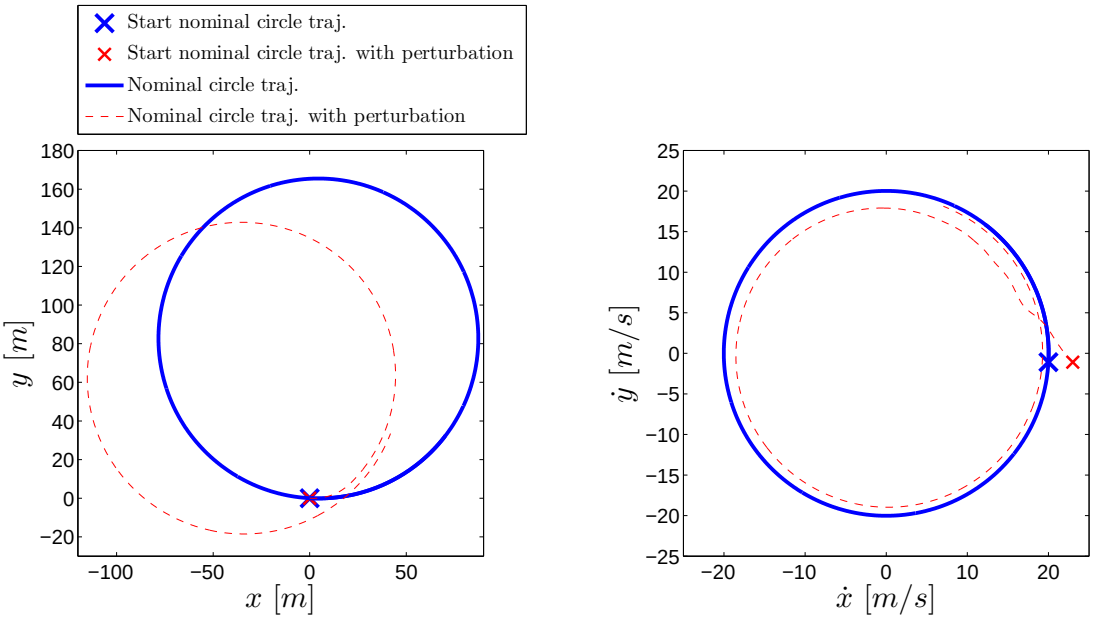


Figure 4.9: Global picture of the stability of the non-linear equations of motion around the nominal circle trajectory

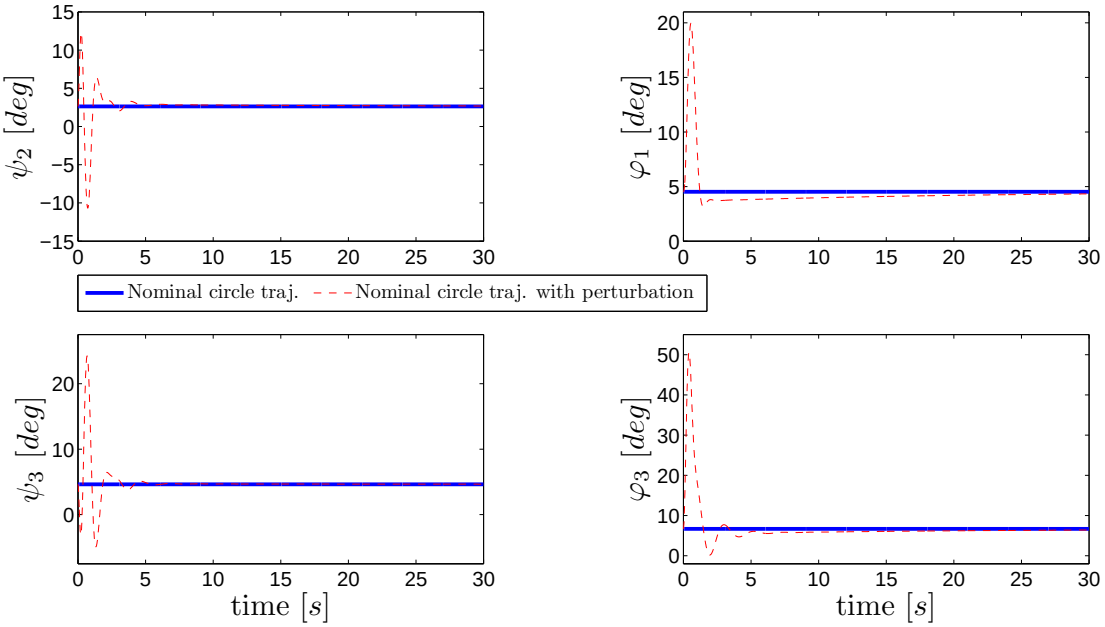


Figure 4.10: Global picture of the stability of yaw and roll angles around the nominal circle trajectory

| **Number** | **Eigenvalue** $[-]$ | **Damping ratio** $[-]$ | **Frequency** $[Hz]$ |
|---|---|---|---|
| 1, 2, 3 | 0 | - | - |
| 4 | -0.0542 | 1 | 0.0086 |
| 5 and 6 | -0.7020 ± 2.8837i | 0.2365 | 0.4724 |
| 7 and 8 | -1.1912 ± 4.9488i | 0.2340 | 0.8101 |
| 9 and 10 | -3.0190 ± 5.3106i | 0.4942 | 0.9722 |
| 11 and 12 | -3.0267 ± 1.7354i | 0.8675 | 0.5553 |
| 13 and 14 | -4.9435 ± 4.7485i | 0.7212 | 1.0910 |

Table 4.5: Eigenvalues, damping and frequency of the autonomous tracking error dynamics of the truck/full-trailer around the nominal circle trajectory

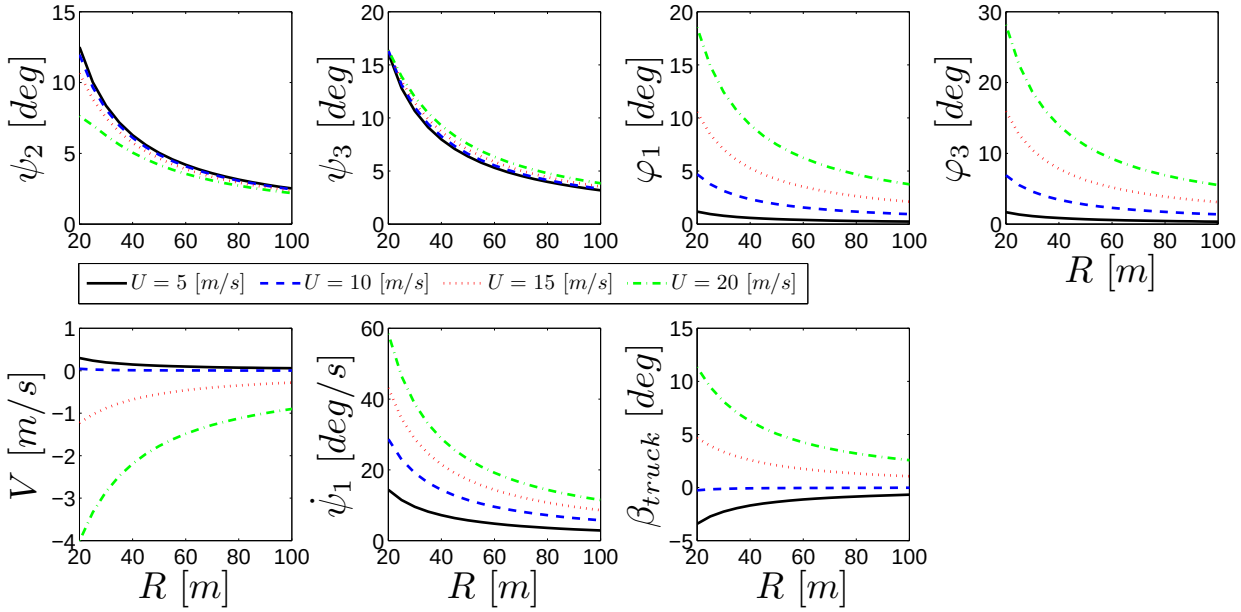


Figure 4.11: Vehicle characteristics of the truck/full-trailer combination for various nominal circle trajectories

Figure 4.10 shows a large magnitude of the roll angles, by which in practice the truck/full-trailer combination can rollover. For that account the rollover will be analyzed in the next section using the rollover criterium as presented in appendix A.

### 4.3.3 Vehicle handling study and stability analysis for various nominal circle trajectories

In this section the truck/full-trailer handling will be studied on the rollover phenomenon and yaw-rate instability. With the derived truck/full-trailer non-linear equations of motion various nominal circle trajectories can be determined for a number of forward velocities and a range of radii. The results of the derived vehicle characteristics and inputs are shown in figures 4.11 and 4.12 respectively.

**Rollover phenomenon**

In practice the truck/full-trailer combination will rollover driving a circle trajectory when

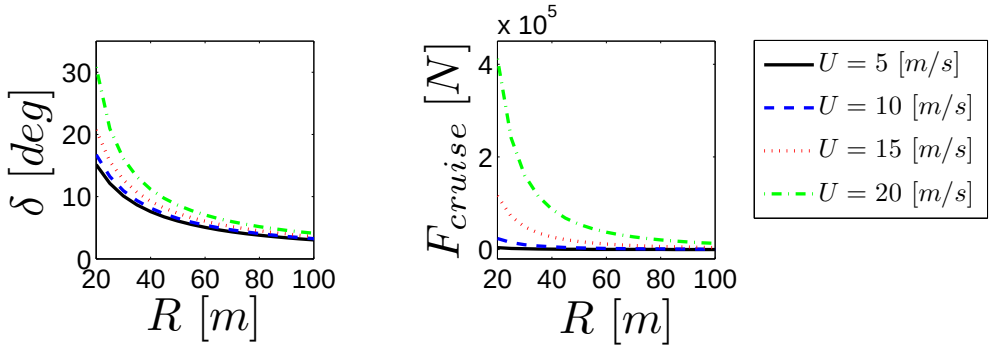


Figure 4.12: Vehicle inputs of the truck/full-trailer combination for various nominal circle trajectories

the lateral acceleration exceeds some threshold value. Appendix A shows how to determine the maximum allowable lateral acceleration by which a vehicle will not rollover. The vehicle combination exists of two elevated rollover masses, which results in two maximum allowable lateral accelerations of the truck and trailer. Because the dynamic vehicle model contains no tyre displacements the maximum lateral acceleration is only dependent on the suspension displacement $x_{susp}$, which results in the maximum lateral acceleration by computation of:

$$\begin{aligned} a_{roll} &= \tfrac{g(T/2-x_{susp})}{H} \\ with \quad x_{susp} &= \tfrac{-M_{susp}^2\ a_y\ H_{susp}^2}{M\ M_{susp}\ g\ H_{susp}-M\ C_\varphi} \end{aligned} \tag{4.18}$$

where $M_{susp} = M_{\varphi 1,\varphi 3}$ is the roll mass, $M = M_{1,3} + M_{\varphi 1,\varphi 3}$ is the total mass, $g$ is the gravitational acceleration, $T/2 = L_{1,3}$ is the virtual distance between the shock observers, $H = h_{\varphi 1,\varphi 3}$ is the height of the roll mass and $C_\varphi = C_{\varphi 1,\varphi 3}$ is the roll stiffness.

Rewriting (4.18) results in:

$$a_{y,roll\_i} = \frac{g\ L_i\,(M_i + M_{\varphi i})\,(M_{\varphi i}\ g\ h_{\varphi i} - C_{\varphi i})}{M_i\ M_{\varphi i}\ g\ h_{\varphi i}^2 - C_{\varphi i}\ h_{\varphi i}\,(M_i + M_{\varphi i})} \qquad with\ i = 1, 3 \tag{4.19}$$

Substitution of the truck/full-trailer parameters of appendix D results in the maximum allowable lateral acceleration of the truck ($i = 1$) and trailer ($i = 3$):

$$a_{y,roll\_truck} = 5.0024\ [\mathrm{m/s^2}]$$

$$a_{y,roll\_trailer} = 4.1661\ [\mathrm{m/s^2}]$$

The maximum allowable lateral acceleration of the truck/full-trailer combination is defined by the smallest $a_{y,roll}$ which is equal to $a_{y,roll\_trailer}$.

Using the SimMechanics model it is possible to determine the lateral acceleration of the truck and trailer for different circle trajectories. In the SimMechanics model a cruise controller has been made to keep a constant forward velocity while driving a circle trajectory. Lateral

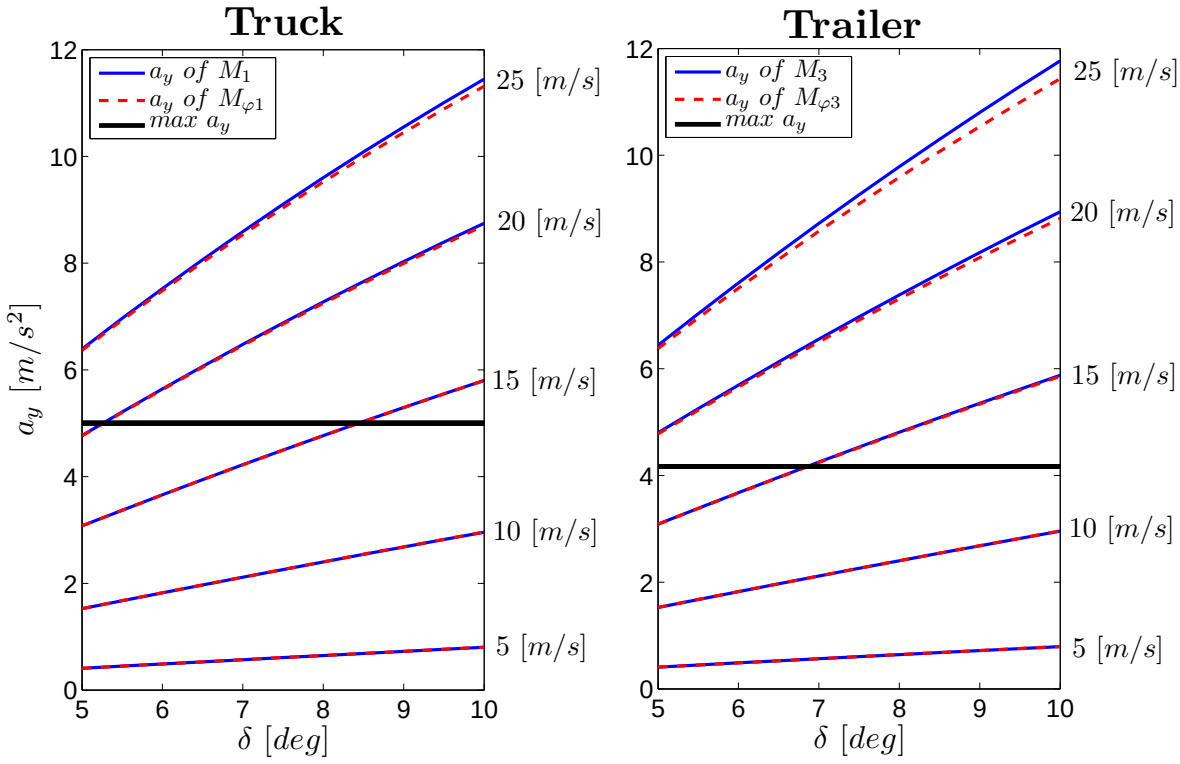


Figure 4.13: SimMechanics model: Lateral accelerations of various $a_y$ sensor locations due to different circle trajectories

acceleration sensors have been placed on the truck/trailer chassis masses and roll masses to analyse the difference in lateral acceleration by the various sensor locations. Figure 4.13 shows the lateral accelerations for different steering angle inputs and forward velocities. For constant circle trajectories this figure shows that there is no difference between the lateral acceleration of the chassis mass and roll mass below the maximum allowable lateral acceleration. Also there is no large difference between the lateral acceleration of the truck and trailer. This implies that a lateral acceleration sensor placed on the truck chassis mass is sufficient to analyse the lateral acceleration of the vehicle combination during a circle trajectory. This result meets one of the requirements of the problem statement, as discussed in section 1.2, which requires that only sensors can be placed on the truck of the vehicle combination.

Using figure 4.13 the critical nominal circle trajectories can be determined. The figure shows that with a forward velocity of 20 and 25 $[m/s]$ the vehicle combination will rollover driving a circle trajectory with a steering angle of 5 $[deg]$. Also with a forward velocity of 15 $[m/s]$ and a steering angle above 6.85 $[deg]$ the vehicle combination will rollover. Using the truck/full-trailer non-linear equations of motion the lateral acceleration of the truck chassis mass can be determined for different nominal circle trajectories as shown in figure 4.14. This figure shows that for the derived nominal circle trajectory, as shown in table 4.4, a lateral acceleration of $a_{y,roll\_truck} = \dot{V}_{traj} + U_{traj}\dot{\psi}_{traj} = 4.8363\ [m/s^2]$ will be reached resulting in a rollover of the trailer.

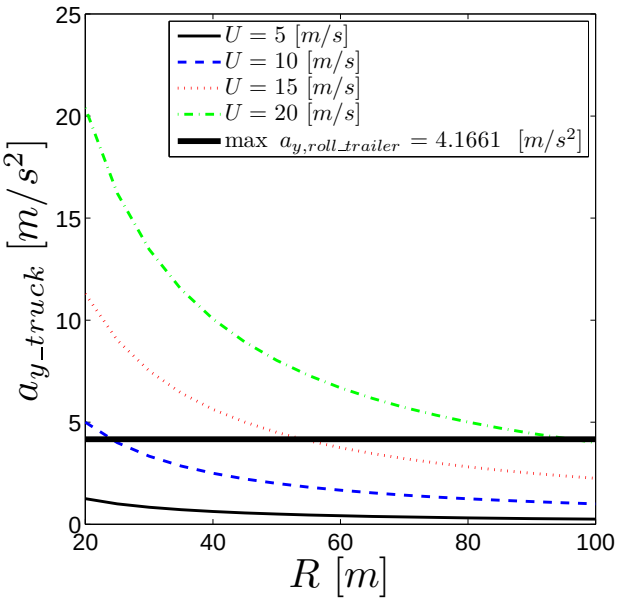


Figure 4.14: Non-linear equations of motion: Lateral acceleration of truck chassis mass for different circle trajectories. The maximum allowable $a_y$ shows the threshold when the vehicle combination will rollover

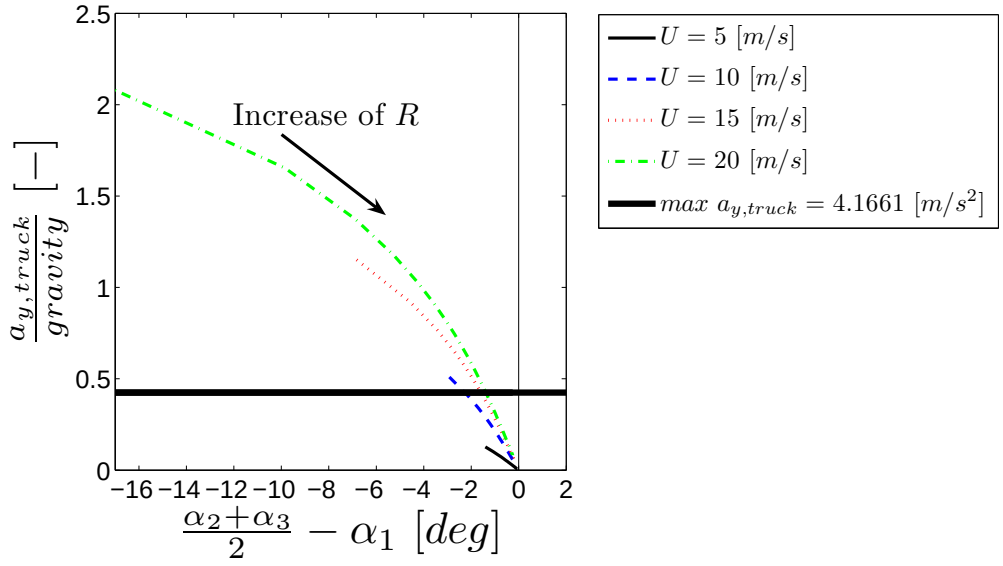


Figure 4.15: Vehicle handling diagram of the truck for various nominal circle trajectories

### Yaw-rate instability

The yaw-rate instability can be analyzed using a vehicle handling diagram, as discussed in section 3.3.9. Therefore the Ackerman steer relation has to be rewritten for the double rear axes of the truck in contrast with the bicycle model, found as [Erv83]:

$$\begin{aligned} &\tfrac{L}{R} - \delta = \alpha_1 - \tfrac{\alpha_2+\alpha_3}{2} \\ &with \quad L = \tfrac{b+c}{2} \end{aligned} \tag{4.20}$$

| | |
|---|---|
| Neutral steer | $\alpha_1 = \frac{\alpha_2+\alpha_3}{2}$ |
| Understeer | $\alpha_1 > \frac{\alpha_2+\alpha_3}{2}$ |
| Oversteer | $\alpha_1 < \frac{\alpha_2+\alpha_3}{2}$ |

Table 4.6: Neutral-, under- and oversteer of the truck of the vehicle combination

For various nominal circle trajectories a vehicle handling diagram has been made, as shown in figure 4.15. This figure has been created for various radii of $5 \leq R \leq 20$ $[m]$ with an iteration step of 5 $[m]$. With this figure and table 4.6 can be concluded that the truck is understeered for the nominal circle trajectories and by increasing $R$ or decreasing the forward velocity $U$ the truck is going to neutral steer.

### Stability analysis

To investigate the stability of the truck/full-trailer combination around various circle trajectories, the nominal circle trajectories have been determined with a lateral acceleration of the truck chassis mass below $a_{y,truck} = 4.1661$ $[m/s^2]$. The derived linearized tracking error dynamics around the nominal circle trajectories are time-invariant and the stability of corresponding autonomous dynamics can be analyzed using the corresponding eigenvalues, as show in figure 4.16.

To study the change in the stability margins of the truck/full-trailer combination using figure 4.16 is difficult. Therefore three situations will be highlighted:

- Various $a_{y,truck}$ at a constant $R$ as show in figure 4.17
  $\Rightarrow a_{y,truck} = 0.3,\ 4.0$ $[m/s^2]$ at $R = 100$ $[m]$
- Constant $a_{y,truck}$ at various $U$ and $R$ as shown in figure 4.17
  $\Rightarrow a_{y,truck} = 4.0$ $[m/s^2]$ at $U = 10,\ 20$ $[m/s]$ and $R = 25,\ 100$ $[m]$
- Eigenvalues around the origin for various $a_{y,truck}$ at a constant $R$ as shown in figure 4.18
  $\Rightarrow a_{y,truck} = 1.0,\ 2.3\ and\ 4.0$ $[m/s^2]$ at $R = 100$ $[m]$

Figure 4.17 shows that by increasing the lateral acceleration $a_{y,truck}$ (near to the rollover threshold) or by increasing the forward velocity $U$ some eigenvalues are moving in the direction of the imaginary axis. This movement of eigenvalues corresponds with a decrease of the truck/full-trailer stability margins and results in a slower system dynamics.

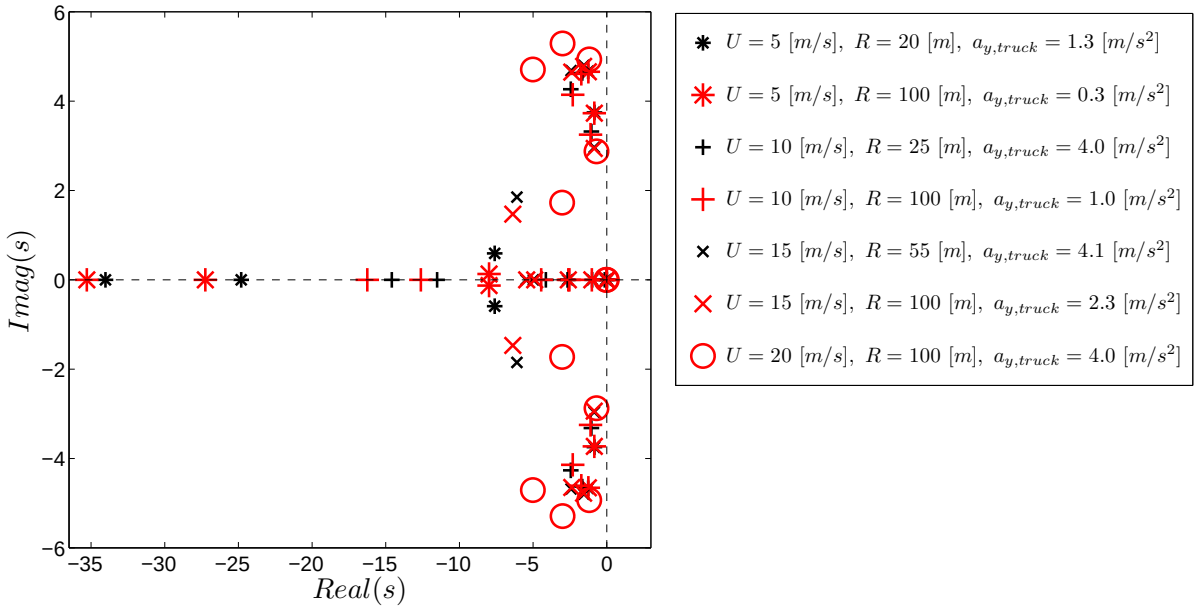


Figure 4.16: Eigenvalues of the autonomous tracking error dynamics of the truck/full-trailer combination around various nominal circle trajectories

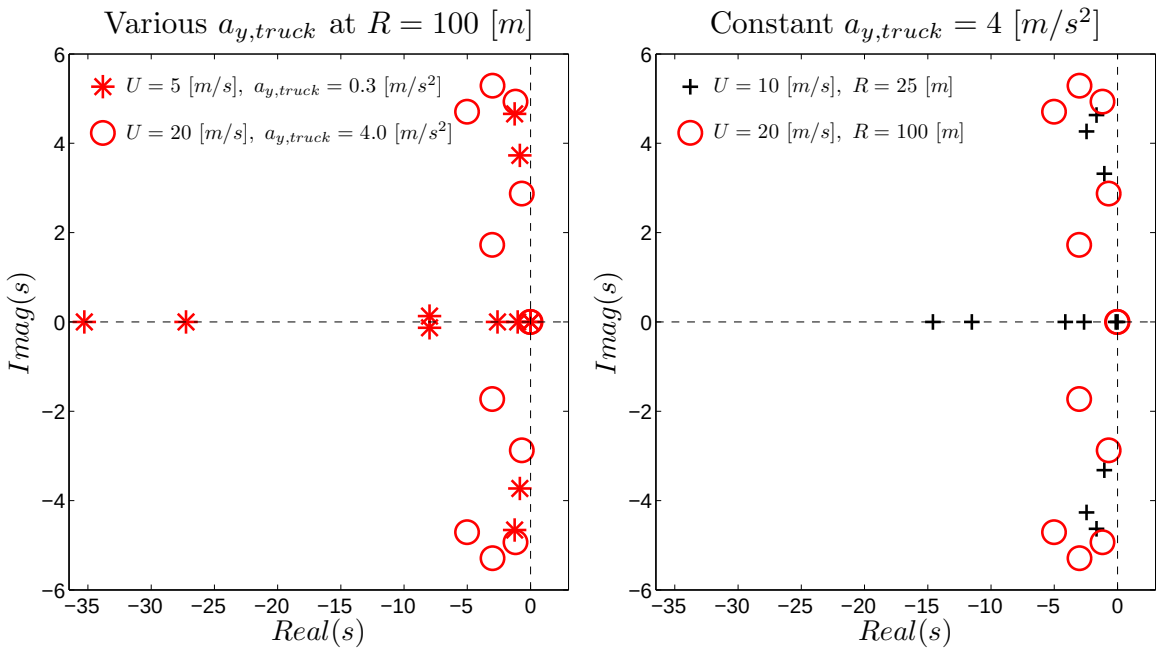


Figure 4.17: Eigenvalues of the autonomous tracking error dynamics of the truck/full-trailer combination around nominal circle trajectories with various and fixed $a_{y,truck}$

Figure 4.18 shows the eigenvalues close to the origin of the complex plane for various $a_{y,truck}$. For all sets of eigenvalues, three eigenvalues are at the origin which is the result by the independency of the generalized displacement coordinates $\int_0^t U\ dt$, $\int_0^t V\ dt$ and $\psi_1$ (as described in section 4.3.2). However in contrast with a previous observation, that by increasing the forward velocity (an increase of $a_{y,truck}$) the corresponding eigenvalues are moving in the direction of the imaginary axis, one eigenvalue moves in opposite direction. This phenomenon can be explained by the fact that the linearized tracking error dynamics with a forward velocity $U \to 0\ [m/s]$, will have an extra zero eigenvalue due to its independency of the forward velocity error in a non-moving mode.

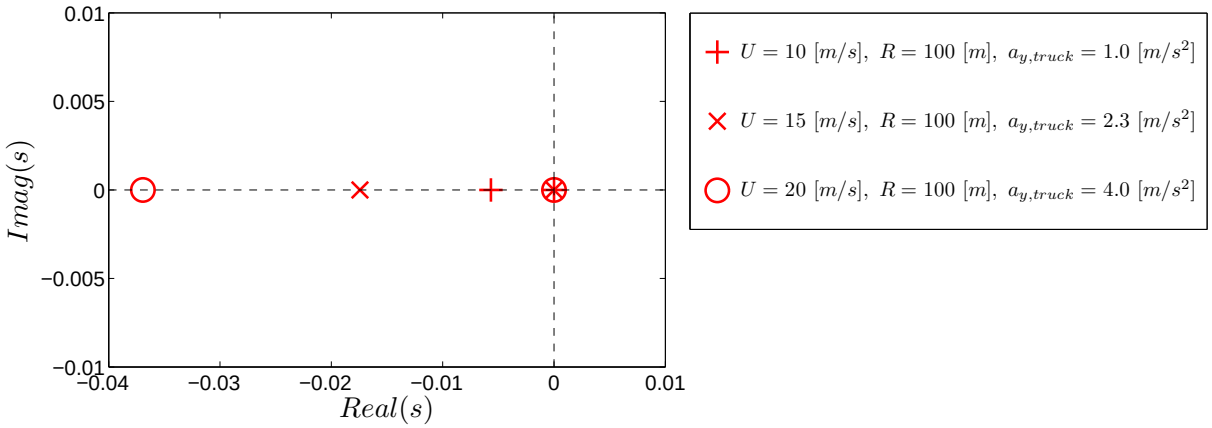


Figure 4.18: Eigenvalues, close to the origin of the complex plane, of the truck/full-trailer autonomous tracking error dynamics around nominal circle trajectories with various $a_{y,truck}$

## 4.4 Preliminary study for controller design

For designing a controller it is helpful to know which sensors and actuators can be used to measure and control all states in a more desirable manner. Therefore a preliminary study will be made using the observability and controllability of the truck/full-trailer combination.

Various sensors and actuators are placed on the truck/full-trailer combination which satisfies the requirements of the problem statement as discussed in section 1.2:

*"The controller design is restricted by the fact that sensors can only be placed on the truck. Control intervention can be applied by braking on both the truck as well on the full-trailer".*

Therefore the available sensors are a forward velocity sensor $U$ (based on the driver model as described in the previous chapter), a yaw-rate sensor $\dot{\psi}_1$ and a lateral acceleration sensor $a_{y,truck}$ placed on the truck chassis mass. An additional yaw-rate sensor will be placed on the trailer $\dot{\psi}_{trailer}$[1] to analyse if this will increase the observability. The available sensors are shown in figure 4.19.

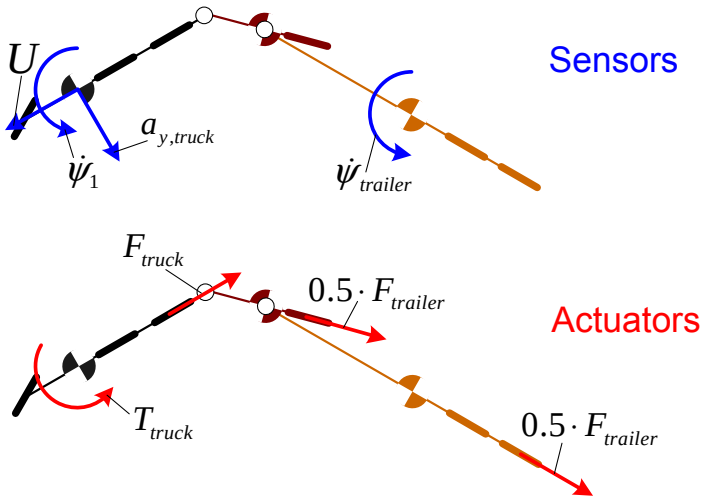


Figure 4.19: Sensors and actuators placed on the truck/full-trailer combination

Control intervention can be made with a force actuator $F_{truck}$ placed on the second rear axle of the truck, a torque actuator $T_{truck}$ acting on the truck chassis mass and a force actuator $F_{trailer}$ distributed (50 percent) over the drawbar axle and the second rear axle of the trailer. The available actuators are shown in figure 4.19. In practice, control intervention by using the force actuators can be done by simultaneous braking of the wheels on an axle. Control intervention of the torque actuator can be realized by selective braking of the individual wheels of the truck.

All error states ($[e, \dot{e}]$) of the linearized tracking error dynamics can be estimated and controlled when the rank of the observability and controllability matrices are equal to 14. However this full observability cannot be achieved by the fact that the non-linear equations of

[1] the equation of the trailer yaw-rate sensor $\dot{\psi}_{trailer} = \dot{\psi}_1 - \dot{\psi}_2 - \dot{\psi}_3$

motion of the truck/full-trailer combination are independent of the 3 generalized displacement coordinates: $\int_0^t U\ dt$, $\int_0^t V\ dt$ and $\psi_1$. Therefore the linearized tracking error dynamics of the truck/full-trailer combination around a nominal trajectory is maximal observable and maximal controllable when the rank of the corresponding matrices are equal to 11.

### 4.4.1 Observability and controllability around nominal straight-line trajectories

For the computation of the observability and controllability by the various sensor and actuator combinations, nominal straight-line trajectories are used with a forward velocity between 5 and 20 $[m/s]$. For each nominal straight-line trajectory the computed observability and controllability are shown in figures 4.21 and 4.22 respectively.

These figures show that by enlarging the forward velocity the observability and controllability increases. This observation is remarkable because the corresponding matrices have the same non-zero element distribution. Only the value of the non-zero cells change for increasing velocities. The change in the rank is caused by the ill-conditioned observability and controllability matrices which effects the numerical rank computation by using the MATLAB function *rank*.

The MATLAB *rank* function provides an estimate of the number of linearly independent rows or columns of a full matrix based on the number singular values of the matrix that are larger than a default tolerance [Mata]. This tolerance is dependent on the size of the matrix and the computers floating-point relative accuracy. Explanation of the numerical rank computation can be done by visualizing the factorized singular values of the matrix, as discussed in [KL80]. An example is given of the numerical rank determination of matrix $\mathbf{A}$ using the MATLAB function *rank*:

$$\mathbf{A} = \begin{bmatrix} 100.00 & 0.01 \\ -100.00 & 0.10 \end{bmatrix} \tag{4.21}$$

Singular values of $\mathbf{A}$:

$$svd(\mathbf{A}) = \begin{bmatrix} 141.4214 & 0.0778 \end{bmatrix}^T \tag{4.22}$$

Factorized singular values of $\mathbf{A}$:

$$20 \cdot \log 10 \left( \frac{svd(\mathbf{A})}{\max(svd(\mathbf{A})} \right) = \begin{bmatrix} 0 & -65.1927 \end{bmatrix}^T \ [db] \tag{4.23}$$

Computers floating-point relative accuracy:

$$eps = 2.2204 \cdot 10^{-16} \tag{4.24}$$

Rank tolerance of $\mathbf{A}$:

$$20 \cdot \log 10 \left( \max \left( size(\mathbf{A}) \right) \cdot eps \left( \max \left( svd(\mathbf{A}) \right) \right) \right) = -264.9064 \ [db] \tag{4.25}$$

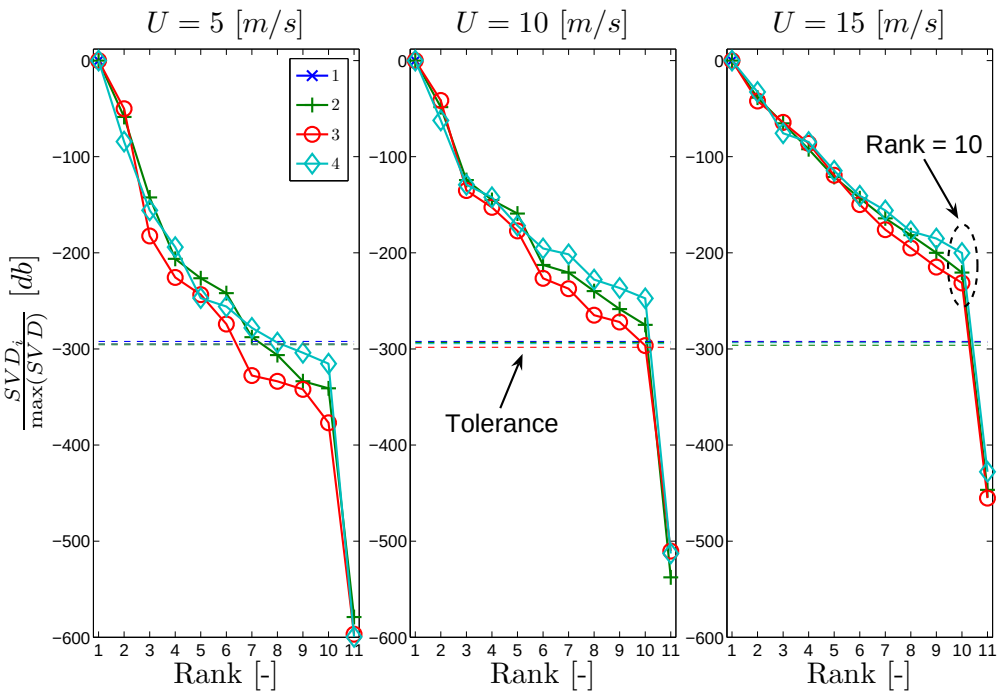


Figure 4.20: Visualization of the rank computation based on the factorized singular values. The rank is computed for the observability matrices using the sensors $1 = U$, $2 = \dot{\psi}_1$, $3 = a_{y,truck}$ and $4 = \dot{\psi}_{trailer}$ around straight-line trajectories with $U = 5, 10$ and $15\ [m/s]$

The factorized singular values (4.23) are above the determined tolerance (4.25) and the MATLAB *rank* function will compute a rank of the matrix $\mathbf{A}$ equal to 2.

The rank computation is visualized in figure 4.20 and shows that by increasing the forward velocity the singular values of observability matrices are moving above the rank tolerance. From this figure can be concluded that by driving a straight-line trajectory with a forward velocity of 15 $[m/s]$ the computed rank's are correct. In practice, truck/full-trailer combinations drive most of the time above this magnitude of forward velocity. Further conclusions of the computed observability and controllability will be draw of straight-line trajectories with $U = 15\ [m/s]$.

Figure 4.21 shows that by using one sensor the system has not the desired maximum observability property around a nominal straight-line trajectory with a forward velocity of 15 $[m/s]$. Using a combination with multiple sensors the system has the desired observability when the sensor combination contains the forward velocity sensors $U$. This sensor is necessary to predict the forward velocity error around a straight-line trajectory.

Concerning the controllability, as shown in figure 4.22, it can be concluded that using one actuator the system is not maximal controllable around a nominal straight-line trajectory with a forward velocity of 15 $[m/s]$. The system is maximal controllable when an actuator combination is used which contains the torque actuator $T_{truck}$.

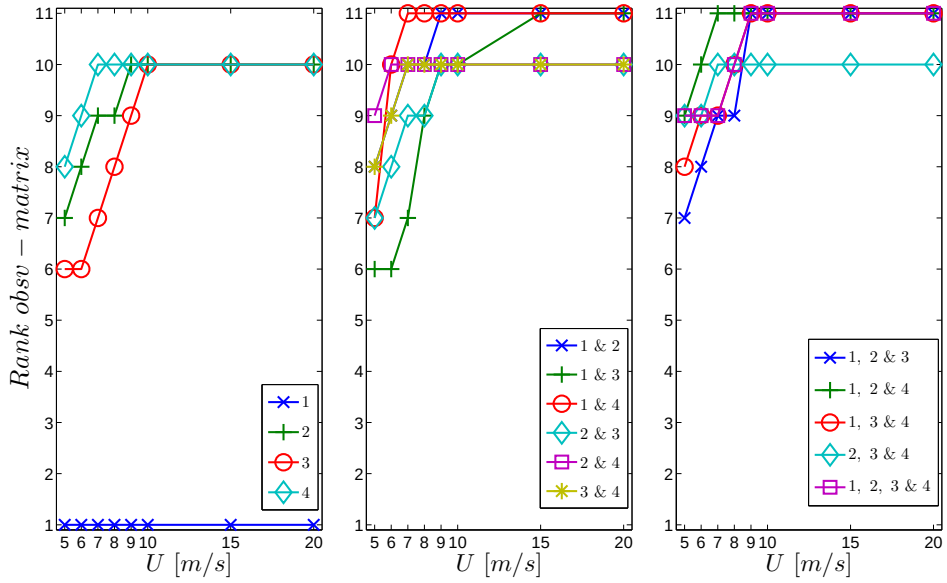


Figure 4.21: Observability of truck/full-trailer error states around nominal straight-line trajectories. Sensor combinations with $1 = U$, $2 = \dot{\psi}_1$, $3 = a_{y,truck}$ and $4 = \dot{\psi}_{trailer}$

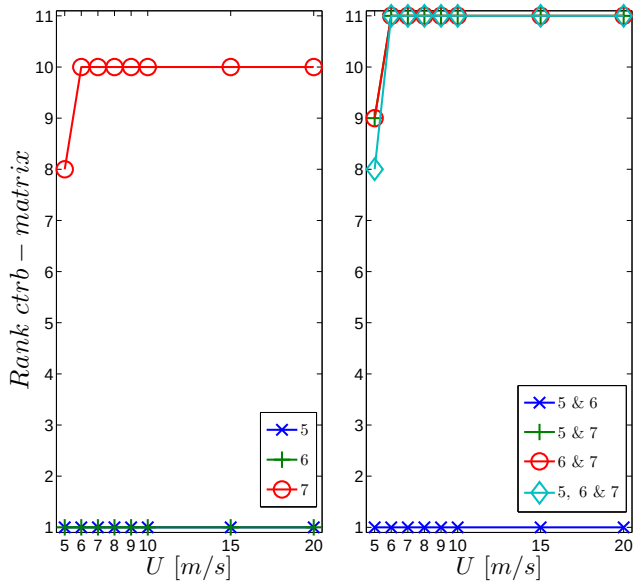


Figure 4.22: Controllability of the truck/full-trailer error states around nominal straight-line trajectories. Actuator combinations with $5 = F_{truck}$, $6 = F_{trailer}$ and $7 = T_{truck}$

### 4.4.2 Observability and controllability around nominal circle trajectories

For the derivation of the observability and controllability of the system around nominal circle trajectories, table 4.7 shows an overview of the different nominal circle trajectories where the lateral acceleration of the truck chassis mass is under the maximum allowable 4.1661 $[m/s^2]$ by which the vehicle combination will not rollover.

| $U\ [m/s]$ | 5 | 6 | 7 | 8 | 9 | 10 | 15 | 20 |
|---|---|---|---|---|---|---|---|---|
| $R < 100\ [m]$ | 20 | 20 | 20 | 20 | 20 | 25 | 55 | |
| $a_{y,truck}\ [m/s^2]$ | 1.2522 | 1.8024 | 2.4521 | 3.2015 | 4.0507 | 4.0000 | 4.0932 | |
| $R = 100\ [m]$ | 100 | 100 | 100 | 100 | 100 | 100 | 100 | 100 |
| $a_{y,truck}\ [m/s^2]$ | 0.2500 | 0.3600 | 0.4900 | 0.6400 | 0.8100 | 1.0000 | 2.2504 | 4.0040 |

Table 4.7: Radii and forward velocity for nominal circle trajectories where $a_{y,truck} < 4.1661\ [m/s^2]$

For these nominal circle trajectories the computed observabilities are shown in figures 4.23 and 4.24. The computed controllabilities are shown in figure 4.25. These figures show also that by enlarging the forward velocity of the nominal circle trajectory, the observability and controllability will increase. This is caused by the numerical rank computation as discussed before. Observing the nominal circle trajectory at a forward velocity of 15 $[m/s]$ the figures show that for all sensor and actuator combinations the system is maximal observable and maximal controllable. The use of a minimal amount of sensors and actuators is cost effective, however using more sensors/actuators can decrease the required controller gains when they are physical impossible, as discussed in section 3.6.2.

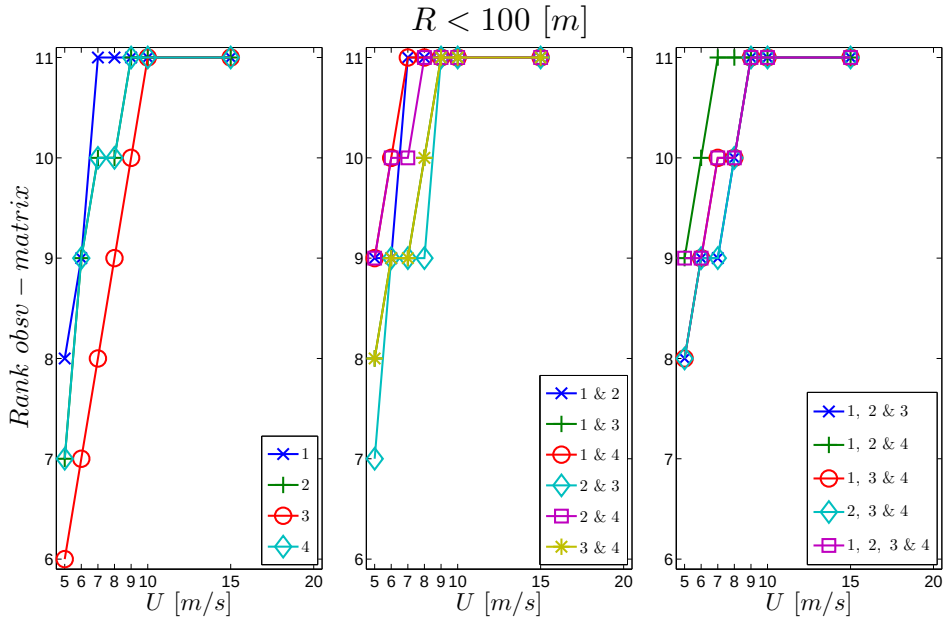


Figure 4.23: Observability of truck/full-trailer error states around nominal circle trajectories with $R < 100$. Sensor combinations with $1 = U$, $2 = \dot{\psi}_1$, $3 = a_{y,truck}$ and $4 = \dot{\psi}_{trailer}$.

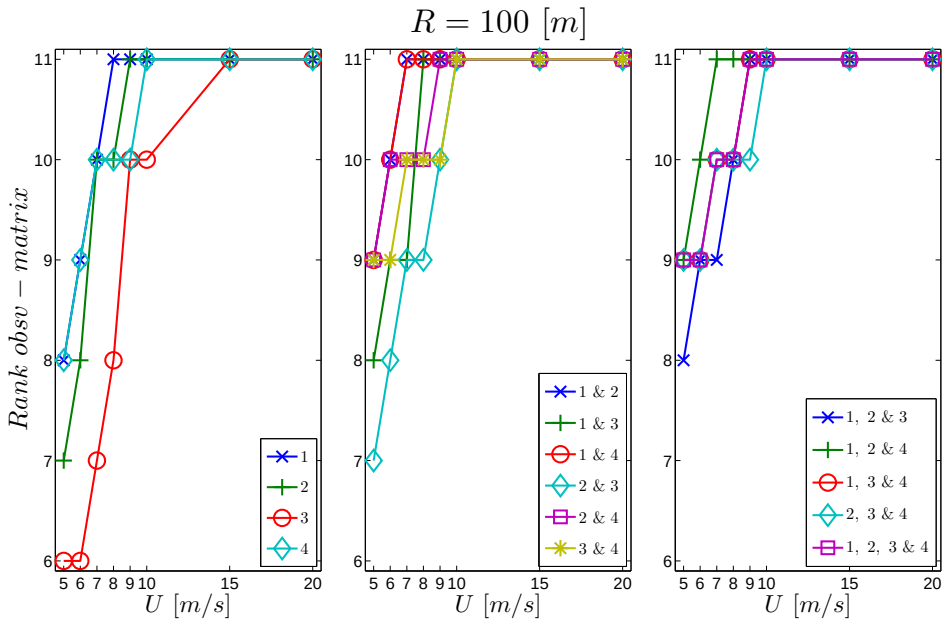


Figure 4.24: Observability of truck/full-trailer error states around nominal circle trajectories with $R = 100$. Sensor combinations with $1 = U$, $2 = \dot{\psi}_1$, $3 = a_{y,truck}$ and $4 = \dot{\psi}_{trailer}$.

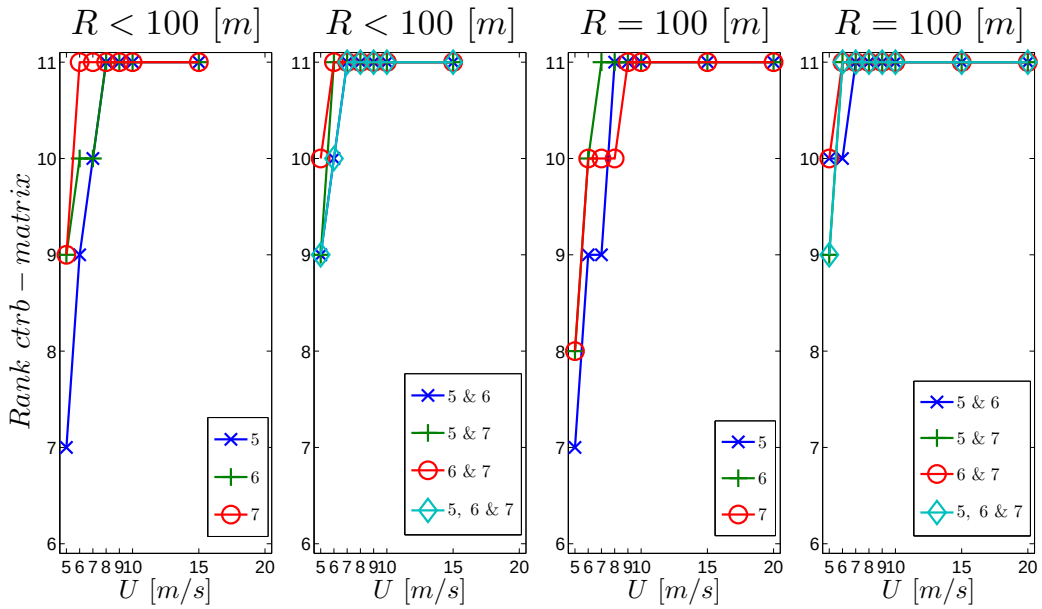


Figure 4.25: Controllability of the truck/full-trailer error states around nominal circle trajectories. Actuator combinations with $5 = F_{truck}$, $6 = F_{trailer}$ and $7 = T_{truck}$.

## 4.5 Conclusions

In this chapter a one-track 3-dimensional dynamic vehicle model and the corresponding non-linear equations of motion have been derived for a truck/full-trailer combination and is used to study the yaw-rate instability and the rollover phenomenon.

To investigate the stability margins of the truck/full-trailer combination, the derived non-linear tracking error dynamics is linearized around a nominal straight-line and a nominal circle trajectory. The same observations as in chapter 3 are derived and show that three eigenvalues are on the imaginary axis which is the result of the independency of the non-linear equations of motion by three generalized coordinates. The linearized tracking error dynamics around a nominal straight-line trajectory show an extra eigenvalue on the imaginary axis since the dynamics is independent of the forward velocity error. The remaining eigenvalues are stable by a negative real part.

A vehicle handling study is carried out by analyzing the rollover phenomenon, yaw-rate instability and the stability margins of the linearized tracking error dynamics around nominal circle trajectories:

- Rollover phenomenon is studied using a rollover threshold by which the maximum allowable lateral acceleration of the truck/full-trailer combination is 4.1661 $[m/s^2]$. With this rollover threshold, realistic nominal circle trajectories are selected for further analysis.
- The yaw-rate instability is studied using a vehicle handling diagram which shows that the truck of the vehicle combination is understeered for the derived nominal circle trajectories. By increasing the radius $R$ of the nominal circle trajectory or decreasing the forward velocity $U$ the truck will have neutral steer.
- The stability analysis shows that by enlarging the lateral acceleration $a_{y,truck}$ or the forward velocity $U$ most eigenvalues are moving in the direction of the imaginary axis, resulting in a decrease of the truck/full-trailer stability margins. One eigenvalue moves in opposite direction by decreasing the forward velocity by the fact that the linearized tracking error dynamics with $U \rightarrow 0$ $[m/s]$, will have an extra zero eigenvalue due to its independency of the forward velocity error in a non-moving mode.

For designing a controller the observability and controllability is studied by various sensors and actuators placed on the truck/full-trailer combination which satisfies the problem statement. Conclusions are draw of nominal trajectories with a forward velocity of 15 $[m/s]$ to ensure that the numerical rank determination is correct.

Around a nominal straight-line trajectory the system is maximal observable and maximal controllable by using a sensor / actuator combination within the forward velocity sensor $U$ and the torque actuator $T_{truck}$ respectively. Possible sensor combinations are $U + \dot{\psi}_1$, $U + a_{y,truck}$ or $U + \dot{\psi}_1 + a_{y,truck}$. Possible actuator combinations are $T_{truck} + F_{truck}$, $T_{truck} + F_{trailer}$ or $T_{truck} + F_{truck} + F_{trailer}$.
Around nominal circle trajectories with $a_{y,truck} < 4.1661$ $[m/s^2]$ the system is maximal observable and maximal controllable using one sensor and one actuator or a combination of the available sensors and actuators. The use of a minimal amount of sensors and actuators is cost effective, however using more sensors/actuators can decrease the required controller gains when they are physical impossible.

# Chapter 5

# Conclusions and recommendations

## 5.1 Conclusions

The presented dynamic vehicle model of the truck/full-trailer combination does not describe the real dynamic behaviour due to the absence of a detailed mass distribution, a low stiffness of the chassis, more realistic tyre dynamics, two-track axles and a complex suspension. The advantage of this dynamic vehicle model representation is that the derived non-linear equations of motion does not contain algebraic loops and can be used for analytic studies.

In this report the autonomous dynamics of the truck/full-trailer combination is analyzed around various trajectories by linearizing the equations of motion with respect to these trajectories. From the studied literature it can be concluded hat the here described and used method is not commonly used in literature. Most authors derive linear equations of motion without linearization to analyze the autonomous dynamics. This approach is only valid when the linear equations of motion can describe local the dynamics around a trajectory. The advantage of the used linearization method is that the linear equations of motion around the trajectory are valid for classic linear stability analysis.

A commonly used test to analyse various vehicle instability phenomena is driving a so-called lane-change manoeuvre. Unfortunately linearizing the non-linear equations of motion around this lane-change manoeuvre is difficult and therefore this manoeuvre has been split up into a straight-line and a circle trajectory.

In this report the truck/full-trailer combination is analyzed on the yaw-rate instability and the rollover phenomenon:

- Yaw-rate instability: the truck part of the vehicle combination is understeered around various nominal circle trajectories. By increasing the forward velocity or decreasing the driven radius it will enlarge the truck understeering. This observation is only valid by driving on a perfect road condition with optimal grip of the tyres.
- Rollover phenomenon: the derived maximal allowable lateral acceleration is a threshold which prevents rollover and is used for deriving realistic nominal circle trajectories for

further analyses in this report. Using this method it is easy to determine rollover thresholds for other vehicle parameters.

Analyzing the autonomous dynamics using the eigenvalue problem show that the stability margins of the truck/full-trailer changes by enlarging the forward velocity or the lateral acceleration, resulting in a less stable dynamic behaviour. This observation corresponds to the physical instability by a more understeered truck and driving near to the rollover threshold.

The observability and controllability are analyzed of the truck/full-trailer combination around specified trajectories. To ensure that the corresponding rank determination is correct a minimal forward velocity is required. The available sensors are a forward velocity sensor $U$, a yaw-rate sensor $\dot{\psi}_1$ and a lateral acceleration sensor $a_{y,truck}$ placed on the truck chassis mass. Control intervention can be made with a force actuator $F_{truck}$ placed on the second rear axle of the truck, a torque actuator $T_{truck}$ acting on the truck chassis mass and a force actuator $F_{trailer}$ distributed (50 percent) over the drawbar axle and the second rear axle of the trailer. Around a nominal straight-line trajectory the system is maximal observable and maximal controllable by using a sensor / actuator combination within the forward velocity sensor $U$ and the torque actuator $T_{truck}$ respectively. Possible sensor combinations are $U + \dot{\psi}_1$, $U + a_{y,truck}$ or $U + \dot{\psi}_1 + a_{y,truck}$. Possible actuator combinations are $T_{truck} + F_{truck}$, $T_{truck} + F_{trailer}$ or $T_{truck} + F_{truck} + F_{trailer}$. Around nominal circle trajectories the system is maximal observable and maximal controllable using one sensor and one actuator or a combination of the available sensors and actuators. The use of a minimal amount of sensors and actuators can be cost effective, however using more sensors/actuators can decrease the required controller gains when they are physical impossible.

## 5.2 Recommendations for future work

- The presented methodology to analyse the dynamic behaviour and controller design (by studying the observability and controllability) can be used to study other vehicle configurations.
- Verification of the derived vehicle handling results of the truck/full-trailer combination can be done using a more complete simulation model, e.g., with a multi-body model. With this verification can be determined if the used dynamic truck/full-trailer model is representative of a real truck/full-trailer combination.
- Investigate a numerical / mathematical way to ensure a correct rank determination for ill-conditioned matrices. This is necessary to determine the observability and controllability below a forward velocity of 15 $[m/s]$. In practice yaw-rate instability can occur at small forward velocities by skidding on a low friction-road
- The presented controller design based on the state-space method, as discussed in section 3.4, is not applied on the truck/full-trailer combination by numerical conflicts due to size of the derived non-linear equations of motion. This results that the corresponding transfer functions where not able to derive. Therefore the controller design has to be carry out in a simulation environment, such as using Simulink, where the non-linear equations of motion can be embedded and a desired controller can be developed.

- The linearized tracking error dynamics and a designed controller can be analyzed with the use of bode frequency functions to provide insights into the benefits or disadvantages of the use of the stability controller. However, the linearized tracking error dynamics is a MIMO system of which the corresponding bode frequency functions are difficult to interpret. The first step is to analyse only the bode frequency functions of the collocated sensors/actuators placed on the truck/full-trailer combination.

# Appendix A

# Static Rollover Indicator

## A.1 Introduction

DAF Trucks used the approach of Ervin [Erv87] to determine the maximum allowable lateral acceleration until a wheel "lift-off", as shown in [Hen04]. If one of the wheels looses contact with the road the complete vehicle is considered to have reached the roll stability boundary.

First, a stability criterion (for a right-turn) is formulated when a wheel "lift-off". The critical lateral acceleration $a_{roll}$ is given by [Erv87]:

$$a_{roll} = \frac{g\ (T/2 - \Delta x)}{H} \tag{A.1}$$

where $\Delta x$ is the overall displacement of c.o.g., $T$ is the track width, $H$ is the height of the c.o.g. and $g$ is the gravitational acceleration.

The overall displacement has been divided into two parts, the tyre displacement $x_{tyre}$ and the suspension displacement $x_{susp}$:

$$\Delta x = x_{tyre} + x_{susp} \tag{A.2}$$

To study the rollover phenomenon Ervin divided the total mass $M$ (point load fixed at the c.o.g.) in an unsprung mass of the chassis $M_{chassis}$ and an elevated sprung mass of the body $M_{susp}$, as shown in figure A.1.

## A.2 Tyre displacement

For the determination of the tyre displacement $x_{tyre}$ it is assumed that the axle roll center is at the ground level and the total load has to be considered, as shown in figure A.2. The corresponding moment balance is:

$$\begin{aligned} &M\ a_y\ H + M\ g\ x_{tyre} = k_{tyre}\ T^2\ \varphi \\ &with \quad \varphi \approx \tan(\varphi) = \tfrac{x_{tyre}}{H} \end{aligned} \tag{A.3}$$

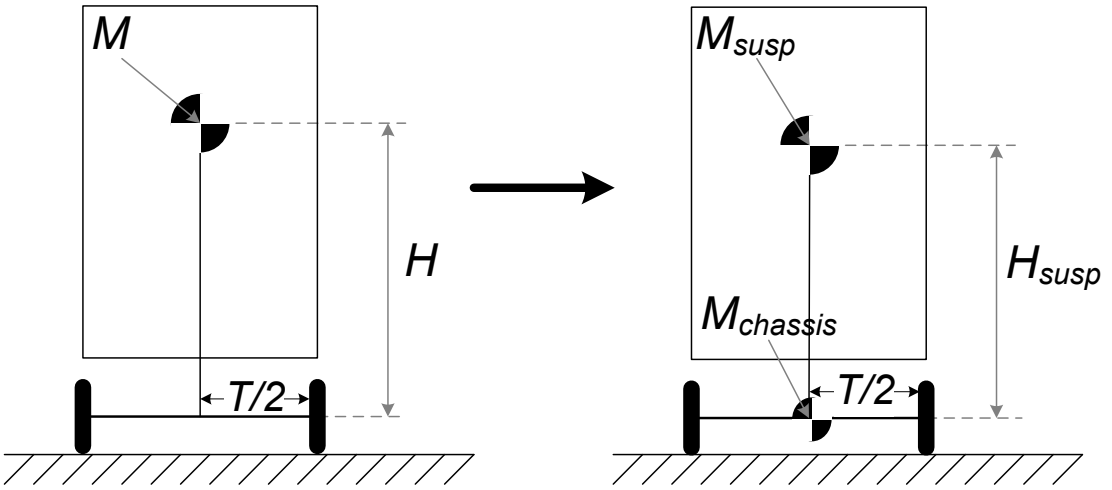


Figure A.1: Mass division

Rewriting of (A.3) results in the tyre displacement:

$$x_{tyre} = \frac{-M\ a_y\ H^2}{M\ g\ H - k_{tyre}\ T^2} \tag{A.4}$$

## A.3 Suspension displacement

For the determination of the suspension displacement, the roll stiffness $C_{roll}$ acts only on the sprung mass $M_{susp}$ on a roll height $H_{susp}$ as shown in figure A.3. The corresponding moment balance is:

$$\begin{aligned} &M_{susp}\ a_y\ H_{susp} + M_{susp}\ g\ x'_{susp} = C_\varphi\ \varphi \\ &with \\ &\varphi \approx \tan(\varphi) = \tfrac{x'_{susp}}{H_{susp}} \end{aligned} \tag{A.5}$$

Rewriting (A.5) results in the suspension displacement:

$$x'_{susp} = \frac{-M_{susp}\ a_y\ H^2_{susp}}{M_{susp}\ g\ H_{susp} - C_\varphi} \tag{A.6}$$

The resulting suspension displacement should be scaled for the computation of the displacement of the total mass, where $x_{susp} = \frac{M_{susp}}{M}\ x'_{susp}$.

## A.4 Static Rollover criterion

The total displacement due to the tyre and suspension displacement of the total axle load is:

$$\Delta x = x_{tyre} + x_{susp} = x_{tyre} + \frac{M_{susp}}{M}\ x'_{susp} \tag{A.7}$$

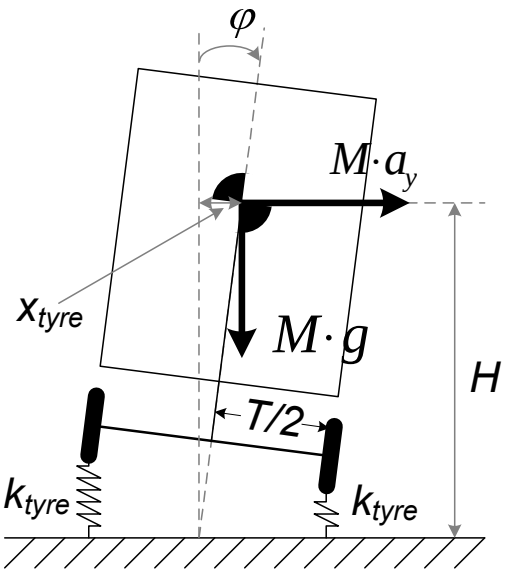


Figure A.2: Determination of the tyre displacement

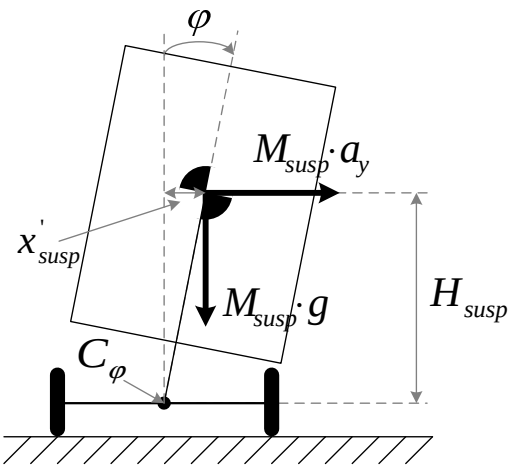


Figure A.3: Determination of the suspension displacement

Substitution in the rollover stability criterion (A.1) gives the maximum allowable lateral acceleration when the complete vehicle have reached the roll stability boundary:

$$a_{roll} = \frac{M\ g\ T\left(k_{tyre}\ T^2 - M\ g\ H\right)\ \left(M_{susp}\ g\ H_{susp} - C_{\varphi}\right)}{2\left[M_{susp}^2\ g\ H_{susp}^2\left(M\ g\ H\ -\ k_{tyre}\ T^2\right) + \cdots \right.} \\ \left. M\ H\ k_{tyre}\ T^2\left(M_{susp}\ g\ H_{susp}\ -\ C_{\varphi}\right)\right] \tag{A.8}$$

# Appendix B

# Lagrange formulation

$$\begin{aligned} &\frac{d}{dt}\frac{\partial T_{kin}}{\partial \dot{q}_i} - \frac{\partial T_{kin}}{\partial q_i} + \frac{\partial U_{pot}}{\partial q_i} + \frac{\partial D_{diss}}{\partial \dot{q}_i} = Q^{ex} \\ &with\ i = 1, \cdots, n \end{aligned} \tag{B.1}$$

$$\begin{aligned} &\frac{d}{dt}\frac{\partial T_{kin}}{\partial U} - \dot{\psi}\frac{\partial T_{kin}}{\partial V} + \frac{\partial U_{pot}}{\partial U} + \frac{\partial D_{diss}}{\partial U} = Q^{ex}_U \\ &\frac{d}{dt}\frac{\partial T_{kin}}{\partial V} + \dot{\psi}\frac{\partial T_{kin}}{\partial U} + \frac{\partial U_{pot}}{\partial V} + \frac{\partial D_{diss}}{\partial V} = Q^{ex}_V \\ &\frac{d}{dt}\frac{\partial T_{kin}}{\partial \dot{\psi}} - V\frac{\partial T_{kin}}{\partial U} + U\frac{\partial T_{kin}}{\partial V} + \frac{\partial U_{pot}}{\partial \dot{\psi}} + \frac{\partial D_{diss}}{\partial \dot{\psi}} = Q^{ex}_{\dot{\psi}} \end{aligned} \tag{B.2}$$

$$\begin{aligned} &Q^{ex}_i = \left(\frac{dr_i}{d\dot{q}}\right)^T \cdot F^{ex}_i \\ &with \quad i = 1, \cdots, n \end{aligned} \tag{B.3}$$

$$\begin{aligned} &\frac{d}{dt}\frac{\partial T_{kin}}{\partial U} - \dot{\psi}_1\frac{\partial T_{kin}}{\partial V} + \frac{\partial U_{pot}}{\partial U} + \frac{\partial D_{diss}}{\partial U} = Q^{ex}_U \\ &\frac{d}{dt}\frac{\partial T_{kin}}{\partial V} + \dot{\psi}_1\frac{\partial T_{kin}}{\partial U} + \frac{\partial U_{pot}}{\partial V} + \frac{\partial D_{diss}}{\partial V} = Q^{ex}_V \\ &\frac{d}{dt}\frac{\partial T_{kin}}{\partial \dot{\psi}_1} - V\frac{\partial T_{kin}}{\partial U} + U\frac{\partial T_{kin}}{\partial V} + \frac{\partial U_{pot}}{\partial \dot{\psi}_1} + \frac{\partial D_{diss}}{\partial \dot{\psi}_1} = Q^{ex}_{\dot{\psi}_1} \\ &\frac{d}{dt}\frac{\partial T_{kin}}{\partial \dot{\psi}_2} - \frac{\partial T_{kin}}{\partial \psi_2} + \frac{\partial U_{pot}}{\partial \psi_2} + \frac{\partial D_{diss}}{\partial \psi_2} = Q^{ex}_{\dot{\psi}_2} \\ &\frac{d}{dt}\frac{\partial T_{kin}}{\partial \dot{\psi}_3} - \frac{\partial T_{kin}}{\partial \psi_3} + \frac{\partial U_{pot}}{\partial \psi_3} + \frac{\partial D_{diss}}{\partial \psi_3} = Q^{ex}_{\dot{\psi}_3} \\ &\frac{d}{dt}\frac{\partial T_{kin}}{\partial \dot{\varphi}_1} - \frac{\partial T_{kin}}{\partial \varphi_1} + \frac{\partial U_{pot}}{\partial \varphi_1} + \frac{\partial D_{diss}}{\partial \dot{\varphi}_1} = Q^{ex}_{\dot{\varphi}_1} \\ &\frac{d}{dt}\frac{\partial T_{kin}}{\partial \dot{\varphi}_3} - \frac{\partial T_{kin}}{\partial \varphi_3} + \frac{\partial U_{pot}}{\partial \varphi_3} + \frac{\partial D_{diss}}{\partial \dot{\varphi}_3} = Q^{ex}_{\dot{\varphi}_3} \end{aligned} \tag{B.4}$$

# Appendix C

# MATLAB function *fsolve.m*

The MATLAB function *fsolve.m* solves systems of nonlinear equations of several variables. *fsolve.m* attempts to solve equations of the form:

$$F(X) = 0 \tag{C.1}$$

Where $F$ and $X$ can be vectors.

## C.1 Deriving the nominal circle trajectory

This example shows how to find the nominal circle trajectory for the non-linear equations of motion of the bicycle model with the use of *fsolve.m*. First, a function has to be defined which contains the non-linear equations of motion and the unknown set of variables, *Solve_Nom_traj.m*:

```
function F = Solve_Nom_Traj(KNOWN,UNKNOWN)

beta    = KNOWN(1);
U       = KNOWN(2);
V       = KNOWN(3);
Fact    = KNOWN(4);

delta   = UNKNOWN(1);
dPsi_1  = UNKNOWN(2);
Fcruise = UNKNOWN(3);

%%%%%%%%%%%%%%%%%%%%%%%%%%%%%%%%%%%%%%%%%%%%%%%%%%%%%%%%%%%%%%%%%%%%%%%%%%%
%%% Non-linear equations of motion of the Bicycle model %%%%%%%%%%%%%%%%%%%
%%%%%%%%%%%%%%%%%%%%%%%%%%%%%%%%%%%%%%%%%%%%%%%%%%%%%%%%%%%%%%%%%%%%%%%%%%%

F = [1/1600*(-60000*delta-60000*atan((-V-7/5*dPsi_1)/U))*sin(delta)+1/1600*Fcruise-1/1600*Fact+dPsi_1*V;
     1/1600*(60000*delta+60000*atan((-V-7/5*dPsi_1)/U))*cos(delta)+75/2*atan((-V+8/5*dPsi_1)/U)-dPsi_1*U;
     1/3600*(84000*delta+84000*atan((-V-7/5*dPsi_1)/U))*cos(delta)-80/3*atan((-V+8/5*dPsi_1)/U)];
```

Finding the nominal circle trajectory with the function *fsolve.m*:

```
%%% --- KNOWN VARIABLES ---
beta = 1*pi/180;         %% <-- Setting of a constant Vehicle Side Slip
```

```
U    = 15;               %% <-- Setting of constant forward velocity
V    = -U*tan(beta);     %% <-- Deriving lateral velocity

KNOWN = [beta,U,V];     %% <-- Set of Known variables

%%% --- UNKNOWN VARIABLES ---
delta   = 1;
dPsi_1  = 1;
Fcruise = 1;

UNKNOWN = [delta,dPsi_1,Fcruise]; %% <-- Set of Unknown variables

options=optimset('Display','iter');
[UNKNOWN FVAL] = fsolve(@(UNKNOWN) Solve_Nom_Traj(KNOWN,UNKNOWN),UNKNOWN,options);

delta   = UNKNOWN(1);
dPsi_1  = UNKNOWN(2);
Fcruise = UNKNOWN(3);
```

This results in:

```
                                    Norm of      First-order   Trust-region
 Iteration  Func-count     f(x)          step         optimality    radius
     0          4         1005.65                    1.36e+003              1
     1          8         71.1816             1           328              1
     2         12         23.1322           2.5          43.5            2.5
     3         16         21.1052           2.5          32.6            2.5
     4         20         19.5433          6.25          39.6           6.25
     5         24         17.7685          6.25          27.6           6.25
     6         28          16.392         15.625          35.6           15.6
     7         32         14.7764         15.625          23.3           15.6
     8         36         13.4204        39.0625          31.6           39.1
     9         40         11.7236        39.0625          18.6           39.1
    10         44          10.023        97.6562          28.1           97.7
    11         48         7.53741        97.6563          11.9           97.7
    12         52         4.28405        244.141          24.4            244
    13         56        0.126234        233.258          2.41            244
    14         60    5.73685e-009        560.358     9.92e-005            583
    15         64    2.06578e-026       0.121563     2.86e-012       1.4e+003
Optimization terminated: first-order optimality is less than options.TolFun.

>> UNKNOWN

UNKNOWN =

    0.0494    0.2179  229.2608

>> FVAL

FVAL =

  1.0e-012 *

    0.1332
   -0.0462
   -0.0280
```

# Appendix D

# Parameters of the truck/full-trailer combination

Truck/full-trailer combination parameters from the report of Zegwaard [Zeg88]:

| Symbol | Description | Value | Unit |
|---|---|---|---|
| $a$ | Distance between truck front axle and truck chassis mass | 3.35 | $[m]$ |
| $b$ | Distance between truck front axle and first rear axle | 4.20 | $[m]$ |
| $c$ | Distance between truck front axle and second rear axle | 5.53 | $[m]$ |
| $d$ | Distance between truck front axle and truck hitch point | 7.00 | $[m]$ |
| $e$ | Distance between dolly axle and dolly chassis mass | 0.03 | $[m]$ |
| $f$ | Distance between truck hitch point and dolly axle | 2.49 | $[m]$ |
| $g$ | Distance between dolly hitch point and trailer chassis mass | 3.42 | $[m]$ |
| $h$ | Distance between dolly hitch point and trailer first rear axle | 4.66 | $[m]$ |
| $k$ | Distance between dolly hitch point and trailer second rear axle | 5.90 | $[m]$ |
| $h_{\varphi 1}$ | Height of truck roll mass $M_{\varphi 1}$ w.r.t. truck chassis mass | 1.56 | $[m]$ |
| $h_{\varphi 3}$ | Height of trailer roll mass $M_{\varphi 1}$ w.r.t. trailer chassis mass | 1.75 | $[m]$ |
| $L_1$ | Virtual distance between shock absorbers of the truck | 0.91 | $[m]$ |
| $L_3$ | Virtual distance between shock absorbers of the trailer | 0.91 | $[m]$ |

| Symbol | Description | Value | Unit |
|---|---|---|---|
| $M_1$ | Chassis mass of the truck | $2.46 \cdot 10^3$ | $[kg]$ |
| $M_2$ | Chassis mass of the drawbar | $1.00 \cdot 10^3$ | $[kg]$ |
| $M_3$ | Chassis mass of the trailer | $1.32 \cdot 10^3$ | $[kg]$ |
| $M_{\varphi 1}$ | Roll mass of the truck | $21.50 \cdot 10^3$ | $[kg]$ |
| $M_{\varphi 3}$ | Roll mass of the trailer | $26.44 \cdot 10^3$ | $[kg]$ |
| $I_1$ | Yaw moment of inertia of the truck | $1.67 \cdot 10^5$ | $[kgm^2]$ |
| $I_2$ | Yaw moment of inertia of the drawbar | $7.50 \cdot 10^2$ | $[kgm^2]$ |
| $I_3$ | Yaw moment of inertia of the trailer | $2.23 \cdot 10^5$ | $[kgm^2]$ |
| $I_{\varphi 1}$ | Roll moment of inertia of the truck | $3.42 \cdot 10^4$ | $[kgm^2]$ |
| $I_{\varphi 3}$ | Roll moment of inertia of the trailer | $4.30 \cdot 10^4$ | $[kgm^2]$ |

| Symbol | Description | Value | Unit |
|---|---|---|---|
| $C_{\varphi 1}$ | Roll stiffness of the tractor<br>**Note:** Zegwaard [Zeg88] uses a roll stiffness of $4.01 \cdot 10^5$ $[Nm/rad]$ which results in a unrealistic large roll angle $\varphi_1$ | $2.38 \cdot 10^6$ | $[Nm/rad]$ |
| $C_{\varphi 3}$ | Roll stiffness of the tractor | $2.38 \cdot 10^6$ | $[Nm/rad]$ |
| $C_1$ | Tyre cornering stiffness of the truck front tyre | $3.65 \cdot 10^5$ | $[N/rad]$ |
| $C_2$ | Tyre cornering stiffness of the truck first rear tyre | $5.88 \cdot 10^5$ | $[N/rad]$ |
| $C_3$ | Tyre cornering stiffness of the truck second rear tyre | $5.18 \cdot 10^5$ | $[N/rad]$ |
| $C_4$ | Tyre cornering stiffness of the drawbar tyre | $6.42 \cdot 10^5$ | $[N/rad]$ |
| $C_5$ | Tyre cornering stiffness of the trailer first rear tyre | $6.74 \cdot 10^5$ | $[N/rad]$ |
| $C_6$ | Tyre cornering stiffness of the trailer second rear tyre | $6.72 \cdot 10^5$ | $[N/rad]$ |
| $K_1$ | Damping factor of a truck shock absorber<br>**Note:** Zegwaard [Zeg88] uses a damping factor of $1.17 \cdot 10^5$ $[Ns/m]$ which results in a unrealistic large roll angle $\varphi_1$ | $4.84 \cdot 10^4$ | $[Ns/m]$ |
| $K_3$ | Damping factor of a trailer shock absorber | $4.84 \cdot 10^4$ | $[Ns/m]$ |

# Appendix E

# Truck/full-trailer velocities and generalized external forces

This appendix shows the determination of the velocities in the dynamic vehicle model of the truck/full-trailer except for the drawbar chassis mass velocities which have been determined in section 4.2.1. The generalized external forces in the dynamic vehicle model will also be determined in this appendix.

## E.1 Velocities in the dynamic vehicle model

With the velocities of the drawbar chassis mass (4.10), the velocities of the drawbar tyre can be determined:

$$\begin{aligned} U_6 &= U_5 \\ V_6 &= U\sin(\psi_2) + V\cos(\psi_2) - (d-a)\dot{\psi}_1\cos(\psi_2) + f(\dot{\psi}_2 - \dot{\psi}_1) \end{aligned} \tag{E.1}$$

For the determination of the velocities of the trailer chassis mass and tyres the spatial positions of the chassis mass of the trailer, expressed in the fixed coordinate system, are:

$$\begin{aligned} X_7 &= X_2 - (d-a)\cos(\psi_1) - (f-e)\cos(\psi_2-\psi_1) - g\cos(\psi_3+\psi_2-\psi_1) \\ Y_7 &= Y_2 - (d-a)\sin(\psi_1) + (f-e)\sin(\psi_2-\psi_1) + g\sin(\psi_3+\psi_2-\psi_1) \end{aligned} \tag{E.2}$$

The corresponding velocities are:

$$\begin{aligned} \dot{X}_7 = \tfrac{dX_7}{dt} &= \dot{X}_2 + (d-a)\dot{\psi}_1\sin(\psi_1) + (f-e)(\dot{\psi}_2-\dot{\psi}_1)\sin(\psi_2-\psi_1) + \dots \\ &\quad g(\dot{\psi}_3+\dot{\psi}_2-\dot{\psi}_1)\sin(\psi_3+\psi_2-\psi_1) \\ \dot{Y}_7 = \tfrac{dY_7}{dt} &= \dot{Y}_2 - (d-a)\dot{\psi}_1\cos(\psi_1) + (f-e)(\dot{\psi}_2-\dot{\psi}_1)\cos(\psi_2-\psi_1) + \dots \\ &\quad g(\dot{\psi}_3+\dot{\psi}_2-\dot{\psi}_1)\cos(\psi_3+\psi_2-\psi_1) \end{aligned} \tag{E.3}$$

Substitution of (4.6) in the velocities of the trailer chassis mass (E.3) gives:

$$\begin{aligned} U_7^* \cos(\psi_1) - V_7^* \sin(\psi_1) &= U_2 \cos(\psi_1) - V_2 \sin(\psi_1) + (d-a)\dot{\psi}_1 \sin(\psi_1) + \dots \\ &\quad (f-e)(\dot{\psi}_2 - \dot{\psi}_1)\sin(\psi_2 - \psi_1) + \dots \\ &\quad (\dot{\psi}_3 + \dot{\psi}_2 - \dot{\psi}_1)\sin(\psi_3 + \psi_2 - \psi_1) \\ U_7^* \sin(\psi_1) + V_7^* \cos(\psi_1) &= U_2 \sin(\psi_1) + V_2 \cos(\psi_1) - (d-a)\dot{\psi}_1 \cos(\psi_1) + \dots \\ &\quad (f-e)(\dot{\psi}_2 - \dot{\psi}_1)\cos(\psi_2 - \psi_1) + \dots \\ &\quad g(\dot{\psi}_3 + \dot{\psi}_2 - \dot{\psi}_1)\cos(\psi_3 + \psi_2 - \psi_1) \end{aligned} \tag{E.4}$$

Rewriting (E.4) results in the forward $U_7^*$ and the lateral $V_7^*$ velocity of the drawbar chassis mass in the $U/V$-direction, respectively:

$$\begin{aligned} U_7^* &= U_2 + (f-e)(\dot{\psi}_2 - \dot{\psi}_1)\sin(\psi_2) + g(\dot{\psi}_3 + \dot{\psi}_2 - \dot{\psi}_1)\sin(\psi_3 - \psi_2) \\ V_7^* &= V_2 - (d-a)\dot{\psi}_1 + (f-e)(\dot{\psi}_2 - \dot{\psi}_1)\cos(\psi_2) + \dots \\ &\quad g(\dot{\psi}_3 + \dot{\psi}_2 - \dot{\psi}_1)\cos(\psi_3 - \psi_2) \end{aligned} \tag{E.5}$$

Final step is to rotate these velocities with the yaw angle between the truck and trailer, $\psi_3 + \psi_2$, and by substitution of $U_2 = U$ and $V_2 = V$ which results in the forward and lateral velocity of the trailer chassis mass, respectively:

$$\begin{aligned} U_7 &= U_7^* \cos(\psi_3 + \psi_2) - V_7^* \sin(\psi_3 + \psi_2) \\ &= U\cos(\psi_3 + \psi_2) - V\sin(\psi_3 + \psi_2) + (d-a)\dot{\psi}_1 \sin(\psi_3 + \psi_2) - \dots \\ &\quad (f-e)(\dot{\psi}_2 - \dot{\psi}_1)\sin(\psi_3) \\ V_7 &= U_7^* \sin(\psi_3 + \psi_2) + V_7^* \cos(\psi_3 + \psi_2) \\ &= U\sin(\psi_3 + \psi_2) + V\cos(\psi_3 + \psi_2) - (d-a)\dot{\psi}_1 \cos(\psi_3 + \psi_2) + \dots \\ &\quad (f-e)(\dot{\psi}_2 - \dot{\psi}_1)\cos(\psi_3) + g(\dot{\psi}_3 + \dot{\psi}_2 - \dot{\psi}_1) \end{aligned} \tag{E.6}$$

With the velocities of trailer chassis mass (E.6) the velocities of the first rear and second rear tyres can be determined:

$$\begin{aligned} U_8 &= U_7 \\ V_8 &= U\sin(\psi_3 + \psi_2) + V\cos(\psi_3 + \psi_2) - (d-a)\dot{\psi}_1 \cos(\psi_3 + \psi_2) + \dots \\ &\quad (f-e)(\dot{\psi}_2 - \dot{\psi}_1)\cos(\psi_3) + h(\dot{\psi}_3 + \dot{\psi}_2 - \dot{\psi}_1) \end{aligned} \tag{E.7}$$

$$\begin{aligned} U_9 &= U_7 \\ V_9 &= U\sin(\psi_3 + \psi_2) + V\cos(\psi_3 + \psi_2) - (d-a)\dot{\psi}_1 \cos(\psi_3 + \psi_2) + \dots \\ &\quad (f-e)(\dot{\psi}_2 - \dot{\psi}_1)\cos(\psi_3) + k(\dot{\psi}_3 + \dot{\psi}_2 - \dot{\psi}_1) \end{aligned} \tag{E.8}$$

Next step is to determine the velocities of the roll masses. Figure E.1 shows the roll masses and the corresponding velocities.

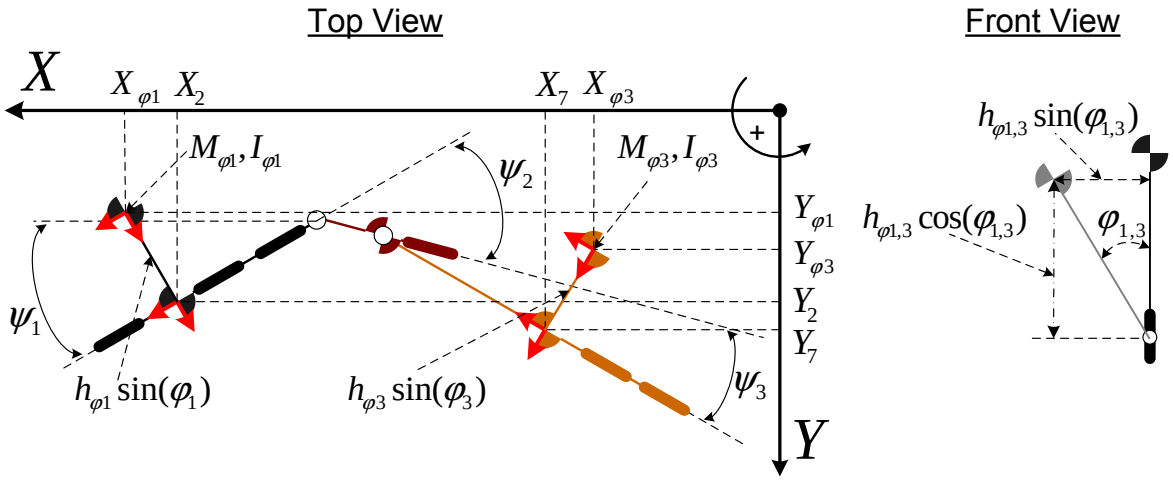


Figure E.1: Velocities of roll masses at truck and trailer

The spatial positions of the roll mass of the truck, expressed in the fixed coordinate system with respect to the truck chassis mass, are:

$$\begin{aligned} X_{\varphi 1} &= X_2 + h_{\varphi 1} \sin(\varphi_1) \sin(\psi_1) \\ Y_{\varphi 1} &= Y_2 - h_{\varphi 1} \sin(\varphi_1) \cos(\psi_1) \end{aligned} \tag{E.9}$$

The corresponding velocities are:

$$\begin{aligned} \dot{X}_{\varphi 1} &= \tfrac{dX_{\varphi 1}}{dt} = \dot{X}_2 + h_{\varphi 1} \dot{\varphi}_1 \cos(\varphi_1) \sin(\psi_1) + h_{\varphi 1} \dot{\psi}_1 \sin(\varphi_1) \cos(\psi_1) \\ \dot{Y}_{\varphi 1} &= \tfrac{dY_{\varphi 1}}{dt} = \dot{Y}_2 - h_{\varphi 1} \dot{\varphi}_1 \cos(\varphi_1) \cos(\psi_1) + h_{\varphi 1} \dot{\psi}_1 \sin(\varphi_1) \sin(\psi_1) \end{aligned} \tag{E.10}$$

Expressing these velocities in the moving coordinate system results in:

$$\begin{aligned} U_{\varphi 1} \cos(\psi_1) - V_{\varphi 1} \sin(\psi_1) &= U_2 \cos(\psi_1) - V_2 \sin(\psi_1) + \ldots \\ &\quad h_{\varphi 1} \dot{\varphi}_1 \cos(\varphi_1) \sin(\psi_1) + h_{\varphi 1} \dot{\psi}_1 \sin(\varphi_1) \cos(\psi_1) \\ U_{\varphi 1} \sin(\psi_1) + V_{\varphi 1} \cos(\psi_1) &= U_2 \sin(\psi_1) + V_2 \cos(\psi_1) - \ldots \\ &\quad h_{\varphi 1} \dot{\varphi}_1 \cos(\varphi_1) \cos(\psi_1) + h_{\varphi 1} \dot{\psi}_1 \sin(\varphi_1) \sin(\psi_1) \end{aligned} \tag{E.11}$$

Rewriting (E.11) results in the forward and lateral velocity of the truck roll mass, respectively:

$$\begin{aligned} U_{\varphi 1} &= U + h_{\varphi 1} \dot{\psi}_1 \sin(\varphi_1) \\ V_{\varphi 1} &= V - h_{\varphi 1} \dot{\varphi}_1 \cos(\varphi_1) \end{aligned} \tag{E.12}$$

The spatial positions of the roll mass of the trailer, expressed in a fixed coordinate system with respect to the trailer chassis mass, are:

$$\begin{aligned} X_{\varphi 3} &= X_7 - h_{\varphi 3}\sin(\varphi_3)\sin(\psi_3+\psi_2-\psi_1) \\ Y_{\varphi 3} &= Y_7 - h_{\varphi 3}\sin(\varphi_3)\cos(\psi_3+\psi_2-\psi_1) \end{aligned} \tag{E.13}$$

Differentiate with respect to time $t$ gives the corresponding velocities:

$$\begin{aligned} \dot{X}_{\varphi 3} = \tfrac{dX_{\varphi 3}}{dt} &= \dot{X}_7 - h_{\varphi 3}\dot{\varphi}_3\cos(\varphi_3)\sin(\psi_3+\psi_2-\psi_1) - \ldots \\ &\quad h_{\varphi 3}(\dot{\psi}_3+\dot{\psi}_2-\dot{\psi}_1)\sin(\varphi_3)\cos(\psi_3+\psi_2-\psi_1) \\ \dot{Y}_{\varphi 3} = \tfrac{dY_{\varphi 3}}{dt} &= \dot{Y}_7 - h_{\varphi 3}\dot{\varphi}_3\cos(\varphi_3)\cos(\psi_3+\psi_2-\psi_1) + \ldots \\ &\quad h_{\varphi 3}(\dot{\psi}_3+\dot{\psi}_2-\dot{\psi}_1)\sin(\varphi_3)\sin(\psi_3+\psi_2-\psi_1) \end{aligned} \tag{E.14}$$

Expressing (E.14) in the $U/V$-direction results in:

$$\begin{aligned} U^*_{\varphi 3}\cos(\psi_1) - V^*_{\varphi 3}\sin(\psi_1) &= U^*_7\cos(\psi_1) - V^*_7\sin(\psi_1) - \ldots \\ &\quad h_{\varphi 3}\dot{\varphi}_3\cos(\varphi_3)\sin(\psi_3+\psi_2-\psi_1) - \ldots \\ &\quad h_{\varphi 3}(\dot{\psi}_3+\dot{\psi}_2-\dot{\psi}_1)\sin(\varphi_3)\cos(\psi_3+\psi_2-\psi_1) \\ U^*_{\varphi 3}\sin(\psi_1) + V^*_{\varphi 3}\cos(\psi_1) &= U^*_7\sin(\psi_1) + V^*_7\cos(\psi_1) - \ldots \\ &\quad h_{\varphi 3}\dot{\varphi}_3\cos(\varphi_3)\cos(\psi_3+\psi_2-\psi_1) + \ldots \\ &\quad h_{\varphi 3}(\dot{\psi}_3+\dot{\psi}_2-\dot{\psi}_1)\sin(\varphi_3)\sin(\psi_3+\psi_2-\psi_1) \end{aligned} \tag{E.15}$$

Rewriting these equations results in the forward $U^*_{\varphi 3}$ and lateral $V^*_{\varphi 3}$ velocity of the trailer roll mass:

$$\begin{aligned} U^*_{\varphi 3} &= U^*_7 - h_{\varphi 3}\dot{\varphi}_3\cos(\varphi_3)\sin(\psi_3+\psi_2) - \ldots \\ &\quad h_{\varphi 3}(\dot{\psi}_3+\dot{\psi}_2-\dot{\psi}_1)\sin(\varphi_3)\cos(\psi_3+\psi_2) \\ V^*_{\varphi 3} &= V^*_7 - h_{\varphi 3}\dot{\varphi}_3\cos(\varphi_3)\cos(\psi_3+\psi_2) + \ldots \\ &\quad h_{\varphi 3}(\dot{\psi}_3+\dot{\psi}_2-\dot{\psi}_1)\sin(\varphi_3)\sin(\psi_3+\psi_2) \end{aligned} \tag{E.16}$$

Final step is to rotate the velocities with the yaw angle between the truck and trailer, $\psi_3+\psi_2$, which results in the forward and lateral velocity of the trailer roll mass:

$$\begin{aligned} U_{\varphi 3} &= U^*_{\varphi 3}\cos(\psi_3+\psi_2) - V^*_{\varphi 3}\sin(\psi_3+\psi_2) \\ &= U^*_7\cos(\psi_3+\psi_2) - V^*_7\sin(\psi_3+\psi_2) - h_{\varphi 3}(\dot{\psi}_3+\dot{\psi}_2-\dot{\psi}_1)\sin(\varphi_3) \\ &= U_7 - h_{\varphi 3}(\dot{\psi}_3+\dot{\psi}_2-\dot{\psi}_1)\sin(\varphi_3) \\ V_{\varphi 3} &= U^*_{\varphi 3}\sin(\psi_3+\psi_2) + V^*_{\varphi 3}\sin(\psi_3+\psi_2) \\ &= U^*_7\sin(\psi_3+\psi_2) + V^*_7\cos(\psi_3+\psi_2) - h_{\varphi 3}\dot{\varphi}_3\cos(\varphi_3) \\ &= V_7 - h_{\varphi 3}\dot{\varphi}_3\cos(\varphi_3) \end{aligned} \tag{E.17}$$

## E.2 Generalized external forces in the dynamic vehicle model

The corresponding velocity vectors $r_i$ for the determination of the generalized external forces are:

$$
\begin{aligned}
r_1 &= \left[ \begin{array}{cc} U_1, & V_1 \end{array} \right]^T \\
r_2 &= \left[ \begin{array}{cc} U_3, & V_3 \end{array} \right]^T \\
r_3 &= \left[ \begin{array}{cc} U_4, & V_4 \end{array} \right]^T \\
r_4 &= \left[ \begin{array}{cc} U_6, & V_6 \end{array} \right]^T \\
r_5 &= \left[ \begin{array}{cc} U_8, & V_8 \end{array} \right]^T \\
r_6 &= \left[ \begin{array}{cc} U_9, & V_9 \end{array} \right]^T
\end{aligned}
\tag{E.18}
$$

The corresponding external forces $F_i$ in the $U/V$-direction are:

$$
\begin{aligned}
F_1 &= \left[ \begin{array}{cc} -F_{y1}\sin(\delta), & F_{y1}\cos(\delta) \end{array} \right]^T \\
F_2 &= \left[ \begin{array}{cc} 0, & F_{y2} \end{array} \right]^T \\
F_3 &= \left[ \begin{array}{cc} 0, & F_{y3} \end{array} \right]^T \\
F_4 &= \left[ \begin{array}{cc} 0, & F_{y4} \end{array} \right]^T \\
F_5 &= \left[ \begin{array}{cc} 0, & F_{y5} \end{array} \right]^T \\
F_6 &= \left[ \begin{array}{cc} 0, & F_{y6} \end{array} \right]^T
\end{aligned}
\tag{E.19}
$$

The lateral tyre forces $F_{yi}$ are dependent on the side slip angles ($\alpha_i$), steering angle ($\delta$), tyre cornering stiffness ($C_i$) and the corresponding velocities ($U_i/V_i$):

$$
\begin{aligned}
&F_{y1} = C_1 \ (\delta + \alpha_1) \\
&F_{y2} = C_2 \ (\alpha_2) \\
&F_{y3} = C_3 \ (\alpha_3) \\
&F_{y4} = C_4 \ (\alpha_4) \\
&F_{y5} = C_5 \ (\alpha_5) \\
&F_{y6} = C_6 \ (\alpha_6) \\
&\textit{with} \quad \alpha_1 = \arctan\left(\tfrac{-V_1}{U_1}\right), \ \alpha_2 = \arctan\left(\tfrac{-V_3}{U_3}\right), \ \alpha_3 = \arctan\left(\tfrac{-V_4}{U_4}\right), \\
&\qquad\quad \alpha_4 = \arctan\left(\tfrac{-V_6}{U_6}\right), \ \alpha_5 = \arctan\left(\tfrac{-V_8}{U_8}\right), \ \alpha_6 = \arctan\left(\tfrac{-V_9}{U_9}\right)
\end{aligned}
\tag{E.20}
$$

With the components $r_i$ (E.18), $F_i$ (E.19) and $F_{yi}$ (E.20) the generalized external forces $Q_i^{ex}$ (B.3) can be determined.

# Appendix F

# Non-linear equations of motion with MATLAB

A MATLAB procedure has been written in a m-file, because the determination of the non-linear equations of motion of the truck/full-trailer combination by handwriting is too difficult. To execute the m-file the MATLAB Symbolic Math Toolbox is required.

```
%%% TRUCK/FULL-TRAILER Combination
%%% -- Derivation of the non-linear equations of motion with Lagrange
%%% -- Final equations are in the form: ddq = inv(MM)*string_right
%%% -- Output of file is: MM and string_right

%%% -- Vehicle Parameters based on report of Zegwaard, J.P.
%%% -- Symbolic Toolbox Necessary

%%% -- Made by R.E. Mansvelders, final thesis DAF-Trucks
%%% -- Date: July 11th, 2006
%%% -- r.e.mansvelders@gmail.com

clear all; close all; clc;

tic

%%%%%%%%%%%%%%%%%%%%%%%%%%%%%%%%%%%%%%%%%%%%%%%%%%%%%%%%%%%%%%%%%%%%%%%%%%%%
%%% Parameters definition (SYMBOLIC) %%%%%%%%%%%%%%%%%%%%%%%%%%%%%%%%%%%%%%%
%%%%%%%%%%%%%%%%%%%%%%%%%%%%%%%%%%%%%%%%%%%%%%%%%%%%%%%%%%%%%%%%%%%%%%%%%%%%
syms IU IV Psi_1 Psi_2 Psi_3 Phi_1 Phi_3
syms U V dPsi_1 dPsi_2 dPsi_3 dPhi_1 dPhi_3
syms dU dV ddPsi_1 ddPsi_2 ddPsi_3 ddPhi_1 ddPhi_3

syms a b c d e f g h k
syms h_r1 h_r3 L_1 L_3
syms M_1 M_2 M_3 I_1 I_2 I_3
syms M_r1 M_r3 I_Phi_1 I_Phi_3
syms C_1 C_2 C_3 C_4 C_5 C_6
syms C_Phi_1 I_Phi_1 C_Phi_3 I_Phi_3
syms K_1 K_3

syms Fy1 Fy2 Fy3 Fy4 Fy5 Fy6
syms gravity
syms delta                  %% <-- Steering angle

syms Fcruise                %% <-- Maintain forward velocity while nominal trajectory
syms Ftruck                 %% <-- Force-Actuator placed on Truck at (a-c)
syms Ftrailer               %% <-- Force-Actuator placed on Trailer at k and (f-e)
```

```
syms Ttruck                %% <-- Torque-Actuator placed on Truck (c.o.g.)
%%%%%%%%%%%%%%%%%%%%%%%%%%%%%%%%%%%%%%%%%%%%%%%%%%%%%%%%%%%%%%%%%%%%%%%%%%%%

%%%%%%%%%%%%%%%%%%%%%%%%%%%%%%%%%%%%%%%%%%%%%%%%%%%%%%%%%%%%%%%%%%%%%%%%%%%%
%%% Velocity of Points %%%%%%%%%%%%%%%%%%%%%%%%%%%%%%%%%%%%%%%%%%%%%%%%%%%%%
%%%%%%%%%%%%%%%%%%%%%%%%%%%%%%%%%%%%%%%%%%%%%%%%%%%%%%%%%%%%%%%%%%%%%%%%%%%%
%%% -- Point 1, Tractor front axis --
U_1 = U;
V_1 = V + a*dPsi_1;

%%% -- Point 2, Tractor Mass --
U_2 = U;
V_2 = V;

%%% -- Point 3, Tractor 1st rear axis --
U_3 = U;
V_3 = V - (b-a)*dPsi_1;

%%% -- Point 4, Tractor 2nd rear axis --
U_4 = U;
V_4 = V - (c-a)*dPsi_1;

%%% -- Point 5, Tractor rear--
U_5 = U;
V_5 = V - (d-a)*dPsi_1;

%%% -- Point 6, Dolly Mass--
U_6 = U + (f-e)*(dPsi_2-dPsi_1)*sin(Psi_2);
V_6 = V - (d-a)*dPsi_1 + (f-e)*(dPsi_2-dPsi_1)*cos(Psi_2);

U_6_rot = U_6*cos(Psi_2) - V_6*sin(Psi_2);
V_6_rot = U_6*sin(Psi_2) + V_6*cos(Psi_2);

%%% -- Point 7, Dolly rear--
U_7 = U + f*(dPsi_2-dPsi_1)*sin(Psi_2);
V_7 = V - (d-a)*dPsi_1 + f*(dPsi_2-dPsi_1)*cos(Psi_2);

U_7_rot = U_7*cos(Psi_2) - V_7*sin(Psi_2);
V_7_rot = U_7*sin(Psi_2) + V_7*cos(Psi_2);

%%% -- Point 8, Trailer Mass rear--
U_8 = U + (f-e)*(dPsi_2-dPsi_1)*sin(Psi_2) + g*(dPsi_3+dPsi_2-dPsi_1)*sin(Psi_3+Psi_2);
V_8 = V - (d-a)*dPsi_1 + (f-e)*(dPsi_2-dPsi_1)*cos(Psi_2) + g*(dPsi_3+dPsi_2-dPsi_1)*cos(Psi_3+Psi_2);

U_8_rot = U_8*cos(Psi_3+Psi_2) - V_8*sin(Psi_3+Psi_2);
V_8_rot = U_8*sin(Psi_3+Psi_2) + V_8*cos(Psi_3+Psi_2);

%%% -- Point 9, Trailer 1st rear axis --
U_9 = U + (f-e)*(dPsi_2-dPsi_1)*sin(Psi_2) + h*(dPsi_3+dPsi_2-dPsi_1)*sin(Psi_3+Psi_2);
V_9 = V - (d-a)*dPsi_1 + (f-e)*(dPsi_2-dPsi_1)*cos(Psi_2) + h*(dPsi_3+dPsi_2-dPsi_1)*cos(Psi_3+Psi_2);

U_9_rot = U_9*cos(Psi_3+Psi_2) - V_9*sin(Psi_3+Psi_2);
V_9_rot = U_9*sin(Psi_3+Psi_2) + V_9*cos(Psi_3+Psi_2);

%%% -- Point 10, Trailer 2nd rear axis --
U_10 = U + (f-e)*(dPsi_2-dPsi_1)*sin(Psi_2) + k*(dPsi_3+dPsi_2-dPsi_1)*sin(Psi_3+Psi_2);
V_10 = V - (d-a)*dPsi_1 + (f-e)*(dPsi_2-dPsi_1)*cos(Psi_2) + k*(dPsi_3+dPsi_2-dPsi_1)*cos(Psi_3+Psi_2);

U_10_rot = U_10*cos(Psi_3+Psi_2) - V_10*sin(Psi_3+Psi_2);
V_10_rot = U_10*sin(Psi_3+Psi_2) + V_10*cos(Psi_3+Psi_2);

%%% --Roll velocities of tractor rollmass--
U_r1 = U + h_r1*sin(Phi_1)*dPsi_1;
V_r1 = V - h_r1*dPhi_1*cos(Phi_1);

%%% --Roll velocities of tractor rollmass--
```

```
U_r3 = U_8_rot - h_r3*sin(Phi_3)*(dPsi_3+dPsi_2-dPsi_1);
V_r3 = V_8_rot - h_r3*dPhi_3*cos(Phi_3);


%%%%%%%%%%%%%%%%%%%%%%%%%%%%%%%%%%%%%%%%%%%%%%%%%%%%%%%%%%%%%%%%%%%%%%%%%%%%%%%
%%% Energy definitions %%%%%%%%%%%%%%%%%%%%%%%%%%%%%%%%%%%%%%%%%%%%%%%%%%%%%%%%
%%%%%%%%%%%%%%%%%%%%%%%%%%%%%%%%%%%%%%%%%%%%%%%%%%%%%%%%%%%%%%%%%%%%%%%%%%%%%%%
%%% --Kinetic Energy--
T_kin = 1/2*M_1*(U_2^2+V_2^2) + 1/2*I_1*dPsi_1^2 + ...
        1/2*M_2*(U_6_rot^2+V_6_rot^2) + 1/2*I_2*(dPsi_2-dPsi_1)^2 + ...
        1/2*M_3*(U_8_rot^2+V_8_rot^2) + 1/2*I_3*(dPsi_3+dPsi_2-dPsi_1)^2 + ...
        1/2*M_r1*(U_r1^2+V_r1^2) + 1/2*I_Phi_1*dPhi_1^2 + ...
        1/2*M_r3*(U_r3^2+V_r3^2) + 1/2*I_Phi_3*(dPhi_3)^2;

%%% --Potential Energy--
U_pot = 1/2*C_Phi_1*Phi_1^2 - M_r1*gravity*h_r1*cos(Phi_1) + ...
        1/2*C_Phi_3*Phi_3^2 - M_r3*gravity*h_r3*cos(Phi_3);

%%% --Dissipation Energy--
D_dis = 1/2*(3*K_1*L_1)*dPhi_1^2 + 1/2*(3*K_3*L_3)*dPhi_3^2;

%%%%%%%%%%%%%%%%%%%%%%%%%%%%%%%%%%%%%%%%%%%%%%%%%%%%%%%%%%%%%%%%%%%%%%%%%%%%%%%
%%% LAGRANGE FORMULATION (Normal and Modified) %%%%%%%%%%%%%%%%%%%%%%%%%%%%%%%%
%%%%%%%%%%%%%%%%%%%%%%%%%%%%%%%%%%%%%%%%%%%%%%%%%%%%%%%%%%%%%%%%%%%%%%%%%%%%%%%
%%% --Generalized coordinates--
q   = [IU, IV, Psi_1, Psi_2, Psi_3, Phi_1, Phi_3];   %% <-- IU / IV and Psi_1 are not in the system!!
dq  = [U, V, dPsi_1, dPsi_2, dPsi_3, dPhi_1, dPhi_3];
ddq = [dU, dV, ddPsi_1, ddPsi_2, ddPsi_3, ddPhi_1, ddPhi_3];

%%% --Differentitae T_kin to q
dT_kin_dq1 = diff(T_kin,q(1));
dT_kin_dq2 = diff(T_kin,q(2));
dT_kin_dq3 = diff(T_kin,q(3));
dT_kin_dq4 = diff(T_kin,q(4));
dT_kin_dq5 = diff(T_kin,q(5));
dT_kin_dq6 = diff(T_kin,q(6));
dT_kin_dq7 = diff(T_kin,q(7));

%%% --Differentitae T_kin to dq
dT_kin_ddq1 = diff(T_kin,dq(1));
dT_kin_ddq2 = diff(T_kin,dq(2));
dT_kin_ddq3 = diff(T_kin,dq(3));
dT_kin_ddq4 = diff(T_kin,dq(4));
dT_kin_ddq5 = diff(T_kin,dq(5));
dT_kin_ddq6 = diff(T_kin,dq(6));
dT_kin_ddq7 = diff(T_kin,dq(7));

%%% --Differentitae U_pot to q
dU_pot_dq1 = diff(U_pot,q(1));
dU_pot_dq2 = diff(U_pot,q(2));
dU_pot_dq3 = diff(U_pot,q(3));
dU_pot_dq4 = diff(U_pot,q(4));
dU_pot_dq5 = diff(U_pot,q(5));
dU_pot_dq6 = diff(U_pot,q(6));
dU_pot_dq7 = diff(U_pot,q(7));

%%% --Differentitae D_dis to dq
dD_dis_ddq1 = diff(D_dis,dq(1));
dD_dis_ddq2 = diff(D_dis,dq(2));
dD_dis_ddq3 = diff(D_dis,dq(3));
dD_dis_ddq4 = diff(D_dis,dq(4));
dD_dis_ddq5 = diff(D_dis,dq(5));
dD_dis_ddq6 = diff(D_dis,dq(6));
dD_dis_ddq7 = diff(D_dis,dq(7));

%%% --Differentitae T_kin to time dq and time
```

```
dt_dT_kin_ddq1 = dq(1)*diff(dT_kin_ddq1,q(1)) + dq(2)*diff(dT_kin_ddq1,q(2)) + dq(3)*diff(dT_kin_ddq1,q(3)) + ...
                 dq(4)*diff(dT_kin_ddq1,q(4)) + dq(5)*diff(dT_kin_ddq1,q(5)) + dq(6)*diff(dT_kin_ddq1,q(6)) + ...
                 dq(7)*diff(dT_kin_ddq1,q(7));
dt_dT_kin_ddq1 = dt_dT_kin_ddq1 + ddq(1)*diff(dT_kin_ddq1,dq(1)) + ddq(2)*diff(dT_kin_ddq1,dq(2)) + ...
                 ddq(3)*diff(dT_kin_ddq1,dq(3)) + ddq(4)*diff(dT_kin_ddq1,dq(4)) + ddq(5)*diff(dT_kin_ddq1,dq(5)) + ...
                 ddq(6)*diff(dT_kin_ddq1,dq(6)) + ddq(7)*diff(dT_kin_ddq1,dq(7));

dt_dT_kin_ddq2 = dq(1)*diff(dT_kin_ddq2,q(1)) + dq(2)*diff(dT_kin_ddq2,q(2)) + dq(3)*diff(dT_kin_ddq2,q(3)) + ...
                 dq(4)*diff(dT_kin_ddq2,q(4)) + dq(5)*diff(dT_kin_ddq2,q(5)) + dq(6)*diff(dT_kin_ddq2,q(6)) + ...
                 dq(7)*diff(dT_kin_ddq2,q(7));
dt_dT_kin_ddq2 = dt_dT_kin_ddq2 + ddq(1)*diff(dT_kin_ddq2,dq(1)) + ddq(2)*diff(dT_kin_ddq2,dq(2)) + ...
                 ddq(3)*diff(dT_kin_ddq2,dq(3)) + ddq(4)*diff(dT_kin_ddq2,dq(4)) + ddq(5)*diff(dT_kin_ddq2,dq(5)) + ...
                 ddq(6)*diff(dT_kin_ddq2,dq(6)) + ddq(7)*diff(dT_kin_ddq2,dq(7));

dt_dT_kin_ddq3 = dq(1)*diff(dT_kin_ddq3,q(1)) + dq(2)*diff(dT_kin_ddq3,q(2)) + dq(3)*diff(dT_kin_ddq3,q(3)) + ...
                 dq(4)*diff(dT_kin_ddq3,q(4)) + dq(5)*diff(dT_kin_ddq3,q(5)) + dq(6)*diff(dT_kin_ddq3,q(6)) + ...
                 dq(7)*diff(dT_kin_ddq3,q(7));
dt_dT_kin_ddq3 = dt_dT_kin_ddq3 + ddq(1)*diff(dT_kin_ddq3,dq(1)) + ddq(2)*diff(dT_kin_ddq3,dq(2)) + ...
                 ddq(3)*diff(dT_kin_ddq3,dq(3)) + ddq(4)*diff(dT_kin_ddq3,dq(4)) + ddq(5)*diff(dT_kin_ddq3,dq(5)) + ...
                 ddq(6)*diff(dT_kin_ddq3,dq(6)) + ddq(7)*diff(dT_kin_ddq3,dq(7));

dt_dT_kin_ddq4 = dq(1)*diff(dT_kin_ddq4,q(1)) + dq(2)*diff(dT_kin_ddq4,q(2)) + dq(3)*diff(dT_kin_ddq4,q(3)) + ...
                 dq(4)*diff(dT_kin_ddq4,q(4)) + dq(5)*diff(dT_kin_ddq4,q(5)) + dq(6)*diff(dT_kin_ddq4,q(6)) + ...
                 dq(7)*diff(dT_kin_ddq4,q(7));
dt_dT_kin_ddq4 = dt_dT_kin_ddq4 + ddq(1)*diff(dT_kin_ddq4,dq(1)) + ddq(2)*diff(dT_kin_ddq4,dq(2)) + ...
                 ddq(3)*diff(dT_kin_ddq4,dq(3)) + ddq(4)*diff(dT_kin_ddq4,dq(4)) + ddq(5)*diff(dT_kin_ddq4,dq(5)) + ...
                 ddq(6)*diff(dT_kin_ddq4,dq(6)) + ddq(7)*diff(dT_kin_ddq4,dq(7));

dt_dT_kin_ddq5 = dq(1)*diff(dT_kin_ddq5,q(1)) + dq(2)*diff(dT_kin_ddq5,q(2)) + dq(3)*diff(dT_kin_ddq5,q(3)) + ...
                 dq(4)*diff(dT_kin_ddq5,q(4)) + dq(5)*diff(dT_kin_ddq5,q(5)) + dq(6)*diff(dT_kin_ddq5,q(6)) + ...
                 dq(7)*diff(dT_kin_ddq5,q(7));
dt_dT_kin_ddq5 = dt_dT_kin_ddq5 + ddq(1)*diff(dT_kin_ddq5,dq(1)) + ddq(2)*diff(dT_kin_ddq5,dq(2)) + ...
                 ddq(3)*diff(dT_kin_ddq5,dq(3)) + ddq(4)*diff(dT_kin_ddq5,dq(4)) + ddq(5)*diff(dT_kin_ddq5,dq(5)) + ...
                 ddq(6)*diff(dT_kin_ddq5,dq(6)) + ddq(7)*diff(dT_kin_ddq5,dq(7));

dt_dT_kin_ddq6 = dq(1)*diff(dT_kin_ddq6,q(1)) + dq(2)*diff(dT_kin_ddq6,q(2)) + dq(3)*diff(dT_kin_ddq6,q(3)) + ...
                 dq(4)*diff(dT_kin_ddq6,q(4)) + dq(5)*diff(dT_kin_ddq6,q(5)) + dq(6)*diff(dT_kin_ddq6,q(6)) + ...
                 dq(7)*diff(dT_kin_ddq6,q(7));
dt_dT_kin_ddq6 = dt_dT_kin_ddq6 + ddq(1)*diff(dT_kin_ddq6,dq(1)) + ddq(2)*diff(dT_kin_ddq6,dq(2)) + ...
                 ddq(3)*diff(dT_kin_ddq6,dq(3)) + ddq(4)*diff(dT_kin_ddq6,dq(4)) + ddq(5)*diff(dT_kin_ddq6,dq(5)) + ...
                 ddq(6)*diff(dT_kin_ddq6,dq(6)) + ddq(7)*diff(dT_kin_ddq6,dq(7));

dt_dT_kin_ddq7 = dq(1)*diff(dT_kin_ddq7,q(1)) + dq(2)*diff(dT_kin_ddq7,q(2)) + dq(3)*diff(dT_kin_ddq7,q(3)) + ...
                 dq(4)*diff(dT_kin_ddq7,q(4)) + dq(5)*diff(dT_kin_ddq7,q(5)) + dq(6)*diff(dT_kin_ddq7,q(6)) + ...
                 dq(7)*diff(dT_kin_ddq7,q(7));
dt_dT_kin_ddq7 = dt_dT_kin_ddq7 + ddq(1)*diff(dT_kin_ddq7,dq(1)) + ddq(2)*diff(dT_kin_ddq7,dq(2)) + ...
                 ddq(3)*diff(dT_kin_ddq7,dq(3)) + ddq(4)*diff(dT_kin_ddq7,dq(4)) + ddq(5)*diff(dT_kin_ddq7,dq(5)) + ...
                 ddq(6)*diff(dT_kin_ddq7,dq(6)) + ddq(7)*diff(dT_kin_ddq7,dq(7));

%%% --Left Side of Modified Lagrange formulation--
Q_q1 = dt_dT_kin_ddq1 - dq(3)*dT_kin_ddq2 + dU_pot_dq1 + dD_dis_ddq1;
Q_q2 = dt_dT_kin_ddq2 + dq(3)*dT_kin_ddq1 + dU_pot_dq2 + dD_dis_ddq2;
Q_q3 = dt_dT_kin_ddq3 - dq(2)*dT_kin_ddq1 + dq(1)*dT_kin_ddq2 + dU_pot_dq3 + dD_dis_ddq3;
%%% --Left Side of Normal Lagrange formulation--
Q_q4 = dt_dT_kin_ddq4 - dT_kin_dq4 + dU_pot_dq4 + dD_dis_ddq4;
Q_q5 = dt_dT_kin_ddq5 - dT_kin_dq5 + dU_pot_dq5 + dD_dis_ddq5;
Q_q6 = dt_dT_kin_ddq6 - dT_kin_dq6 + dU_pot_dq6 + dD_dis_ddq6;
Q_q7 = dt_dT_kin_ddq7 - dT_kin_dq7 + dU_pot_dq7 + dD_dis_ddq7;

%%%%%%%%%%%%%%%%%%%%%%%%%%%%%%%%%%%%%%%%%%%%%%%%%%%%%%%%%%%%%%%%%%%%%%%%%%%
%%% Left Side of the Lagrange formulation %%%%%%%%%%%%%%%%%%%%%%%%%%%%%%%%%
%%%%%%%%%%%%%%%%%%%%%%%%%%%%%%%%%%%%%%%%%%%%%%%%%%%%%%%%%%%%%%%%%%%%%%%%%%%
string_tot_left = [Q_q1; Q_q2; Q_q3; Q_q4; Q_q5; Q_q6; Q_q7];

%%%%%%%%%%%%%%%%%%%%%%%%%%%%%%%%%%%%%%%%%%%%%%%%%%%%%%%%%%%%%%%%%%%%%%%%%%%
%%% External applied Forces %%%%%%%%%%%%%%%%%%%%%%%%%%%%%%%%%%%%%%%%%%%%%%%
```

```
%%%%%%%%%%%%%%%%%%%%%%%%%%%%%%%%%%%%%%%%%%%%%%%%%%%%%%%%%%%%%%%%%%%%%%%%%%%%
F_appl_1 = [-Fy1*sin(delta);Fy1*cos(delta)];
F_appl_2 = [Fcruise;Fy2];           %% <-- Fcruise to maintain forward vel U
F_appl_3 = [-Ftruck;Fy3];           %% <-- Force Actuator on Truck
F_appl_4 = [-0.5*Ftrailer ;Fy4];    %% <-- 50 percent (brake force distribution) Force Actuator on Truck
F_appl_5 = [0 ;Fy5];
F_appl_6 = [-0.5*Ftrailer; Fy6];    %% <-- 50 percent (brake force distribution) Force Actuator on Truck

T_appl_1 = Ttruck;                  %% <-- Torque actuator on truck chassis mass

%%% --Velocities External applied forces--
R_1 = [U_1;V_1];
R_2 = [U_3;V_3];
R_3 = [U_4;V_4];
R_4 = [U_7_rot;V_7_rot];
R_5 = [U_9_rot;V_9_rot];
R_6 = [U_10_rot;V_10_rot];
R_7 = dPsi_1;

R_1_ddq_1 = []; R_1_ddq_2 = [];
R_2_ddq_1 = []; R_2_ddq_2 = [];
R_3_ddq_1 = []; R_3_ddq_2 = [];
R_4_ddq_1 = []; R_4_ddq_2 = [];
R_5_ddq_1 = []; R_5_ddq_2 = [];
R_6_ddq_1 = []; R_6_ddq_2 = [];
R_7_ddq   = [];

for i=1:length(dq)
    dR_1 = diff(R_1(1),dq(i));
    dR_2 = diff(R_1(2),dq(i));
    R_1_ddq_1 = [R_1_ddq_1,dR_1];
    R_1_ddq_2 = [R_1_ddq_2,dR_2];
end
R_1_ddq = [R_1_ddq_1;R_1_ddq_2];

for i=1:length(dq)
    dR_1 = diff(R_2(1),dq(i));
    dR_2 = diff(R_2(2),dq(i));
    R_2_ddq_1 = [R_2_ddq_1,dR_1];
    R_2_ddq_2 = [R_2_ddq_2,dR_2];
end
R_2_ddq = [R_2_ddq_1;R_2_ddq_2];

for i=1:length(dq)
    dR_1 = diff(R_3(1),dq(i));
    dR_2 = diff(R_3(2),dq(i));
    R_3_ddq_1 = [R_3_ddq_1,dR_1];
    R_3_ddq_2 = [R_3_ddq_2,dR_2];
end
R_3_ddq = [R_3_ddq_1;R_3_ddq_2];

for i=1:length(dq)
    dR_1 = diff(R_4(1),dq(i));
    dR_2 = diff(R_4(2),dq(i));
    R_4_ddq_1 = [R_4_ddq_1,dR_1];
    R_4_ddq_2 = [R_4_ddq_2,dR_2];
end
R_4_ddq = [R_4_ddq_1;R_4_ddq_2];

for i=1:length(dq)
    dR_1 = diff(R_5(1),dq(i));
    dR_2 = diff(R_5(2),dq(i));
    R_5_ddq_1 = [R_5_ddq_1,dR_1];
    R_5_ddq_2 = [R_5_ddq_2,dR_2];
end
R_5_ddq = [R_5_ddq_1;R_5_ddq_2];
```

```
for i=1:length(dq)
    dR_1 = diff(R_6(1),dq(i));
    dR_2 = diff(R_6(2),dq(i));
    R_6_ddq_1 = [R_6_ddq_1,dR_1];
    R_6_ddq_2 = [R_6_ddq_2,dR_2];
end
R_6_ddq = [R_6_ddq_1;R_6_ddq_2];

for i=1:length(dq)
    dR_1 = diff(R_7,dq(i));
    R_7_ddq = [R_7_ddq,dR_1];
end

%%% --Total External applied Forces--
Q = conj(R_1_ddq')*F_appl_1 + conj(R_2_ddq')*F_appl_2 + conj(R_3_ddq')*F_appl_3 + ...
    conj(R_4_ddq')*F_appl_4 + conj(R_5_ddq')*F_appl_5 + conj(R_6_ddq')*F_appl_6 + ...
    conj(R_7_ddq')*T_appl_1;

%%%%%%%%%%%%%%%%%%%%%%%%%%%%%%%%%%%%%%%%%%%%%%%%%%%%%%%%%%%%%%%%%%%%%%%%%%%
%%% Values of the External applied forces %%%%%%%%%%%%%%%%%%%%%%%%%%%%%%%%
%%% dependent on Side Slip angles (velocities) at different points,  %%%%%
%%% where the external applied forces acts. %%%%%%%%%%%%%%%%%%%%%%%%%%%%%%
%%%%%%%%%%%%%%%%%%%%%%%%%%%%%%%%%%%%%%%%%%%%%%%%%%%%%%%%%%%%%%%%%%%%%%%%%%%
F_y1 = C_1 * (delta + atan(-V_1/U_1));
F_y2 = C_2 * atan(-V_3/U_3);
F_y3 = C_3 * atan(-V_4/U_4);
F_y4 = C_4 * atan(-V_7_rot/U_7_rot);
F_y5 = C_5 * atan(-V_9_rot/U_9_rot);
F_y6 = C_6 * atan(-V_10_rot/U_10_rot);

%%% --Substitution in total External applied Forces--
Q = subs(Q,Fy1,F_y1); Q = subs(Q,Fy2,F_y2); Q = subs(Q,Fy3,F_y3);
Q = subs(Q,Fy4,F_y4); Q = subs(Q,Fy5,F_y5); Q = subs(Q,Fy6,F_y6);

%%%%%%%%%%%%%%%%%%%%%%%%%%%%%%%%%%%%%%%%%%%%%%%%%%%%%%%%%%%%%%%%%%%%%%%%%%%
%%% Right Side of the Lagrange formulation %%%%%%%%%%%%%%%%%%%%%%%%%%%%%%%%
%%%%%%%%%%%%%%%%%%%%%%%%%%%%%%%%%%%%%%%%%%%%%%%%%%%%%%%%%%%%%%%%%%%%%%%%%%%
string_force = Q;

%%%%%%%%%%%%%%%%%%%%%%%%%%%%%%%%%%%%%%%%%%%%%%%%%%%%%%%%%%%%%%%%%%%%%%%%%%%
%%% Rewrite Left and Right side of the Lagrange formulation %%%%%%%%%%%%%%%
%%% to ddq = inv(MM)*string_total_right %%%%%%%%%%%%%%%%%%%%%%%%%%%%%%%%%%
%%%%%%%%%%%%%%%%%%%%%%%%%%%%%%%%%%%%%%%%%%%%%%%%%%%%%%%%%%%%%%%%%%%%%%%%%%%
MM_II = [diff(string_tot_left(1),ddq(1)),diff(string_tot_left(1),ddq(2)),diff(string_tot_left(1),ddq(3)),...
         diff(string_tot_left(1),ddq(4)),diff(string_tot_left(1),ddq(5)),diff(string_tot_left(1),ddq(6)),...
         diff(string_tot_left(1),ddq(7));
         diff(string_tot_left(2),ddq(1)),diff(string_tot_left(2),ddq(2)),diff(string_tot_left(2),ddq(3)),...
         diff(string_tot_left(2),ddq(4)),diff(string_tot_left(2),ddq(5)),diff(string_tot_left(2),ddq(6)),...
         diff(string_tot_left(2),ddq(7));
         diff(string_tot_left(3),ddq(1)),diff(string_tot_left(3),ddq(2)),diff(string_tot_left(3),ddq(3)),...
         diff(string_tot_left(3),ddq(4)),diff(string_tot_left(3),ddq(5)),diff(string_tot_left(3),ddq(6)),...
         diff(string_tot_left(3),ddq(7));
         diff(string_tot_left(4),ddq(1)),diff(string_tot_left(4),ddq(2)),diff(string_tot_left(4),ddq(3)),...
         diff(string_tot_left(4),ddq(4)),diff(string_tot_left(4),ddq(5)),diff(string_tot_left(4),ddq(6)),...
         diff(string_tot_left(4),ddq(7));
         diff(string_tot_left(5),ddq(1)),diff(string_tot_left(5),ddq(2)),diff(string_tot_left(5),ddq(3)),...
         diff(string_tot_left(5),ddq(4)),diff(string_tot_left(5),ddq(5)),diff(string_tot_left(5),ddq(6)),...
         diff(string_tot_left(5),ddq(7));
         diff(string_tot_left(6),ddq(1)),diff(string_tot_left(6),ddq(2)),diff(string_tot_left(6),ddq(3)),...
         diff(string_tot_left(6),ddq(4)),diff(string_tot_left(6),ddq(5)),diff(string_tot_left(6),ddq(6)),...
         diff(string_tot_left(6),ddq(7));
         diff(string_tot_left(7),ddq(1)),diff(string_tot_left(7),ddq(2)),diff(string_tot_left(7),ddq(3)),...
         diff(string_tot_left(7),ddq(4)),diff(string_tot_left(7),ddq(5)),diff(string_tot_left(7),ddq(6)),...
         diff(string_tot_left(7),ddq(7))];
```

```
MM = simple(MM_II);

string_right = string_tot_left - MM*conj(ddq');
string_right = simple(string_right);
string_right_tot_II = string_force - string_right;


%%%%%%%%%%%%%%%%%%%%%%%%%%%%%%%%%%%%%%%%%%%%%%%%%%%%%%%%%%%%%%%%%%%%%%%%%%%%
%%% Substitution of Zegwaard vehicle parameters %%%%%%%%%%%%%%%%%%%%%%%%%%%%
%%%%%%%%%%%%%%%%%%%%%%%%%%%%%%%%%%%%%%%%%%%%%%%%%%%%%%%%%%%%%%%%%%%%%%%%%%%%
%% --Note C_Phi_1 and K_1 has been changed, because of an unrealistic roll angle!!
M_r1 = 21500; M_r3 = 26440; M_1 = 23960-M_r1; M_2 = 1e3; M_3 = 27760-M_r3;
a = 3.35; b = 4.2; c = 5.53; d = 7; e = 0.03; f = 2.49; g = 3.42; h = 4.66; k = 5.9;
L_1 = 0.91; L_3 = 0.91; h_r1 = 1.56; h_r3 = 1.75;
C_Phi_3 = 2.38e6; C_Phi_1 = C_Phi_3; % C_Phi_1 = 4.01e5;
I_1 = 1.67e5; I_2 = 7.5e2; I_3 = 2.23e5; I_Phi_1 = 3.42e4; I_Phi_3 = 4.3e4;
C_1 = 3.65e5; C_2 = 5.88e5; C_3 = 5.18e5; C_4 = 6.42e5; C_5 = 6.74e5; C_6 = 6.72e5;
K_3 = 4.84e4; K_1 = K_3; % K_1 = 1.17e5;

gravity = -9.81;

MM = eval(MM);
string_right = eval(string_right_tot_II);

%%% --Save Mass matrix and right-side
save MM_string_right.mat MM string_right

toc
```

# Appendix G

# System matrix $\mathbf{A}_{Circle}$ of the truck/full-trailer combination

$$\mathbf{A}_{Circle}\,(14\times 14) = \begin{bmatrix} \mathbf{0} & \mathbf{I} \\ \mathbf{A}^{e}_{Circle} & \mathbf{A}^{\dot{e}}_{Circle} \end{bmatrix}$$

$$\mathbf{A}^{e}_{Circle}\,(7\times 7) = \begin{bmatrix} 0 & 0 & 0 & -3.7103 & -3.0111 & -1.7702 & 2.7577 \\ 0 & 0 & 0 & 0.2243 & -0.5291 & -71.9742 & 0.3811 \\ 0 & 0 & 0 & 0.0049 & 0.1744 & -0.2573 & -0.1350 \\ 0 & 0 & 0 & -63.7310 & -29.6484 & 28.2582 & 23.4623 \\ 0 & 0 & 0 & 59.8306 & 17.2107 & -28.4115 & -22.5969 \\ 0 & 0 & 0 & 0.0870 & -0.2052 & -51.8378 & 0.1478 \\ 0 & 0 & 0 & 63.5934 & 44.0533 & 0.1549 & -39.2482 \end{bmatrix}$$

$$\mathbf{A}^{\dot{e}}_{Circle}\,(7\times 7) = \begin{bmatrix} -0.0683 & -0.2205 & 0.0309 & -0.4870 & -0.3507 & -0.4236 & 0.6028 \\ -0.6220 & -6.5813 & -17.8578 & -0.2947 & -0.1813 & -4.6376 & -0.0169 \\ 0.0320 & 0.1087 & -2.1805 & 0.0784 & 0.0490 & -0.0114 & -0.0055 \\ -0.2641 & -0.2092 & 20.9249 & -15.4208 & -7.7232 & 1.8215 & 1.5551 \\ 0.2317 & 0.1383 & -18.5976 & 11.6617 & 4.3910 & -1.8237 & -1.4892 \\ -0.1475 & -2.5529 & 0.8540 & -0.1143 & -0.0703 & -3.3318 & -0.0065 \\ 0.5416 & 3.1320 & -30.9102 & 19.4327 & 11.6391 & 0.0326 & -2.6273 \end{bmatrix}$$

# Bibliography


[AB98] Odenthal D. Ackermann, J. and T. Bnte (eds.), *Advantages of active steering for vehicle dynamics control*, DLR, German Aerospace Center, Institute of Robotics and System Dynamics, Proceedings of International Symposium on Automotive Technology and Automation, Vienna, 1999, 1998.

[AO88] J. Ackermann and D. Odenthal (eds.), *Damping of vehicle roll dynamics by gain scheduled active steering*, DLR, German Aerospace Center, Institute of Robotics and System Dynamics, Proceedings of European Control Conference. Karlsruhe, Germany, 1988.

[AO03] T. Acerman and Ü. Özgüner (eds.), *Rollover prevention for heavy trucks using frequency shaped sliding mode control*, pp. 7-12, vol. 1, IEEE Conference on Control Applications, 2003, 2003.

[BC04] Staals H. Liebregts R. Jongerius C. Besselink, I.J.M. and S. de Cock, *Advanced vehicle dynamics, lecture notes course 4j570*, Tech. report, University of Technology, Eindhoven, The Netherlands. Department Mechanical Engineering, 2004.

[BV03] I.J.M. Besselink and P. Veldpaus, *Vehicle dynamics, lecture notes course 4l150*, Tech. report, University of Technology, Eindhoven, The Netherlands. Department Mechanical Engineering, 2003.

[Dah01] E. Dahlberg, *Commercial vehicle stability - focussing on rollover*, Issn: 1103-470x, Royal Institute of Technology, Stockholm, Sweden. Department of Vehicle Engineering, 2001.

[Erv83] R.D. Ervin, *Chapter 18: The cornering response of commercial vehicles in the nonlinear regime, engineering summer conferences, mechanics of heavy-duty trucks and truck combinations, volume ii*, Tech. report, The University of Michigan - College of Engineering, 1983.

[Erv87] ———, *Mechanics of the rollover process, engineering summer conferences, mechanics of heavy-duty trucks and truck combinations*, Tech. report, The University of Michigan - College of Engineering, 1987.

[FEN94] Powell J.D. Franklin, G.F and A. Emami-Naeini, *Feedback control of dynamic systems*, third ed., no. ISBN 0-201-53487-8, Addison-Wesley Publishing Company, Inc., 1994.

[fSN04a] NHTSA's Notional Center for Statistics and Analysis (NCSA), *Traffic safety facts 2004, a compilation of motor vehicle crash data from the fatality analysis reporting system and the general estimates system*, Tech. Report DOT HS 809 919, `http://www.nhtsa.dot.gov`, NHTSA, 2004, page 77.

[fSN04b] ———, *Traffic safety facts, data 2004, overview*, Tech. Report `http://www.nhtsa.dot.gov`, NHTSA, 2004.

[Gmb] Bosch GmbH, *http://rb-k.bosch.de/en/start/s0_safety.html*.

[Gol01] R.W. Goldman, *Development of a rollover-warning device for road vehicles*, Tech. report, The Pennsylvania State University, department of Mechanical and Nucliar Engineering, 2001.

[HB00] Schramm H. Beyer C. Holler G. Hecker, F. and M. Bennet (eds.), *Heavy vehicle stability notification and assistance*, no. 2000-01-3481, SAE, 2000.

[Hen04] R. Hensen, *Roll stability criterion for special vehicles english market*, Tech. Report Internal report, 51051/04/081, DAF Trucks, 2004.

[HS97] Hummel S. Jundt O. Leimbach K.-D. Faye I. Hecker, F. and H. Schramm (eds.), *Vehicle dynamics control for commercial vehicles*, no. 973284, SAE, 1997.

[KdCv01] B. Kraker de and D.H. Campen van, *Mechanical vibrations*, no. ISBN 90-423-0165-1, Shaker Publishing BV, 2001.

[KL80] V.C. Klema and A.J. Laub, *The singular value decomposition: Its computation and some applications*, IEEE Transactions on Automatic Control **AC-25** (1980), no. 2, 164–176.

[LA97] Rakheja S. Liu, P.J. and A.K.W. Ahmed (eds.), *Detection of dynamic roll instability of heavy vehicles for open-loop rollover control*, no. 973263, SAE, 1997.

[LZ04] Huang R. Liu, Y. and J. Zhu (eds.), *Nonlinear system control using neural networks based on trajectory linearization*, vol. International Conference on Control Applications, Taipei, Taiwan, University of Ohio, department Electrical Engineering and Computer Science, IEEE, 2004.

[Mata] The MathWorks, *http://www.mathworks.com/access/helpdesk/help/techdoc/ref/index.html?/access/helpdesk/help/techdoc/ref/rank.html*.

[Matb] ———, *http://www.mathworks.com/access/helpdesk/help/toolbox/control/ref/place.html*.

[(NH02] The National Highway Traffic Safety Administration (NHTSA), *Rating system for rollover resistance*, Tech. report, Transportation Research Board, The National Academies, 2002.

[NHT] NHTSA, *http://www.safercar.gov/Rollover/*.

[Ode02] D. Odenthal, *Ein robustes fahrdynamik-regelungskonzept fr die kippvermeidung von kraftfahrzeugen*, Isbn: 3183505126, University of Technology, Munich, Germany. Department Steuerungs- und Regelungstechnik, 2002.

[oMVAA06] American Association of Motor Vehicle Administrators (AAMVA), *Florida commercial driver license (cdl) handbook 2006*, Tech. Report `http://www.aamva.org` and `http://www.hsmv.state.fl.us/handbooks/Commercial/`, 2006.

[Pac02] H.B. Pacejka, *Tyre and vehicle dynamics*, no. ISBN 0-7506-5141-5, Butterworth-Heinemann, 2002.

[PL99] M. Plöchl and P. Lugner (eds.), *Passenger car and passenger car-trailer, different tasks for the driver*, vol. 20, pp. 543-548, no. 4, JSAE Review, 1999.

[Raj06] R. Rajamani, *Vehicle dynamics and control*, no. ISBN 0-387-26396-9, Springer, 2006.

[Sko05] Postlethwaite I. Skogestad, S., *Multivariable feedback control: Analysis and design*, second ed., no. ISBN: 0-470-01168-8 (pb). - 0-470-01167-X (hb). - 978-0-470-01168-3 (pb). - 978-0-470-01167-6 (hb), John Wiley & Sons, Ltd, 2005.

[SS04a] Ricalde L.J. Langari R. Sanchez, E.N. and D. Shahmirzadi (eds.), *Recurrent neural control for rollover prevention on heavy vehicles*, pp. 1841-1846, vol. 3, IEEE International Joint Conference, 2004.

[SS04b] Ricalde L.J. Langari R. Sanchez, E.N. and D. Shahmirzadi (eds.), *Rollover prediction and control in heavy vehicles via recurrent neural networks*, pp. 5210-5215, vol. 5, 43rd IEEE Conference, 2004.

[TH02] Nagai M. Taniguchi T. Takano, S. and T. Hatano (eds.), *Study on a vehicle dynamics model for improving roll stability*, pp. 149-156, vol. 24, JSAE Review, 2002.

[Win00] C. Winkler, *Rollover of heavy commercial vehicles*, Tech. Report Volume 31, Number 4, UMTRI Research Review, University of Michigan Transportation Research Institute, 2000.

[Zan03] A Zanten, *Fahrdynamik und fahrdynamikregelsysteme*, Tech. report, Bosch GmbH, 2003, ESP Course.

[Zeg88] J.P. Zegwaard, *Modelling and analysis of the behaviour of a truck-trailer-combination during lane-change manoeuvres*, 88.3.vt.2478, University of Technology, Delft, The Netherlands, 1988.

# List of Figures